REVIEWS OF MODERN PHYSICS, VOLUME 77, OCTOBER 2005

Isotope effects on the optical spectra of semiconductors

Manuel Cardona*

Max-Planck-Institut fuer Festkoerperforschung, Heisenbergstrasse 1, D-70569 Stuttgart, Germany

M. L. W. Thewalt

Physics Department, Simon Fraser University, Burnaby, B.C. V5A 1S6, Canada

(Published 7 November 2005)

Since the end of the cold war, macroscopic amounts of separated stable isotopes of most elements have been available "off the shelf" at affordable prices. Using these materials, single crystals of many semiconductors have been grown and the dependence of their physical properties on isotopic composition has been investigated. The most conspicuous effects observed have to do with the dependence of phonon frequencies and linewidths on isotopic composition. These affect the electronic properties of solids through the mechanism of electron-phonon interaction, in particular, in the corresponding optical excitation spectra and energy gaps. This review contains a brief introduction to the history, availability, and characterization of stable isotopes, including their many applications in science and technology. It is followed by a concise discussion of the effects of isotopic composition on the vibrational spectra, including the influence of average isotopic masses and isotopic disorder on the phonons. The final sections deal with the effects of electron-phonon interaction on energy gaps, the concomitant effects on the luminescence spectra of free and bound excitons, with particular emphasis on silicon, and the effects of isotopic composition of the host material on the optical transitions between the bound states of hydrogenic impurities.

CONTENTS

*Electronic address: m.cardona@fkf.mpg.de

I. INTRODUCTION

Soddy (1913) realized that there are mixtures of elements which cannot be separated by chemical means. He then postulated that such elements, usually obtained by radioactive transmutation, have the same intra-atomic charge but different atomic masses. He called them isotopes because they occupy the same place in the periodic table (Greek: *topos*=place). At about the same time Thomson (1913) found the presence of neon in gas discharge tubes, with atomic masses 20 and 22 and an average mass 20.2, which agreed with the accepted mass of this element. Those experiments, which were discontinued because of the war, were not sufficiently convincing to establish the existence in nature of two stable isotopes of Ne (Aston, 1920). After the war Aston restarted this work with a greatly improved mass spectrometer, confirmed the existence of ^{20}Ne and ^{22}Ne and discovered the two stable isotopes of chlorine (^{35}Cl and ^{37}Cl). Thus the presence on Earth of stable isotopes of some elements was established. The three authors of the discovery were awarded separate Nobel prizes (Chemistry: Soddy, 1921 and Aston, 1922; Thomson had already received the Physics Nobel Prize in 1905).

The separation of isotopes received great impetus during World War II because of the military uses of ^{235}U, which although radioactive through nuclear fission, can almost be considered stable (7×10^8 yr half-life) and is found in natural uranium with an abundance of 0.7% [see Emsley (1990)]. For more recent listings of stable isotopes and their abundances, see http://physics.nist.gov/PhysRefData/Compositions/index.html. The isotopic abundances are rather constant throughout our planetary system. There is considerable literature covering the generation of isotopes after the Sun was formed. For recent reviews see Mason (1991) and Manuel (2001). The state of the art around 1956 was reviewed by Suess and Urey (1956).

The first large-scale separation of isotopes involved the production of heavy water by electrolysis in Norway in the 1930s. The initial purpose was merely academic, but after the discovery of nuclear fission, it became evident that heavy water (as well as highly pure graphite) would be the ideal neutron energy moderator for use in nuclear reactors. This fact probably played a role in the invasion of Norway by Germany. Attempts by the Allies to thwart the acquisition of the precious liquid by the Germans have even made it to a Hollywood movie (*The Heroes of Telemark*, with Kirk Douglas, 1965).

The second large-scale separation, at the opposite end of the atomic mass spectrum, dealt with ^{235}U for nuclear warfare (Manhattan project). This separation was performed, in kilogram quantities, by electromagnetic means, analogous in principle to the mass spectrometers used by Aston (1920). For the separation of ^{235}U from ^{238}U a large number of such spectrometers, called *calutrons*, were set up at the Oak Ridge National Laboratory (Love, 1973).

Several other methods for separating isotopes have been developed. They involve such diverse techniques as laser excitation, thermal diffusion, gas centrifugation, and chemical exchange. For a review, see Villani (1976). When the element to be separated can be prepared as a gaseous compound (e.g., Si as SiF_4), the technique of choice for separating large amounts of material is gas centrifugation (Olander, 1978). Isotopes of the following elements are at present separated using this procedure: Si, S, Cl, Ar, Ti, Cr, Ni, Cu, Zn, Ga, Ge, Se, Br, Kr, Mo, Cd, Sn, Te, Xe, W, Ir, and U. There are nowadays only a few separation plants in operation for civilian use, most of them in Russia (Kurchatov Institute[1]) or in Western Europe, although the separation facility at Oak Ridge, which had been shut down, is operating again.

In spite of the small number of isotope separation facilities, the University of Vermont lists under http://www.uvm.edu/~geology/geowww/suppliers.html 80 isotope suppliers and dealers worldwide. They make contacts with the producers, negotiate wholesale agreements, sometimes check the quality (chemical purity, isotopic composition) of the isotopes, and arrange the production of chemical compounds with specific isotopic composition. The main consumers of stable isotopes are the pharmaceutical and biomedical industries. They use them for diagnostic purposes, such as markers of products whose final bodily destination is known. For instance, ^{13}C, with a nuclear magnetic moment, can be applied to studies with NMR scanners. Chemicals containing stable isotopes can be kept on the shelf and activated by neutron irradiation shortly before using them in cancer therapy (for instance, $^{88}\mathrm{Sr}+n=^{89}\mathrm{Sr}$, which is radioactive and has found application in bone cancer therapy). Stable isotopes have also found application in the laser industry (He-Cd lasers with isotopically pure Cd produce a strong uv line, which is hard to obtain with natural Cd). ^{113}Cd is used as a neutron absorber in reactor technology. Many more applications can be found by searching the Web for "applications of stable isotopes."

The elements used in the work on semiconductors described in this review are listed in Table I. Note that aluminum, phosphorus, arsenic, and iodine, which are components of some of the semiconductors discussed here, have only one stable isotope. It is highly recommended, in order to avoid unpleasant surprises, that one check the agreement of the actual chemical purity and isotopic composition with the assay provided by the suppliers and to report to them as soon as possible any important deviations before embarking on costly crystal growth and experimentation. Isotopic analysis is usually performed by mass spectroscopy (if spatial resolution is

[1]Russian isotopes became widely available in the West after the fall of the Iron Curtain.

TABLE I. Stable isotopes of elements used for the work described in this review. Phosphorus, aluminum, arsenic, and iodine have only one stable isotope and are thus not listed. Some of the isotopes listed (e.g., ^{115}In, half-life 6×10^{14} yr; ^{76}Ge, half-life $\sim10^{20}$ yr) undergo radioactive decay. However, their half-life is larger than that of the solar system. The nuclear spins are given in boldface parentheses (if they are not zero). From www.webelements.com and Emsley (1990).

Carbon	^{12}C: 98.9%; ^{13}C: 1.1% (**3/2**)
Silicon	^{28}Si: 92.2%; ^{29}Si: 4.7% (**3/2**); ^{30}Si: 3.1%
Germanium	^{70}Ge: 20.8%; ^{72}Ge: 27.5%; ^{73}Ge: 7.7% (**9/2**); ^{74}Ge: 36.3%; ^{76}Ge: 7.6%
Tin (gray)	^{112}Sn: 1%; ^{114}Sn: 0.7%; ^{115}Sn: 0.3% (**1/2**); ^{116}Sn: 14.5%; ^{117}Sn: 7.7% (**1/2**); ^{118}Sn: 24.2%; ^{119}Sn: 8.6% (**1/2**); ^{120}Sn: 32.6%; ^{122}Sn: 4.6%; ^{124}Sn: 5.8%
Boron	^{10}B: 19.9% (**3**); ^{11}B: 80.1% (**3/2**)
Gallium	^{69}Ga: 60.1% (**3/2**); ^{71}Ga: 39.9% (**3/2**)
Indium	^{113}In: 4.3% (**9/2**); ^{115}In: 95.7% (**9/2**)
Zinc	^{64}Zn: 48.6%; ^{66}Zn: 27.9%; ^{67}Zn: 4.1% (**5/2**); ^{68}Zn: 18.8%; ^{70}Zn: 0.6%
Cadmium	^{106}Cd: 1.3%; ^{108}Cd: 0.9%; ^{110}Cd: 12.5%; ^{111}Cd: 12.8% (**3/2**); ^{112}Cd: 24.1%; ^{113}Cd: 12.2% (**1/2**); ^{114}Cd: 28.7%; ^{116}Cd: 7.5%
Copper	^{63}Cu: 69.2% (**3/2**); ^{65}Cu: 30.8% (**3/2**)
Chlorine	^{35}Cl: 75.8% (**3/2**); ^{37}Cl: 24.2% (**3/2**)
Bromine	^{79}Br: 50.7% (**3/2**); ^{81}Br: 49.3% (**3/2**)
Oxygen	^{16}O: 99.8%; ^{17}O: 0.05% (**3/2**); ^{18}O: 0.2%
Sulfur	^{32}S: 95%; ^{33}S: 0.8% (**3/2**); ^{34}S: 4.2%; ^{36}S: 0.02%
Selenium	^{74}Se: 0.9%; ^{76}Se: 9.4%; ^{77}Se: 7.6% (**1/2**); ^{78}Se: 23.8%; ^{80}Se: 49.6%; ^{82}Se: 8.8%
Tellurium	^{122}Te: 2.5%; ^{123}Te: 0.9% (**1/2**); ^{124}Te: 4.7%; ^{125}Te: 7.1% (**1/2**); ^{128}Te: 31.7%; ^{130}Te: 34%
Nitrogen	^{14}N: 99.6% (**1**); ^{15}N: 0.4% (**1/2**)
Antimony	^{121}Sb: 57.2% (**5/2**); ^{123}Sb: 42.8% (**7/2**)

required, with secondary-ion-mass spectroscopy). In some cases, a quick determination of the isotopic abundances can be obtained with Raman spectroscopy (see Sec. III) or, if the materials are compact, by Archimedian measurement of their density (the volume changes at most by $\lesssim$0.05% with isotopic mass, see Sec. III.B.2). A nuclear resonance fluorescence technique for evaluating the ^{13}C concentration has recently been reported (Beck *et al.*, 1998).

The prices of the elements in Table I with abundances higher than 5% lie between 1000 and 20 000 USD per gram. The amount needed to grow high-quality single crystals depends on the method of growth. Since the amounts required by most of the work discussed here are rather small, typical quantities of material needed are of the order of 1 g. The most economical growth technique is molecular-beam epitaxy. Commercial molecular-beam-epitaxy machines are designed to operate with natural elements as sources. Hence loss of material is not important and the substrate can be placed quite far away from the sources. When using separated isotopes, however, it is convenient to decrease this distance so as to lower the loss of expensive isotopes. With 1 g of isotope it is then possible to grow several tens of samples with thicknesses of the order of 1 μm. When growing bulk crystals with Bridgman (Itoh *et al.*, 1993), Czochralski, or floating-zone (Bulanov, 2000) techniques, it is also important to redesign the growth apparatus so as to be able to use only a few grams of each isotope. The same applies to crystal growth within an ampoule by either sublimation or chemical transport techniques (Debernardi *et al.*, 1997; Serrano, Manjón, *et al.*, 2003).

Semiconductors are often doped, either intentionally or not, and the doping impurities are in many instances dominant factors in the optical spectroscopy of the material. Impurities can introduce electronic levels in the gap (and transitions between these levels) and can localize excitons forming bound excitons. They can also change the phonon spectrum of the material by introducing local vibrational modes, which result in new absorption and Raman transitions. Variations of the isotopic mass of the impurity species will have a strong and direct effect on the frequency of the impurity local vibrational modes and may also have a small effect on the electronic binding energies of impurity levels, as first observed by Dingle (1959) and reviewed by Heine and Henry (1975). The present review deals primarily with isotopic effects related to the host material, and not the impurities.

II. PHONONS

A. Introduction

Lattice vibrations were probably first invoked by Einstein (1907) in order to explain the specific heat of insulators by means of a single quantized (Einstein) oscillator. In order to improve this theory, Nernst and Lindemann (1911) used two single oscillators, thus intro-

ducing a simplified model of the lattice vibrations, which will be very useful here for interpreting the temperature dependence of excitation energies. Debye (1912) introduced the long-wavelength elastic vibrations of the crystal in order to account for the dependence on temperature of the specific heat at low temperatures. The frequency spectrum of the lattice vibrations thus becomes a continuum (in the limit of a very large crystal) contrary to the discrete oscillators introduced by Einstein (1907) and by Nernst and Lindemann (1911). The Debye model led to the famous T^3 dependence of the specific heat at low temperatures. A review of these and more recent developments can be found in Born and Huang (1956) and in Srivastava (1990).

More realistic models involve the introduction of interatomic potentials and their dependence on the atomic coordinates. A power-series expansion around the equilibrium position leads to a quadratic dependence of the interatomic potentials on either atomic coordinates or interatomic distances, the harmonic approximation. Extending this expansion to higher-order terms, usually up to the fourth order, leads to anharmonic effects.

The translational symmetry operations of a perfect crystal (i.e., made out of isotopically pure atoms) imply that the eigenstates of the lattice vibrations must fulfill Bloch's theorem and thus depend on a vector $\boldsymbol{q}$ called a wave vector or crystal momentum (not to be confused with linear momentum). This dependence of the (angular) frequency ω on $\boldsymbol{q}$ gives rise to the dispersion relations $\omega(\boldsymbol{q})$, which can be restricted in $\boldsymbol{q}$ space, without loss of generality, to the first Brillouin zone (BZ). This restriction leads to $3s$ branches of $\omega(\boldsymbol{q})$, where s is the number of atoms in the primitive cell, the smallest possible translational unit that generates the crystal. The first calculation of a realistic and nontrivial dispersion relation was performed by Born and von Kármán (1912).

The total number of states belonging to each branch of the first BZ equals N, where N is the number of primitive cells in the crystal. Another interesting concept is that of the density of phonon states $N_d(\omega)$, which is defined by considering the number of states $N_d d\omega$ that fall within the frequency range ω and $\omega+d\omega$. The density of states can be calculated, usually numerically, from the dispersion relations $\omega(\boldsymbol{q})$. Per unit volume of crystal we find for each branch

$$N_d(\omega) = \frac{1}{8\pi^3} \int \frac{dS_{\boldsymbol{q}}(\omega)}{|\nabla_{\boldsymbol{q}}\omega|}, \tag{2.1}$$

where $dS_{\boldsymbol{q}}(\omega)$ represents an element of surface in $\boldsymbol{q}$ space whose points correspond to frequencies lying between ω and $\omega+d\omega$. Equation (2.1) yields the density of states of a single branch of the dispersion relation. The total density of states is obtained by summing over all $3s$ branches. Since the density of states is proportional to the volume of crystal under consideration, in order to define it uniquely we must choose a specific volume of crystal. The simplest choice is to normalize $N_d(\omega)$ over a primitive cell, which leads to a total number of states $3s$ and the normalization (for the total density of states):

$$\int_0^\infty N_d(\omega) d\omega = 3s. \tag{2.2}$$

The density of states $N_d(\omega)$ can also be generalized to represent its projection $N_d(\omega)$ on each of the atoms of the unit cell. For its evaluation we must then use, per unit volume of crystal and branch j,

$$N_d(\omega, r) = \frac{1}{8\pi^3} \int |\boldsymbol{e}_{r\boldsymbol{q}j}|^2 \frac{dS_{\boldsymbol{q}}(\omega)}{|\Delta_{\boldsymbol{q}}\omega|}, \tag{2.3}$$

where the vector $\boldsymbol{e}_{r\boldsymbol{q}j}$ represents the component of the eigenvector at atom r, corresponding to the BZ point $\boldsymbol{q}$ and branch j, and $\omega_{\boldsymbol{q}j}$ the corresponding frequency [see Eqs. (2.6) and (2.7)]. $\boldsymbol{q}$ must be summed over all N discrete values within the first BZ (N is the number of unit cells per unit volume), whereas j must be summed over all branches of the dispersion relations ($j=1-3s$). The orthonormal eigenvectors are normalized according to

$$\sum_r |\boldsymbol{e}_{r\boldsymbol{q}j}|^2 = 1, \tag{2.4}$$

where $r=1,\ldots,s$ must be summed over the total number of atoms in the unit cell s.

The vibrational frequencies and amplitudes follow from the classical equation of motion, force=mass $\times$acceleration (Menéndez, Page, and Guha, 1994),

$$-\boldsymbol{M}\cdot\boldsymbol{\chi}\omega^2 + \boldsymbol{\Phi}\cdot\boldsymbol{\chi} = 0, \tag{2.5}$$

where $\boldsymbol{M}$ and $\boldsymbol{\Phi}$ are matrices with $3s\times 3s$ rows and columns, representing the three directions of motion of each of the various atoms, and $\boldsymbol{\chi}$ is a vector with similar $3s$ components. The matrix $\boldsymbol{M}$ is diagonal in r and its components are the masses of the s atoms. $\boldsymbol{\Phi}$ is the force constant matrix.

Notice that Eq. (2.5) differs from a standard eigenvalue equation for which $\boldsymbol{M}$ is a multiple of the unit matrix. However, since $\boldsymbol{M}$ is positive definite, Eq. (2.5) can be transformed into a standard eigenvalue equation by multiplying the right- and left-hand side by $\boldsymbol{M}^{-1/2}$ and $\boldsymbol{M}^{+1/2}$, respectively, and introducing $\boldsymbol{M}^{-1/2}\cdot\boldsymbol{M}^{+1/2}=\boldsymbol{1}$ between $\boldsymbol{M}$ and both $\boldsymbol{\Phi}$ and $\boldsymbol{\chi}$. We thus find

$$-\boldsymbol{e}\omega^2 + \boldsymbol{D}\cdot\boldsymbol{e} = 0, \tag{2.6}$$

where

$$\boldsymbol{D} = \boldsymbol{M}^{-1/2}\boldsymbol{\chi}\boldsymbol{M}^{-1/2},$$

$$\boldsymbol{e} = \boldsymbol{M}^{1/2}\boldsymbol{\chi}. \tag{2.7}$$

$\boldsymbol{D}$ is the so-called dynamical matrix and $\boldsymbol{e}$ is the eigenvector (with $3s$ components), which we take to be normalized according to Eq. (2.4). When handling lattice vibrational problems we must always keep in mind the difference between $\boldsymbol{\chi}(\omega)$, which represents atomic displacements, and $\boldsymbol{e}(\omega)$, which represents the orthonormal set of $3r$ eigenvectors of Eq. (2.6).

Diagonalization of Eq. (2.6) leads to the $3r$ eigenfrequencies $\omega(\boldsymbol{q}j)$ and the corresponding eigenvectors $\boldsymbol{e}_{r\boldsymbol{q}j}$, with a total of $3s\times 3s$ components for each value of $\boldsymbol{q}$

and j. The problem is then reduced to that of $3s$ decoupled harmonic oscillators per primitive cell (hence the name harmonic for the approximation used, in which the force matrix $\mathbf{\Phi}$ is independent of the atomic displacement). Each of these oscillators can be quantized by using second quantization techniques, i.e., introducing creation ($a^{\dagger}_{\boldsymbol{q}j}$) and annihilation ($a_{\boldsymbol{q}j}$) operators. We thus find for each oscillator, labeled by $\boldsymbol{q}$ and j, the Hamiltonian (Srivastava, 1990)

$$H_{\boldsymbol{q}j} = \hbar\omega_{\boldsymbol{q}j}\left(a^{\dagger}_{\boldsymbol{q}j}a_{\boldsymbol{q}j} + \frac{1}{2}\right). \tag{2.8}$$

The ensemble average of Eq. (2.8) at temperature T gives the average thermal energy

$$\langle\hbar\omega_{\boldsymbol{q}j}\rangle = \frac{1}{2}\hbar\omega_{\boldsymbol{q}j}(2n_B + 1), \tag{2.9}$$

with the Bose-Einstein factor n_B,

$$n_B(\omega_{\boldsymbol{q}j}) = [e^{\hbar\omega_{\boldsymbol{q}j}/kT} - 1]^{-1}. \tag{2.10}$$

Equation (2.10) indicates that each oscillator has an average energy $\frac{1}{2}\hbar\omega_{\boldsymbol{q}j}$ at $T=0$ for each atom, the zero-point energy. This energy corresponds to a finite average vibrational amplitude at $T=0$, the zero-point amplitude, given by

$$\langle u^2_{\boldsymbol{q}j}\rangle_r = \frac{\hbar}{2M_r\omega N}|\boldsymbol{e}_{\boldsymbol{q}jr}|^2, \tag{2.11}$$

where N is the total number of primitive cells in the sample under consideration. For a finite temperature T, Eq. (2.11) must be multiplied by $2n_B+1$. In the limit of $T\to\infty$ (temperatures higher than the average Debye temperature of the crystal), $n_B\to kT/\hbar\omega$. In this limit, the average squared vibrational amplitude of any of the atoms, and also the total vibrational energy, are proportional to T.

We consider next the simplest possible case of a monatomic crystal (e.g., diamond). In this case the low-temperature vibrational amplitude (2.11) and also the vibrational energy are inversely proportional to $M^{1/2}$. At high temperatures, however, the dependence on mass disappears because of the proportionality of n_B to $kT/\hbar\omega$ and the fact that $\omega\propto M^{-1/2}$. This confirms that the zero-point vibrational amplitude is a true quantum effect. It vanishes for $M\to\infty$ and also for finite M at high temperatures. The zero-point properties can thus be modified by changing the isotopic mass, a fact that is the basis of most of the work discussed in this review. Hence if we want to observe isotopic effects, we must work at low temperatures, which means at temperatures well below the Debye temperature of the crystal T_D. For diamond, $T_D\approx 2200$ K (Debye, 1912) and isotopic mass effects become fully observable even at room temperature. For germanium $T_D=370$ K and for silicon $T_D=640$ K and quantum effects are small, but nonnegligible, at room temperature. However, they reach magnitudes close to their maximum already at 100 K (Sozontov *et al.*, 2001).

B. Force constants, dynamical matrix

In Eqs. (2.5) and (2.6) we have introduced the concepts of the force constant matrix and the dynamical matrix. The corresponding matrix elements have been treated, until recently, as adjustable parameters determined by fitting the dispersion relations measured by means of inelastic neutron scattering (Brockhouse and Iyengar, 1958).

The set of parameters to be fitted is not uniquely determined. It is usually specified within one of a number of more or less physical models. The simplest is the springs-and-balls or Born–von Kármán model (Born and von Kármán, 1912; Srivastava, 1990) in which the ions are assumed to be rigid with springs which determine the force constants connecting them. Springs connecting nearest neighbors as well as farther ones can be considered. As shown by Brockhouse and Iyengar (1958), the fit of the first- and second-neighbor Born–von Kármán model to the measured dispersion relations of germanium is rather poor. In particular, it cannot represent the very flat dispersion of the lowest transverse-acoustic modes of the group-IV semiconductors, which requires up to fifth-neighbor force constants for a reasonable fit (Herman, 1959).

The realization that long-range forces are important even in nonpolar crystals suggested models in which electron coordinates are introduced in a phenomenological way, e.g., as spherical shells surrounding the otherwise rigid ions. This led to the shell models, which require a large number of parameters in order to describe the measured dispersion relations of the covalent semiconductors (Waugh and Dolling, 1963). For covalent semiconductors, the most successful phenomenological force-constant model has been the bond-charge model introduced by Weber (1977). In this model shells are replaced by bond charges placed, in equilibrium, midpoint between nearest-neighbor atoms so as to simulate the covalent bonds. The additional electronic coordinates are eliminated by the condition of adiabaticity, which follows from the fact that the electronic mass is much smaller than the ionic mass. We show in Fig. 1 the dispersion relations of germanium measured by inelastic neutron scattering (Nilsson and Nelin, 1971; Nelin and Nilsson, 1972) together with a fit to Weber's bond-charge model (Weber, 1977) with four adjustable parameters. Although the fit is not perfect [see, e.g., the transverse-optical (TO) modes at the X point of the BZ], the very flat measured transverse-acoustic bands near the X_3 and L_3 points are represented rather well by the model.

As a by-product of a fit to measured dispersion relations, a set of eigenvectors is obtained. One must keep in mind, however, that at a given point of the BZ there are $3s$ (six for diamond) values of the frequency but $3s\times 3s$ eigenvector components (36 for diamond). Hence a good fit to the six frequencies does not guarantee the correctness of the corresponding calculated eigenvectors, which, ideally, should be measured directly. Measurements of eigenvectors over the whole BZ by inelastic neutron scattering require careful determination of

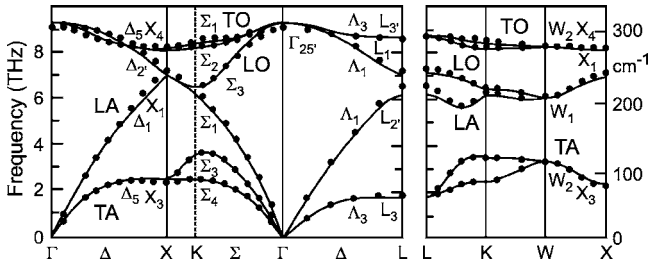

FIG. 1. Phonon dispersion relations of natural Ge. The solid lines show the adiabatic bond-charge-model calculations of Weber (1977), the dots the experimental values from neutron scattering (Nilsson and Nelin, 1971; Nelin and Nilsson, 1972). The frequency scale is in THz. For convenience we have given the equivalent scale in cm^{-1} on the vertical axis at the right.

the relative intensities of all scattering peaks and has only been performed in a limited number of cases (Strauch and Dorner, 1986; Strauch, Mayer, and Dorner, 1990). Eigenvectors at some special points of the BZ can also be determined by measuring the frequency shifts induced by isotopic substitution (Zhang *et al.*, 1996, 1997). This will be discussed in Sec. III.B.5.

C. *Ab initio* calculations

It follows from the Born-Oppenheimer approximation (Born and Huang, 1956) that the interatomic force constants, i.e., the matrix elements of the dynamical matrix, can be obtained by taking the second derivatives of the total energy (including electron-electron, electron-ion, and ion-ion interactions) with respect to the atomic displacements. This is, in general, a rather formidable undertaking. Such calculation requires an accurate theoretical description of the occupied electronic states of the crystal, their mutual interactions, their interactions with the constituent ions, and derivatives of these states with respect to the nuclear positions.[2] The most difficult part of this problem is the many-body aspect of the electron-electron interaction. When treated in a one-body mean-field framework, the electron-electron interaction can be split into a Hartree and a Fock (exchange) term. The solution of the corresponding quantum-mechanical problem, including these many-body effects, can be simplified considerably using the density-functional theorem (Hohenberg and Kohn, 1964; Kohn and Sham, 1965), which states that the electron-electron interaction can be described as a functional of the density of occupied electrons and does not require the details of the individual complex wave functions. This functional has three terms, the straightforward Hartree term representing the Coulomb interaction between the electronic charges, the exchange term, and a correlation correction to the Hartree term. The exchange and correlation functionals, are, in principle, not known. They are often approximated by the local electron-density functional, an algebraic function of the local density that corresponds to the exchange and correlation terms in a uniform electron gas (Kohn and Sham, 1965).

Once the electronic charge density is known, e.g., by means of a calculation using the local-density approximation to the exchange and correlation potentials, plus the kinetic-energy functional for noninteracting electrons, the force induced on an ion by its displacement can be obtained with the Hellmann-Feynman theorem. This theorem states that such force is produced by the interaction of the moving ion with all other ionic charges plus its interaction with the unperturbed electronic charge density. The calculation of the electronic charge density requires, within the local-density approximation, the solution of a set of Schrödinger-like differential equations, coupled through the Hartree and local-density-approximation potentials. These solutions are expressed as linear combinations of a set of orthornormal functions. Lack of completeness can lead to considerable errors in the Hellmann-Feynman forces, which have been discussed by Srivastava (1990) and Baroni *et al.* (2001).

An early road map for the calculation of phonon dispersion relations was given by Sham (1974). It is based on the concept of polarizability $\tilde{\chi}_0$, which gives the charge density induced in a crystal by a small change in the total crystal potential. The change induced by an ionic motion is actually that induced by the change in the potential of the moving ion plus that which corresponds to the self-consistent charge in the electronic potential. In order to determine the density response function we must thus calculate the susceptibility and invert the corresponding self-consistency equation, which means that one must perform an inversion of the dielectric matrix.

Such inversion is possible when local potentials are used, as was suggested by Martin (1969) in connection with phonon calculations. He also implemented in this manner a calculation of the dispersion relations of silicon. This calculation, however, led to dispersion curves that differ considerably from those measured by inelastic neutron scattering (especially for the transverse-acoustic modes).

The dielectric screening method has given way to more accurate techniques, especially after the introduction of nonlocal pseudopotentials together with local-density-approximation functionals. This method leads to rather accurate calculations of total energies, lattice constants, elastic constants, and other macroscopic properties of semiconductors. The calculation of dynamical matrices is most easily implemented by using density-functional perturbation theory (Baroni, de Gironcoli, and dal Corso, 2001). Excellent agreement between calculated dispersion relations and those measured by inelastic neutron scattering has been achieved for Si, Ge, and a few III-V compounds by Giannozzi *et al.* (1991).

Density-functional perturbation theory has also been used in connection with other types of electronic band-

[2]In a realistic calculation the occupied electronic states are usually divided into two groups: valence electrons and core electrons. The ionic potential is that of the atomic core screened by valence electrons.

structure calculations such as the linear muffin-tin orbital method (for silicon, see Savrasov, 1996) and the linearized augmented plane-wave method (Wang, Yu, and Krakauer, 1994). The latter method was applied to CuCl, a zinc-blende-structure semiconductor with interesting anharmonic effects which will be discussed in Sec. III.B.3. The valence bands of this material, such as those of the other cuprous halides, CuBr and CuI, show strong hybridization of the standard p valence electrons of the halogen with the $3d$ electrons of the copper. The latter are difficult to treat with plane-wave pseudopotential techniques. The linearized augmented plane-wave method, in which the electron orbitals near the core are chosen to be atomiclike, is ideally suited to handle these materials.

A problem that will also be of interest in connection with isotopic substitution is that of the transferability of force constants from one compound (e.g., GaAs) to a similar one (AlAs). The interest lies in the fact that for GaAs there are excellent inelastic neutron-scattering data (Strauch and Dorner, 1986), whereas for AlAs no such data are available (because of the unavailability of large single crystals). It is therefore tempting to generate the dispersion relations of AlAs from those of GaAs by taking the same force constants and simply changing the masses in the corresponding dynamical matrix [Eq. (2.7)]. This is the basis of the mass approximation. Because of the lack of experimental data, the density-functional perturbation-theory calculations for GaAs and AlAs have been used to check the adequacy of this approximation (Giannozzi *et al.*, 1991). It was found that the anion mass substitution, applied to the calculated dynamical matrix of GaAs, reproduces rather well the directly calculated dispersion relations of AlAs. It is worth noting, however, that such an agreement is not necessarily obtained if the mass approximation is applied to the usual six-parameter bond-charge model of GaAs. A set of bond-charge-model parameters fitted not only to phonon frequencies but to their eigenvectors, however, restores the validity of the mass approximation (Colombo and Gianozzi, 1995; Baroni *et al.*, 2001).

The mass approximation will implicitly be used in Sec. IV.B to treat the effect of isotopic substitution. In this case, however, the transferability of the force constants is to be regarded as very accurate since the band structure is altered little by isotopic substitution. We shall see in Sec. V that the isotopic substitution effects on the electronic states amount to a few meV, except for materials with atoms in the first row of the periodic table where they can be an order of magnitude larger (Manjón *et al.*, 2003).

Before closing this section, we would like to mention another *ab initio* method for calculating force constants and phonon eigenvectors, namely, the frozen-phonon technique. In this conceptually simple but somewhat limited method, the total energy is calculated for the unperturbed crystal and for a crystal with a small phononlike displacement as a perturbation. The second-order terms in the expansion of the energy versus displacement correspond to force constants. This method is particularly useful if one has a computer code for the calculation of the total energy in a crystal with a given translational lattice. The force constants are obtained directly from this code provided one considers only phonons at the center of the BZ (Γ point). It is, however, possible to extend the method to other high-symmetry points by increasing the size of the primitive cell and bringing the corresponding $\boldsymbol{q}$ point to the center of the BZ. This increases the complexity of the method while limiting the usefulness to only a few points in the BZ. For early application of frozen-phonon methods to semiconductors, see Kunc and Martin (1982) and Yin and Cohen (1982).

In Sec. III we shall not only make use of the dispersion relations, densities of states, and eigenvectors of phonons, but also of their anharmonic properties. Such properties are related to terms of third and fourth order in the expansion of the total energy versus phonon displacements. Partial information about these terms can be obtained by frozen-phonon methods (Vanderbilt *et al.*, 1984).

We close this section by mentioning that Baroni *et al.* (2001) have made available an open source code for density-functional-theory–density-functional perturbation-theory pseudopotentional calculations at http://www.pwscf.org. Another such code is described by Gonze *et al.* (2002) and can be found at http://www.abinit.org.

III. PHONON EFFECTS RELATED TO AVERAGE ISOTOPIC MASSES

A. Introduction

The vast majority of isotope effects in semiconductors arise from the dependence of phonon frequencies and eigenvectors, as well as their lifetimes, on isotopic masses.[3]

These phonon parameters depend on isotopic mass in a way that can usually be described by the mass approximation (Sec. II.C), which implies that the force constants do not depend on isotopic mass. This assumption does not necessarily hold when substituting an atom by a different one (e.g., Ge by Si, Buchenauer *et al.*, 1971, or Ga by Al, Baroni *et al.*, 2001).

The mass effects on the phonons can be divided into two categories:

(a) Effects of the average mass, which correspond to the virtual-crystal approximation when more than one isotope of a given atom is present.

(b) Effects of the mass fluctuations in materials with a mixture of several isotopes of a given atom.

The average virtual-crystal approximation is introduced in a crystal with several isotopes in order to recover the translational invariance lifted by the isotopic

[3]For effects of the nuclear magnetic moment, see Sec. IV.D.

disorder (most natural crystals fall into this category, see Table I). For this purpose, the masses of these isotopes are replaced in the dynamical matrix, Eq. (2.7), by their average, weighted by the corresponding isotopic abundances.[4] The site-dependent difference between the actual isotopic masses and their average, which lifts translational invariance, is then treated as a perturbation.

The use of the virtual-crystal approximation for the unperturbed crystal leads to a vanishing of the first-order perturbation of the mass fluctuations because the average mass fluctuation, defined as

$$g_1 = \sum_i c_i \frac{\langle M\rangle - M_i}{\langle M\rangle}, \tag{3.1}$$

with $\langle M\rangle = \Sigma c_i M_i$, vanishes [in Eq. (3.1) c_i represents the abundance of isotope i]. Terms of higher order in perturbation theory do not vanish, and will be discussed below (Tamura, 1983; Widulle *et al.*, 2001).

For a monatomic crystal, the virtual-crystal approximation results in a proportionality of any of the phonon frequencies to $\langle M\rangle^{-1/2}$ since the force constants do not depend on $\langle M\rangle$. In a crystal with different elements in the primitive cell, each element acts differently on the virtual-crystal-approximation frequency. The effects of the changes in the average mass at r, induced by the isotopic substitution, must be weighted by the corresponding eigenvector components (Menéndez, Page, and Guha, 1994). This fact provides a method for determining eigenvectors if samples of different isotopic compositions are available (Zhang *et al.*, 1997; see also Sec. III.B.5).

The effects of the average isotopic mass just mentioned are the simplest isotopic effects possible since they appear in the harmonic approximation. They also result in a dependence of the specific heat on isotopic mass below the Debye temperature T_D because of the proportionality of T_D to $\langle M\rangle^{-1/2}$ (Plekhanov, 2001; Schnelle and Gmelin, 2001). Other effects of $\langle M\rangle$ are related to the anharmonic terms in the interatomic potentials. The simplest of these effects corresponds to the thermal expansion, which vanishes in the harmonic approximation where the average positions of the atoms are independent of temperature (London, 1958; Buschert *et al.*, 1988; Sozontov *et al.*, 2001). Third-order anharmonic terms are responsible for the thermal expansion. These terms are proportional to the square of the vibrational amplitudes, which for a monatomic crystal is proportional to $\langle M\rangle^{-1/2}$ (Barron and Klein, 1974).

Most of the extant work on the dependence of anharmonic effects on the average mass is concerned with phonon frequencies and linewidths (Cardona and Ruf, 2001; Widulle *et al.*, 2001, 2002; Serrano, Widulle, *et al.*, 2003). The linewidths (and the corresponding lifetimes) at low temperatures are also governed by anharmonic decay processes, which for monatomic crystals result in linewidths proportional to $\langle M\rangle^{-1}$ (Widulle *et al.*, 2001). These linewidths can be regarded as the imaginary part of an anharmonic self-energy whose real part results in frequency shifts with respect to the predictions of harmonic calculations (Widulle *et al.*, 2001; Sanati and Estreicher, 2003).

Among the effects of isotopic mass fluctuations we mention first what is probably the largest of such effects, namely, the effect on the thermal conductivity (Wei *et al.*, 1993; Asen-Palmer *et al.*, 1997; Ruf, Henn, *et al.*, 2000).

Smaller, but important effects have been observed in the phonon linewidths (Cardona and Ruf, 2001). Frequency shifts related to the real part of the corresponding self-energy have also been reported (Hass *et al.*, 1992; Widulle *et al.*, 2001). The partial breakdown in translational invariance effected by the isotopic disorder results in a partial lifting of $\boldsymbol{q}$ conservation. Correspondingly, not only phonons at $\boldsymbol{q}=\boldsymbol{0}$ can be excited with optical spectroscopy (Raman as well as IR). Therefore the optical spectra of samples with isotopic disorder include a weak component that mimics the density of phonon states (Fuchs *et al.*, 1993). Brillouin as well as two-phonon scattering and absorption measurements have also been performed for isotopically controlled diamonds (Vogelgesang *et al.*, 1996, 1998).

B. Effects of the average isotopic masses on lattice properties

1. Dependence of the specific heat C_p on isotopic mass

Measurements of C_p have been performed for germanium with three different average isotopic masses ($\langle \boldsymbol{M}\rangle = 70.01$, 72.71, and 73.12; Schnelle and Gmelin, 2001). At low temperatures ($T \ll T_D \simeq 360$ K) C_p is expected to be proportional to T_D^{-3} for a given T, i.e.,

$$C_p = AM^{3/2}T^3. \tag{3.2}$$

The T^3 dependence of Eq. (3.2) is only valid for $T < 6$ K, a region that corresponds to $T_D \simeq 360$ K. For $T > 6$ K one has to increase A in Eq. (3.2). This fact is due to the strong nonlinearity of the dispersion relations of the transverse-acoustic phonons (see Fig. 1) represented with a temperature dependent T_D reaching a minimum $T_D(\min) \simeq 260$ K at $T(\min) \simeq 22$ K. This effective Debye temperature corresponds to an average phonon frequency and is thus also expected to be proportional to $\langle M\rangle^{-1/2}$. Thus the specific heat at $T(\min)$ should be proportional to $\langle M\rangle^{3/2}$. The change in $\langle M\rangle^{3/2}$ between $\langle M\rangle = 70.02$ and 73.12 is 4.27%, the corresponding change in $C_p(T_D(\min))$ should then be 6.4%. The measured change is 6.3%, in agreement with the prediction from the change in $\langle M\rangle$. Because of the strong dependence of A on T, the most accurate measurement of the dependence of C_p on M is that performed at $T(\min)$. At higher temperatures C_p must tend to a constant value, indepen-

[4]Note that according to Eq. (2.7) one should average the inverse isotopic masses. However, because of the small spread in those masses (Table I), averaging $\boldsymbol{M}^{-1}$ is nearly equivalent to averaging $\boldsymbol{M}$.

dent of $\langle M\rangle$, dictated by the Dulong and Petit law. The temperature dependence of C_p is indeed found to decrease above T(min) and at 100 K is no longer observable (see Fig. 2 of Schnelle and Gmelin, 2001). *Ab initio* calculations of the dependence of $C_p(T)$ on isotopic mass have been recently published (Sanati, Estreicher, and Cardona, 2004). Measurements for diamond and silicon have also been recently performed (Cardona *et al.*, 2005; Gibin *et al.*, 2005).

2. Effects of isotopic masses on lattice parameters: Thermal expansion

The effect of lattice vibrations on the lattice parameter a_0 of a cubic crystal can be expressed in terms of the mode Grüneisen parameters $\gamma_{\boldsymbol{q}j}$ as (Pavone and Baroni, 1994; Debernardi *et al.*, 1996)

$$\frac{\Delta a_0}{a_0} = \frac{\hbar}{3BV}\sum_{\boldsymbol{q}j} \gamma_{\boldsymbol{q}j}\omega_{\boldsymbol{q}j}\left[n_B(\omega_{\boldsymbol{q}j}) + \frac{1}{2}\right], \tag{3.3}$$

where V is the volume of the crystal, B its bulk modulus, and $\gamma_{\boldsymbol{q}j}$ is defined as

$$\gamma_{\boldsymbol{q}j} = -\frac{\partial \ell n \omega_{\boldsymbol{q}j}}{\partial \ell n V}. \tag{3.4}$$

At high temperatures ($T > T_D$) $n_B \to kT/\hbar\omega$ and the thermal expansion is proportional to T:

$$\frac{\Delta a_0}{a_0} \to \frac{2kT}{BV_c}\langle\gamma_{\boldsymbol{q}j}\rangle, \tag{3.5}$$

where V_c is the volume of the primitive cell and $\langle\gamma_{\boldsymbol{q}j}\rangle$ the average of $\gamma_{\boldsymbol{q}j}$ over all branches of the Brillouin zone. We have implicitly assumed a crystal with two atoms per primitive cell. The linear dependence on T found experimentally at high T extrapolates for $T \to 0$ to the bare value of $\Delta a_0/a_0$. This extrapolation enables us to estimate the renormalization of $\Delta a_0/a_0$ due to zero-point vibrations:

$$\left(\frac{\Delta a_0}{a_0}\right)_{T=0} = \frac{\hbar}{BV_c}\langle\gamma_{\boldsymbol{q}j}\omega_{\boldsymbol{q}j}\rangle \simeq \frac{\hbar}{BV_c}\langle\omega_{\boldsymbol{q}j}\rangle\langle\gamma_{\boldsymbol{q}j}\rangle. \tag{3.6}$$

Note that the average of $\gamma_{\boldsymbol{q}j}$ that appears in Eq. (3.6) may differ somewhat from that in Eq. (3.5).

The use of Eqs. (3.5) and (3.6) for estimating the zero-point renormalization of $\Delta a_0/a_0$ is illustrated in Fig. 2 for the case of silicon. The renormalization turns out to be $\Delta a_0/a_0 = 1.9\times10^{-3}$. The procedure illustrated above will also be very useful for the determination of zero-point renormalization for other physical properties, including the elastic constants (Cardona, 2001a, 2001b), phonon frequencies, and electronic energy-band states (Secs. III.B.3 and V). It may seem surprising that such a construction should enable us to obtain bare quantities from measured experimental data since bare parameters are basically not observable. The clue to this philosophical question was given by Allen (1994). The bare quantities determined by the linear extrapolation procedure (and also the isotopic mass substitution method to be described next) are not exact. The procedure is based on the treatment of the anharmonic interactions by perturbation theory, keeping only second-order terms proportional to $\langle u^2\rangle$ ($\sim T$ at high T). Higher-order terms would lead to higher powers of T which are not included in the linear extrapolation procedure.

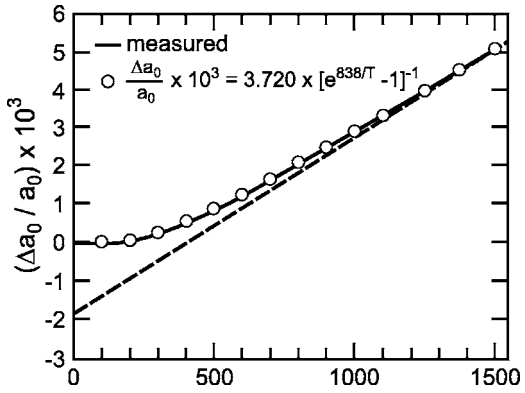

FIG. 2. Dependence on temperature of the linear expansion of silicon $\Delta a_0/a_0$. The solid curve represents x-ray data. The points are a fit to these data using the single-oscillator frequency as given (with T in K). The dashed line extrapolated to $T=0$ determines the zero-point renormalization of $\Delta a_0/a_0$. From Cardona, 2001b.

Equation (3.6) provides another way to determine zero-point renormalizations in monatomic crystals. For these crystals this equation can be written as

$$\left(\frac{\Delta a_0}{a_0}\right)_{T=0} = C\langle\omega_{\boldsymbol{q}j}\rangle = D\langle M\rangle^{-1/2}. \tag{3.7}$$

The determination of a_0 for two values of $\langle M\rangle$ thus allows us to determine D and, correspondingly, the zero-point renormalization for any values of $\langle M\rangle$. Measurements of $(\Delta a_0/a_0)_{T\simeq0}$ for several values of the average isotopic mass $(\Delta a_0/a_0)_{T\simeq0}$ have been performed for diamond (Holloway *et al.*, 1991), germanium (Buschert *et al.*, 1988; Sozontov *et al.*, 2001; Hu *et al.*, 2003; and Cardona, 2005, see Fig. 4), and silicon (Sozontov *et al.*, 2001). The following values of $(\Delta a_0/a_0)_{T=0}$ for a change of 1 amu in $\langle\Delta M\rangle$ have been reported: 7.5×10^{-5} for diamond, 3×10^{-5} for Si, and 8.8×10^{-6} for Ge. These values correspond, according to Eq. (3.7), to zero-point renormalizations of $(\Delta a_0/a_0)_{T=0}$ equal to -3.9×10^{-3} for diamond, -1.7×10^{-3} for Si, and -1.3×10^{-3} for Ge. These values are in good agreement with the values obtained with the linear extrapolation method: -3.7×10^{-3} for diamond (from Reeber and Wang, 1996), -1.9×10^{-3} for Si (see Fig. 2), and -1.2×10^{-3} for Ge (from Singh, 1968).

Another prescription for estimating the zero-point renormalization is based on Eqs. (3.5) and (3.6). The zero-point renormalization can be obtained from the asymptotic (high T) slope of $\Delta a_0/a_0$ versus T provided one knows the approximate average frequency $\langle\omega_{\boldsymbol{q}j}\rangle$. The latter can be obtained from a single-oscillator fit to $\Delta a_0/a_0$ versus T using Eq. (3.3). This fit has been performed for diamond (Cardona, 2001a) and Si (Cardona, 2001b). The values of the $\Delta a_0/a_0$ renormalization at T

$=0$ obtained with this procedure for diamond and Si are -3.9×10^{-3} and -2.0×10^{-3}, respectively. Using the slope found in the article by Singh (1968), we obtained for Ge $(\Delta a_0/a_0)_T=-1.8\times10^{-3}$.

One may at this point wonder why a single oscillator gives such an excellent fit to the data for Si (Fig. 2) and to those for diamond (Fig. 3 of Cardona, 2001a) without taking into account the Debye spectrum which represents the low-frequency acoustic phonons. Using the Debye spectrum we obtain from Eq. (3.3) the following temperature behavior for $\Delta a_0/a_0$ at low T:

$$\frac{\Delta a_0}{a_0} \propto \int_0^{T_D} \langle \gamma_{\boldsymbol{q}j} \rangle_\omega \omega^3 \left[\frac{1}{e^{\hbar\omega/kT}-1} + \frac{1}{2} \right] d\omega, \tag{3.8}$$

where $\langle \gamma_{\boldsymbol{q}j} \rangle$ is the average of $\gamma_{\boldsymbol{q}j}$ over a $\boldsymbol{q}$-space surface of constant frequency ω. If we assume that this average is independent of ω, we can take it out of the integral sign and Eq. (3.8) becomes proportional to T^4 at low T, and equivalent to that which represents the thermal energy in the Debye model. However, the assumption that $\langle \gamma_{\boldsymbol{q}j} \rangle_\omega$ is independent of ω is actually incorrect. It is well known that $\langle \gamma_{\boldsymbol{q}j} \rangle_\omega$ reverses sign twice at low T for most tetrahedral semiconductors and thus never reaches very high values in this region (Bienenstock, 1964; Debernardi and Cardona, 1996). This may explain the failure to observe a Debye term in $\Delta a_0/a_0$ at low temperatures.

The discussion above applies to monatomic crystals. Note, however, that Eq. (3.3) also applies to cubic crystals containing different elements.[5] In the case of polyatomic crystals, however, isotopic substitution will produce different effects on a_0 depending on which element is being substituted. Such different effects have not yet been observed experimentally. Calculations involving GaAs and ZnSe have, however, appeared. They are based on the equation

$$\frac{1}{a_0}\frac{\partial a_0}{\partial M_r} = -\frac{\hbar}{6B_0}\sum_{\boldsymbol{q}j} \frac{\partial^2 \omega(\boldsymbol{q}j)}{\partial V \partial M_r}. \tag{3.9}$$

An evaluation with Eq. (3.9) of the effects of changing either the cation or the anion mass of ZnSe and GaAs on the lattice parameter a_0 was given by Debernardi *et al.* (1996) and Garro *et al.* (1996).

We conclude this section by mentioning that the harmonic lattice dynamics of a crystal can be calculated for lattice parameters which include the temperature- and mass-dependent renormalization just discussed. This is the quasiharmonic approximation. It yields a contribution to the temperature- and mass-dependent shift of the phonon frequencies which must be included in the effects and discussed in Sec. III.B.3.

[5]The theory of $\Delta a_0/a_0$ for noncubic crystals can be found in Barron and Klein, 1974.

3. Anharmonic effects on phonon frequencies and linewidths

In the harmonic approximation the frequency is a well-defined function of $\boldsymbol{q}$ for each phonon branch. Anharmonic effects, and also isotopic mass fluctuations (see Sec. IV.B), replace this sharp dependence of ω on $\boldsymbol{q}$ by a spectral function, usually a Lorentzian function of ω centered at $\tilde{\omega}_{\boldsymbol{q}j}$. The Lorentzian has a full width at half maximum (FWHM) $\Gamma_{\boldsymbol{q}j}$ and is shifted slightly, by an amount $\Delta_{\boldsymbol{q}j}$, with respect to its harmonic value ($\tilde{\omega}_{\boldsymbol{q}j} = \omega_{\boldsymbol{q}j}+\Delta_{\boldsymbol{q}j}$). It would be very interesting to determine $\Gamma_{\boldsymbol{q}j}$ and $\Delta_{\boldsymbol{q}j}$, and their dependence on T and isotopic composition, for all $\boldsymbol{q}$ points and branches of the BZ. Unfortunately, the standard inelastic neutron-scattering techniques usually do not have enough resolution to perform this job, nor does the recently developed technique of x-ray Raman scattering with synchrotron radiation (Ruf *et al.*, 2001a). Nevertheless, some BZ points have been investigated for germanium (Fuchs *et al.*, 1993; Göbel, Wang, *et al.*, 1998) and for diamond (Ruf *et al.*, 2001b). Measurements of phonon frequencies versus T at several points of the BZ have been performed by Nelin and Nilsson (1974). More recently, very accurate investigations of Γ and Δ have been performed for the phonons at the X point of Ge (Kulda *et al.*, 2003) using neutron spin echoes.

In spite of its limited applicability to inelastic neutron-scattering measurements, isotopic substitution has been very useful for measuring phonon dispersion relations in crystals that contain natural isotopes that are strong neutron absorbers. The most conspicuous case is cadmium compounds that contain ^{113}Cd, one of the strongest absorbers of slow neutrons. Inelastic neutron-scattering measurements have been performed for ^{114}CdTe (zinc-blende structure) by Rowe *et al.* (1974) and for ^{114}CdS by Debernardi *et al.* (1997). We show in Fig. 3 the experimental points for $\omega_{\boldsymbol{q}j}$ obtained for ^{114}CdS, the prototype of the wurtzite-type materials, together with the dispersion relations calculated *ab initio*.

The main mechanism that determines $\Gamma_{\boldsymbol{q}j}$, and the corresponding lifetimes, is decay into two phonons with energy and wave-vector conservation. The lifetime is related to Γ through

$$\tau_{\boldsymbol{q}j} \simeq \Gamma_{\boldsymbol{q}j}^{-1}, \tag{3.10}$$

where τ is given in seconds and Γ in units of angular frequency, i.e., rad/sec. We shall confine most of our discussion to phonons at $\boldsymbol{q}=\boldsymbol{0}$ (Γ point, center of the BZ) since these are the ones that can be easily investigated by Raman spectroscopy.

The anharmonic decay of one phonon into two is represented, to lowest order in anharmonicity, by the Feynman diagram of Fig. 4(a). We have assumed, for simplicity, that for the $\boldsymbol{q}j$ decaying phonon $\boldsymbol{q}$ is at the center of the BZ. Thus for the two phonons into which it decays we have

$$\omega_{0j} = \omega_{\boldsymbol{q}_1 j_1} + \omega_{-\boldsymbol{q}_1 j_2}. \tag{3.11}$$

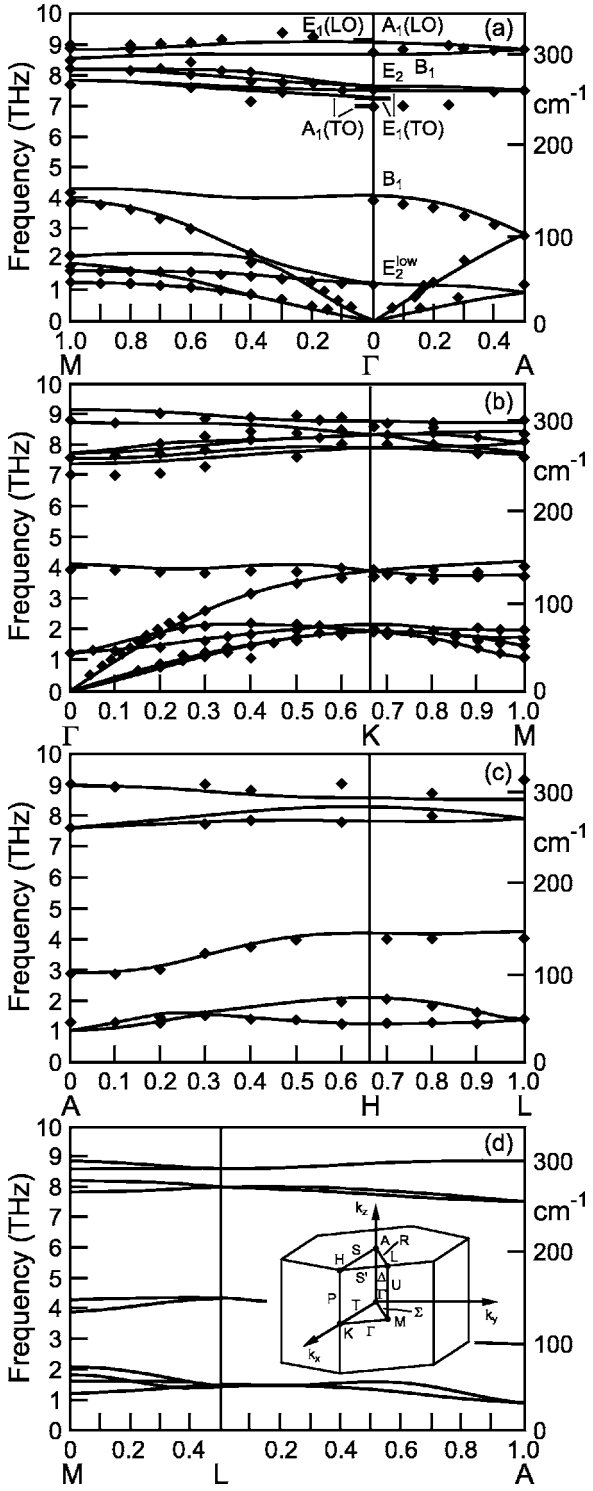

FIG. 3. Phonon dispersion of wurtzite-type CdS along different high-symmetry directions in the Brillouin zone: (a) M-Γ-A, (b) Γ-K-M, (c) A-H-L, and (d) M-L-A. The symbols represent the measured phonon frequencies; the solid curves correspond to the *ab initio* calculation. The irreducible representations of the modes at the Γ point are given in (a). The horizontal bars in (a) denote zone-center phonon frequencies from Raman spectroscopy. The inset in (d) shows the Brillouin zone and indicates the choice of axes and the notation of high-symmetry points and lines used in the text. The distances between some points are $\overline{\Gamma K}=4\pi/3a$ (along k_z), $\overline{\Gamma K}=2\pi/3^{1/2}a$ (along k_z), and $\overline{\Gamma K}=2\pi/c$. From Debernardi *et al.*, 1997.

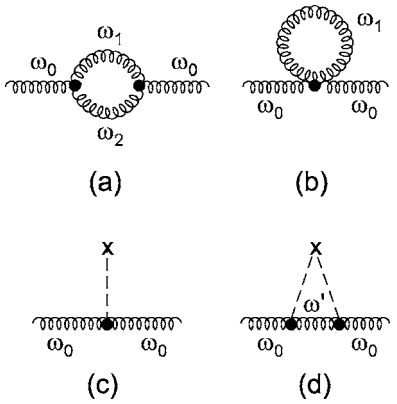

FIG. 4. (a) Feynman diagram that represents the third-order anharmonic self-energy for a phonon of frequency ω_0. (b) Diagram representing the fourth-order anharmonic correction to the frequency ω_0. (c) First-order correction due to a mass difference at a given site. This term vanishes in the virtual-crystal approximation. (d) Self-energy diagram corresponding to scattering of a phonon with frequency ω_0 to an intermediate frequency ω' by a mass defect.

This is the only third-order anharmonic process that is possible at $T=0$. At finite temperature some phonons are already excited and it is possible to create a phonon while destroying another one already present:

$$\omega_{0j} = \omega_{\boldsymbol{q}_1 j_1} - \omega_{\boldsymbol{q}_1 j_2}. \tag{3.12}$$

The processes (3.11) are called down-conversion or sum processes whereas those that correspond to Eq. (3.12) are called up-conversion or difference processes. Since they only appear at relatively high temperatures, the latter do not play an important role when considering isotope effects.

The evaluation of diagram 4(a) leads to a complex quantity called the anharmonic self-energy $\Sigma=\Sigma_r+i\Sigma_i$, which is, in principle, frequency dependent. The spectral function, a delta function of ω in the harmonic approximation for an isotopically pure crystal, can be written as

$$A_{0j}(\omega) = \frac{1}{\pi}\frac{\Gamma/2}{[\omega-\omega_{0j}-\Delta]^2+(\Gamma/2)^2}, \tag{3.13}$$

where $\Gamma/2=-\Sigma_i$ and $\Delta=\Sigma_r$ (note that Σ_i is defined as negative). In Eq. (3.13) we have implicitly assumed that Δ and Γ are small compared to ω_{0j}.

The diagram in Fig. 4(b) represents the fourth-order anharmonicity taken as a first-order perturbation, whereas in Fig. 4(a) the third-order vortex appears twice, i.e., corresponding to a second-order perturbation. The effect of the diagram in Fig. 4(b) is a real frequency shift which must be added to the Δ of Fig. 4(a) but does not contribute to the linewidth Γ. Both contributions to Δ have similar temperature and mass dependence and will be treated as a single $\Delta(\omega)$ unless otherwise specified. We must also add to Δ the effect of thermal expansion, including zero-point effects, which affect the harmonic frequency in the quasiharmonic ap-

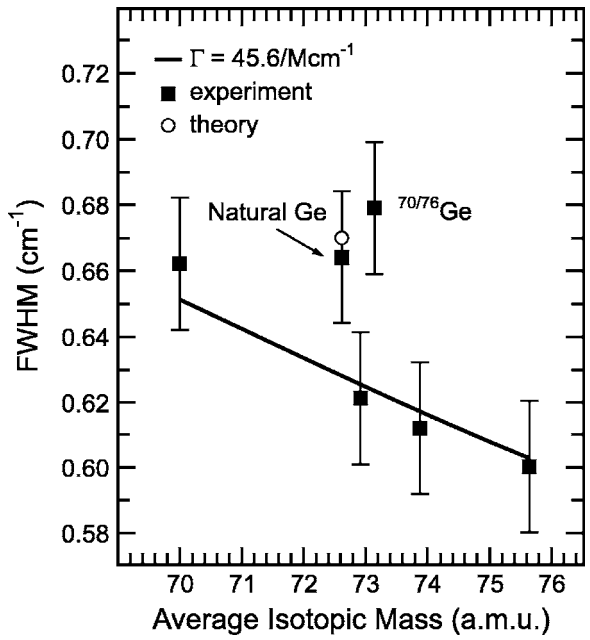

FIG. 5. Intrinsic Raman phonon linewidth of isotopic Ge vs the average mass $\langle M\rangle$ measured at 10 K with a laser excitation of 6471 Å. The straight line represents the predicted proportionality to $\langle M\rangle^{-1}$ for the anharmonic linewidth. The circle represents the anharmonic linewidth of natural Ge plus the calculated effect of the mass disorder. From Cardona and Ruf, 2001, with permission from Elsevier.

proximation through the corresponding Grüneisen parameter.

The linewidth for the down-conversion in terms of Eq. (3.11) is given by Fermi's golden rule:

$$\Gamma(\omega_{0j}) = |V_3|^2 N_{d2}(\omega_{0j})(1 + n_{B1} + n_{B2}), \tag{3.14}$$

where V_3 is an anharmonic matrix element, $N_{d2}(\omega_{0j})$ represents the density of states for the sum of two phonons into which the phonon of frequency ω_{0j} decays, and n_{B1}, n_{B2} are the Bose-Einstein factors that correspond to those two phonons. For the up-conversion processes we obtain a similar expression with the term in parentheses replaced by $n_{B2} - n_{B1}$. This term obviously vanishes for $T \to 0$. Equation (3.14) becomes linear in T at high T and for $T \to 0$ extrapolates to a finite value, which corresponds to the zero-point effect.

Let us examine next the dependence of Eq. (3.14) on M for a monatomic crystal. The anharmonic matrix element $|V_3|^2$ is proportional to the product of phonon amplitudes $\langle u_0^2\rangle \cdot \langle u_1^2\rangle \cdot \langle u_2^2\rangle$, i.e., to $M^{-3/2}$ for $T \to 0$. The density of states is inversely proportional to the maximum frequency, i.e., to $M^{1/2}$, hence $\Gamma(\omega_{0j})$ should be proportional to M^{-1} for $T \to 0$. For $T \to \infty$ it is proportional to $M^{-1/2}$ but the ratio $\Gamma(\omega_{0j})/\omega_{0j}$ becomes independent of M. The dependence on M^{-1} for $T \simeq 0$ is illustrated in Fig. 5 for the Raman frequencies of four nearly isotopically pure germanium samples ($M \simeq 70, 73, 74, 76$). The widths of two additional isotopically mixed samples (a natural one and a $^{70}Ge_{0.5}$ $^{76}Ge_{0.5}$ sample) have also been displayed in Fig. 5 in order to illustrate the effect of mass fluctuations, which will be discussed in Sec. V.B.

In order to describe the temperature dependence of $\Gamma(\omega_0)$ we must decide how to split ω_0 into $\omega_1 + \omega_2$. This depends on which are the most important contributions to the density of states $N_{d2}(\omega_0)$.

In the cases of Ge and Si it has been shown both experimentally and theoretically that the simplest possible ansatz $\omega_1 = \omega_2 = \omega_0/2$ does not work as well as the ansatz $\omega_1 = 2\omega_0/3$ and $\omega_2 = \omega_0/3$ (Menéndez and Cardona, 1984; Debernardi *et al.*, 1995). Figure 6 illustrates the measured shift of the frequency of the Raman phonon of silicon with increasing temperature. As already mentioned, this shift has three contributions: that of thermal expansion plus those represented diagrammatically in Figs. 4(a) and 4(b). Conceptually, the most complicated one is that which corresponds to the real part of the self-energy Σ_r [Fig. 4(a)], which can be written as (Barron and Klein, 1974)

$$\Sigma_r(\omega_0) = \frac{|V_3|^2}{\pi} \int_0^\infty \frac{\omega' N_{d2}(\omega')}{\omega_0^2 - \omega'^2}(1 + n_{B1} + n_{B2}) d\omega', \tag{3.15}$$

where the integral is to be understood as the Cauchy principal part and $|V_3|$ as an average value.

For Si and Ge $N_{d2}(\omega)$ extends from $\omega' = 0$ to $\omega' = 2\omega_0$. The portions of N_{d2} for $\omega' > \omega_0$ contribute a negative term to Eq. (3.15), whereas those for $\omega' < \omega_0$ contribute a positive term. It is easy to speculate that the latter are smaller than the former because they involve acoustic phonons and the corresponding matrix elements should

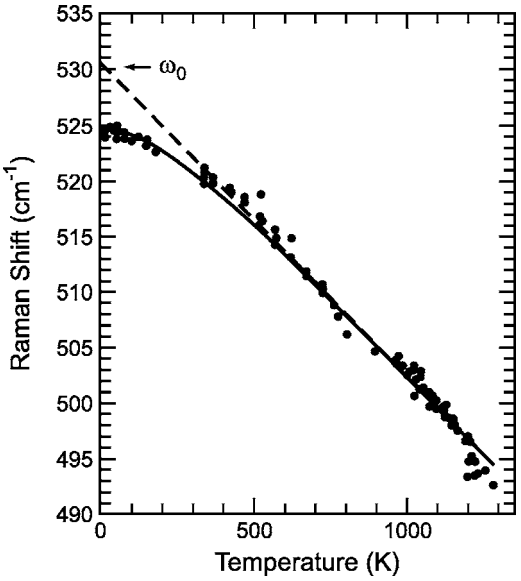

FIG. 6. Temperature dependence of the Raman frequency of silicon. The solid curve represents a fit with the ansatz $\omega_1 = 2\omega_2 = 2\omega_R/3$, including the thermal-expansion effect. The dotted asympotic line illustrates the construction described in the text to estimate the bare harmonic frequency ω_0 from the linear extrapolation to $T \to 0$. From Widulle *et al.*, 2001, with permission from Elsevier.

vanish for either ω_1 or $\omega_2 \to 0$ (Barron and Klein, 1974). Hence the overall shift given in Eq. (3.15) should have the sign revealed in Fig. 6. Lang *et al.* (1999) and Debernardi (2000) have shown by means of *ab initio* calculations that the contribution of Fig. 4(b) to Δ is also negative and so is the contribution of the thermal expansion. Moreover, these contributions can all be represented by Bose-Einstein factors similar to those of Eq. (3.14) (with $\omega_1 = \omega_2$) for the contributions of thermal expansion and Fig. 4(b). Note that the frequency of the intermediate state $\omega = \omega_1 + \omega_2$ need not be equal to ω_0 in Eq. (3.15). Fits to the experimental points can be attempted with a sum of two average Bose-Einstein factors $\Delta_0 \propto 1 + n_{B1} + n_{B2}$, using ω_1 and ω_2 as adjustable parameters. Figure 6 shows such a fit for the Raman frequency of Si. Accidentally, the best fitting frequencies are the same as those that determine the temperature dependence of Γ_0. Note that at the lowest temperatures the variation of Δ with T should be proportional to T^5 (see Sec. III.B.2). Neither the existing experimental data nor the calculations are, at present, sufficiently accurate and detailed to reveal this dependence.

The linear extrapolation method has been used in Fig. 6 to extract the $T=0$ anharmonic renormalization $\Delta_0(0) = -6\ \mathrm{cm}^{-1}$. Another method to determine $\Delta_0(0)$ is to fit the Raman frequencies measured for ^{28}Si and ^{30}Si with the expression

$$\omega_0(\langle M \rangle) = \omega_0 \sqrt{\frac{28}{\langle M \rangle}} + \Delta_0(0)\frac{28}{\langle M \rangle}, \tag{3.16}$$

which gives $\Delta_0(0) = -5.4\ \mathrm{cm}^{-1}$ and a bare frequency $\omega_0 = 530.2$ for natural Si. The latter agrees astoundingly well with recent *ab initio* calculations ($\omega_0 = 531\ \mathrm{cm}^{-1}$, Sanati and Estreicher, 2003). Measurements for diamond have also recently been performed (Cardona *et al.*, 2005).

The anharmonic linewidths at $T \simeq 0$ and their dependence on M have also been determined for diamond ($\approx -3\ \mathrm{cm}^{-1}$, Spitzer *et al.*, 1993), germanium (Zhang, Giehler, *et al.*, 1998), and α-Sn (Wang *et al.*, 1997). The anharmonic renormalization of the Raman frequency of diamond has been found to be $-20\ \mathrm{cm}^{-1}$ (Herchen and Capelli, 1981) while that of α-Sn was $-1\ \mathrm{cm}^{-1}$ (Zhang *et al.*, 1997).

4. Fermi resonances

In the previous section we have implicitly assumed that $N_{d2}(\omega_{0j})$ in Eq. (3.14) is a smooth and well-behaved function of the Raman frequency ω_{0j}. However, a density of states is known to have singularities of various types, especially at high-symmetry points in the BZ. They are called van Hove singularities or critical points (Yu and Cardona, 2005). The number of such singularities is small, typically about a dozen for a crystal with two atoms per primitive cell. Among these crystals we consider those with either diamond or zinc-blende structure. The former have one Raman frequency ω_0 whereas the latter have two, ω_{TO} and ω_{LO}. The chances that one of these Raman frequencies is close to one of the approximately 12 van Hove singularities are therefore small, but nevertheless twice as large for a zinc-blende crystal as for one with the diamond structure. The large variety of crystals with zinc-blende structure enhances even more the probability of finding such a coincidence. Indeed, no accidental proximities of ω_0 to critical points in $N_{d2}(\omega)$ have been found for group-IV semiconductors.[6]

Near-degeneracies of Raman phonons with critical points of $N_{d2}(\omega)$ have been found for GaP (Weinstein, 1976), ZnS (Tallman *et al.*, 2004), CuCl (Ulrich *et al.*, 1999), CuBr (Manjón *et al.*, 2001), and ZnO (Serrano, Manjón *et al.*, 2003). We discuss first one of the most striking examples of the coupling of a Raman phonon to a singularity in $N_{d2}(\omega)$, which is found in ZnO. The resulting phenomenon is often called a Fermi resonance.

ZnO, the mineral zincite, crystallizes under normal conditions in the hexagonal wurtzite structure, with four atoms per unit cell. There are therefore nine phonons at the center of the BZ, some of which (those with E_2 symmetry) are doubly degenerate. There are a total of six different Raman frequencies. One of them, E_2^{high} at $\approx 420\ \mathrm{cm}^{-1}$, corresponds to nearly pure vibrations of two neighboring oxygen atoms against each other, whereas for the $E_2^{low} \approx 100\ \mathrm{cm}^{-1}$ phonons the neighboring Zn atoms vibrate against each other. The latter phonons are very sharp at low T. Their width is probably determined by up-conversion processes (Serrano, Widulle, *et al.*, 2003).

Here we shall be concerned with the E_2^{high} processes. Figure 7 indicates that they occur, for a large number of isotopic compositions investigated, around singularities in $N_{d2}(\omega)$ (Serrano, Manjón, *et al.*, 2003). The frequency of the E_2^{high} phonons of ZnO is approximately proportional to $M_O^{-1/2}$, where M_O is the atomic mass of oxygen. N_{d2} at this frequency corresponds to a sum of a transverse-acoustic and a longitudinal-acoustic (LA) phonon near the edge of the BZ. Such acoustic phonons should have frequencies nearly proportional to $M_{Zn}^{-1/2}$. Hence by varying the isotopic masses of O and Zn we can sweep with the E_2^{high} frequency, a highly structured region of $N_{d2}(\omega)$, as shown in Fig. 7. The various $N_{d2}(\omega)$ that correspond to different Zn masses have been shifted in frequency in Fig. 7 so as to make them coincide. The result is rather striking. A fit with Eq. (3.14) leads to the value $|V_3|^2 = 57\ \mathrm{cm}^{-2}$ for the anharmonic coupling constant.

The strong variation of Γ throughout the various isotopic ZnO samples is due to the fact that E_2^{high} depends on $M_O^{-1/2}$, whereas the transverse-acoustic and longitudinal-acoustic frequencies depend almost exclusively on $M_{Zn}^{-1/2}$. Another way of sweeping $N_{d2}(\omega)$ with

[6] *Ab initio* calculations suggested that such coincidences may appear for silicon under a pressure of ~7 GPa. Experiments showed, however, that the coincidence occurs at pressures well beyond the experimental range of ~10 GPa (Ulrich *et al.*, 1997).

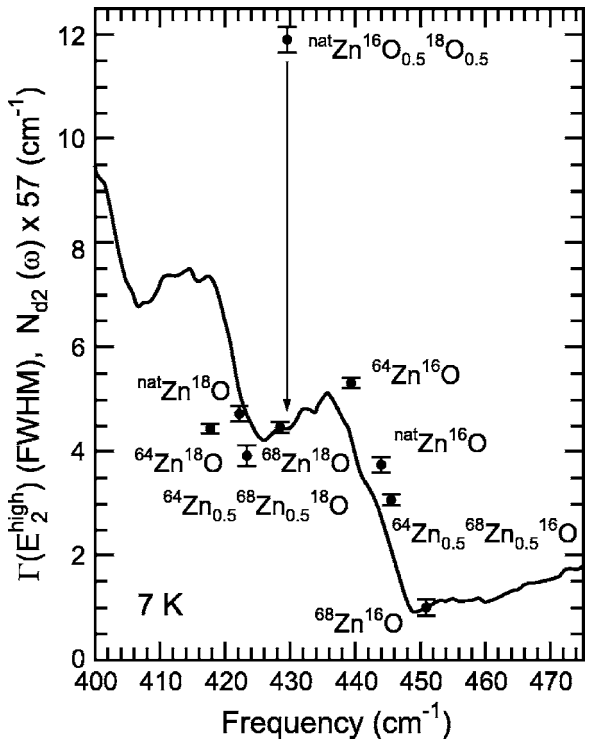

FIG. 7. Resolution-corrected FWHM of the E_2^{high} phonons obtained from Raman spectra measured at 7 K for several isotopic compositions. The points corresponding to $^{64}Zn^xO$ samples are plotted at the measured frequencies. The others have been shifted as explained in the text. The solid line displays the calculated $N_{d2}(\omega)$ scaled by a factor of 57 cm^{-2}. The large width observed for $^{nat}Zn^{16}O_{0.5}{}^{18}O_{0.5}$ illustrates the effect of isotopic mass fluctuations. From Serrano, Manjón, *et al.*, 2003.

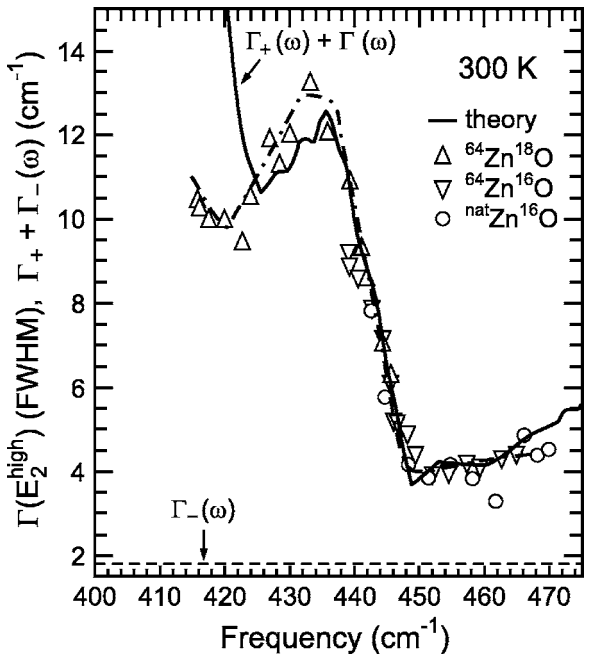

FIG. 8. Measured linewidths of the E_2^{high} phonons of ZnO replotted vs peak frequency, with the frequency shifts required to compare them with the calculations based on a single $N_{d2}(\omega)$. The solid line was obtained by adding to the down-conversion contribution $\Gamma_+(\omega)$ a constant attributed to up-conversion processes $\Gamma_-(\omega)$ (dashed line). From Serrano, Manjón, *et al.*, 2003.

the E_2^{high} frequency is achieved by applying a high hydrostatic pressure. The E_2^{high} frequency shifts by +5 cm^{-1}/GPa with increasing pressure, whereas the corresponding ridge in $N_{d2}(\omega)$ shifts by only +1.5 cm^{-1}. The combined effect is similar to that obtained in Fig. 7 by varying the isotopic masses. Figure 8 shows a large number of E_2^{high} frequencies obtained either by applying pressure or by mass substitution on the corresponding $N_{d2}(\omega)$ calculated *ab initio* (Serrano, Manjón, *et al.*, 2003) and shifted so as to be able to compare the phonon widths with the same $N_{d2}(\omega)$ curve for all frequencies and isotopic masses.

The widths Γ plotted in Figs. 7 and 8 have been obtained through fits with Eq. (3.13) under the assumption of frequency-independent values of Γ and Δ for each individual sample. This assumption represents an approximation that neglects, for instance, asymmetries in A_{oj} due to the frequency dependence of Γ and Δ. Although such asymmetries have indeed been observed for some of the samples, the excellent fit displayed in Fig. 8 confirms the validity of the procedure used. However, in the other zinc-blende materials mentioned earlier (GaP, ZnS, CuCl, CuBr), the frequency dependence of Γ and Δ is of the essence for the understanding of the Fermi-resonance phenomena related to the decay of the TO (GaP, ZnS, CuCl) and longitudinal-optical (LO) (CuBr) phonons. We consider next the case of GaP, where Ga has two stable isotopes (^{69}Ga and ^{71}Ga) but P only has one. We show in Fig. 9 the Raman spectra measured for four samples, one with the natural isotopic composition of Ga ($^{69}Ga_{0.4}{}^{71}Ga_{0.6}P$), another with a so-called anti-natural composition ($^{69}Ga_{0.6}{}^{71}Ga_{0.4}P$), and two with pure Ga isotopes. The dashed curves in the figure represent the corresponding $N_{d2}(\omega)$, with a van Hove singularity, and their shift with isotopic composition induced by the change in the Ga mass since the corresponding two phonons are acoustic (longitudinal acoustic + transverse acoustic near the X point of the BZ). The TO Raman frequency shifts like the reduced mass $\mu^{-1} = M_{\text{Ga}}^{-1} + M_{\text{P}}^{-1}$. Because $M_{\text{P}} \ll M_{\text{Ga}}$, the shift in μ^{-1} with M_{Ga} is strongly reduced, as illustrated in Fig. 9. The change in the masses allows us to sweep the van Hove singularity of $N_{d2}(\omega)$ through ω_{TO} and thus through the Fermi resonance, which is almost exactly achieved for the natural samples. Two structures, labeled A and B, are seen in the clearly non-Lorentzian spectra. The curves through the experimental points were obtained by substituting the $\Gamma(\omega)$ and $\Delta(\omega)$ obtained with Eqs. (3.14) and (3.15) into Eq. (3.13). The anharmonic coupling parameter (Widulle, Ruf, Göbel, *et al.*, 1999) resulting from the fit turns out to be $|V_3|^2 = 114$ cm^{-2}. As in the case of ZnO, the Fermi resonance can also be swept through for GaP by the application of hydrostatic pressure. Figure 10 shows Raman spectra of the TO phonons

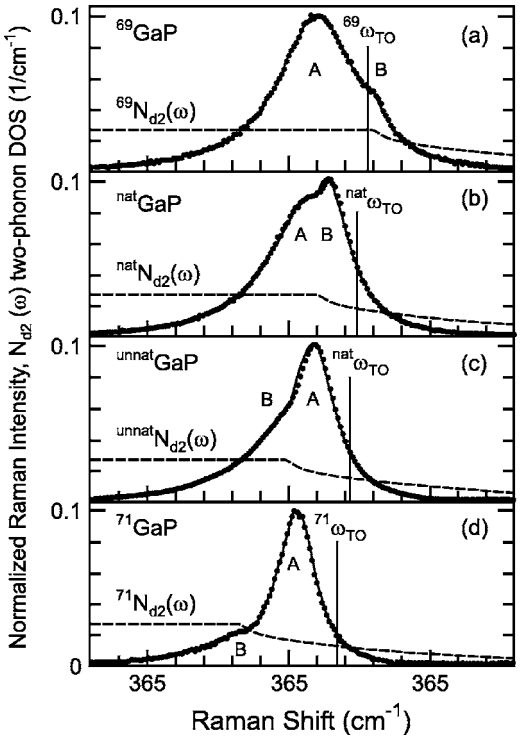

FIG. 9. Raman spectra of the transverse-optical (TO) phonon of (a) ^{69}GaP; (b) ^{nat}GaP; (c) $^{69}Ga_{0.4}{}^{71}Ga_{0.6}P$; (d) ^{71}GaP. The measurements were performed at $T=6$ K. The solid lines are fits to the experimental data (symbols) using the indicated N_{2d} (dashed lines). The vertical lines represent the δ-function peaks which correspond to the TO phonons in the harmonic approximation. From Widulle, Ruf, Göbel, *et al.*, 1999.

of ^{69}GaP measured at several pressures and for $T=10$ K. The spectra sharpen up considerably with increasing pressure as the phonon frequency shifts away from the van Hove singularity (Ves *et al.*, 2001). Similar effects have been observed for ZnS (Tallman *et al.*, 2004).

We shall not go into the details of the Fermi resonance observed for the TO Raman phonons of CuCl (Göbel *et al.*, 1997) and the LO phonons of CuBr (Serrano *et al.*, 2001). The corresponding line shapes are rather complex and have received a lot of attention since the presence of a Fermi resonance was suggested by Krautzman *et al.* (1974) for the TO spectrum of CuCl.

5. Isotopic substitution and phonon eigenvectors

The E_2^{high} and E_2^{low} phonons of wurtzite materials are an ideal pair to illustrate the determination of eigenvectors by isotopic substitution. These eigenvectors depend only on one parameter that represents the mixture of the vibrations of the low-mass atom E_2^{high} with those of the high-mass counterpart E_2^{low}. Isotope substitution for only one of the constituent atoms suffices to obtain the mixing parameter. This was done for GaN since only N-substituted samples were available. For CdS (Zhang *et al.*, 1996) and ZnO (Serrano, Widulle, *et al.*, 2003) both isotopes were substituted (see Sec. III.B.4) and the problem became overdetermined. This led to a more accurate determination of the admixture parameter. Some work has also been performed for several polytypes of SiC (Widulle, Ruf, Buresch, *et al.*, 1999).

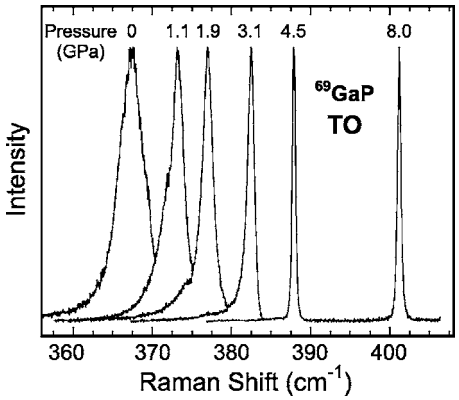

FIG. 10. Pressure dependence of the Raman spectrum of the TO phonon of GaP at 10 K. Note the sharpening of the measured peak with increasing pressure. From Ves *et al.*, 2001.

The change in a phonon frequency ω_{qj} induced by a change in the isotopic mass at site r is given by (Menéndez *et al.*, 1994; Zhang *et al.*, 1997)

$$\frac{\partial \omega_{qj}}{\partial M_r} = -\frac{1}{2M_r}\omega_{qj}|\boldsymbol{e}_{qjr}|^2, \tag{3.17}$$

where the vector $\boldsymbol{e}_{qjr}$ represents the component of the orthonormal eigenvector at site r corresponding to the qj phonon. Equation (3.17) allows us to determine the absolute value of this component (usually complex except at the center of the BZ) if we measure the derivative of ω_{qj} with respect to the mass M_r. For the E_2 modes of wurtzite (e.g., GaN), the eigenvector, which describes the E_2^{high}-E_2^{low} admixture, is real and can be found by solving the following secular equation (Zhang *et al.*, 1997):

$$\begin{pmatrix} -\omega^2 + \dfrac{k_{Ga}}{M_{Ga}} & \dfrac{k_{Ga\,N}}{\sqrt{M_{Ga}M_N}} \\ \dfrac{k_{Ga\,N}}{\sqrt{M_{Ga}M_N}} & -\omega^2 + \dfrac{k_N}{M_N} \end{pmatrix} \cdot \begin{pmatrix} \boldsymbol{e}_{Ga} \\ \boldsymbol{e}_N \end{pmatrix} = 0, \tag{3.18}$$

where k_{Ga} and k_N represent force constants for the Ga—Ga and N—N vibrations, respectively, and k_{GaN} the coupling of these two modes. The two observed frequencies of the E_2^{high} and E_2^{low} phonons do not suffice to determine k_{Ga}, k_N, and k_{GaN}. However, if we include the derivative of Eq. (3.17) we obtain, either from Eq. (3.18) or from Eq. (3.17), the eigenvectors ($|\boldsymbol{e}_{Ga}| = 0.204 \pm 0.0045$; $|\boldsymbol{e}_N| = 0.677 \pm 0.012$) for the E_2^{high} phonons and ($|\boldsymbol{e}_{Ga}| = 0.677 \pm 0.012$; $|\boldsymbol{e}_N| = 0.204 \pm 0.0045$) for the E_2^{low} phonons. Because of the presence of four atoms in the primitive cell these eigenvectors have been normalized according to

$$2(|\boldsymbol{e}_{Ga}|^2 + |\boldsymbol{e}_N|^2) = 1. \tag{3.19}$$

As indicated in Eq. (3.19) the relative sign of $\boldsymbol{e}_{Ga}$ and

e_N cannot be determined by isotopic substitution. *Ab initio* calculations give magnitudes of e_{Ga} and e_N that agree with those determined experimentally and for Ga and N neighboring atoms placed along the *c* direction, parallel (antiparallel) displacements for the E_2^{high} (E_2^{low}) modes. The E_2^{high}-E_2^{low} admixture is somewhat larger in CdS, as expected from the smaller frequency splitting of these modes (Zhang *et al.*, 1996). For ZnO, the eigenvectors are nearly the same as for GaN (Serrano, Widulle, *et al.*, 2003).

We close this section by mentioning that isotopic substitution has been used rather successfully to obtain information about phonon eigenvectors in high-T_c superconductors (Henn *et al.*, 1997). These materials have a large number of atoms per unit cell and reliable information about eigenvectors is otherwise difficult to obtain.

IV. PHONON EFFECTS RELATED TO ISOTOPIC DISORDER

A. Thermal conductivity

In insulators and semiconductors (at temperatures below that of the gap) the thermal conduction is effected by phonons, predominantly acoustic ones. The simplest expression for the thermal conductivity κ is

$$\kappa(T) = \frac{1}{3}\langle v_{ph}\rangle \ell_{ph}(T) C_p(T), \tag{4.1}$$

where $\langle v_{ph}\rangle$ is an average phonon velocity, $\ell_{ph}(T)$ their mean free path, and $C_p(T)$ the corresponding specific heat. A theory of $\kappa(T)$ requires basically the calculation of $\ell_{ph}(T) = \tau_{ph}(T)\langle v_{ph}\rangle$,[7] a rather formidable task since several scattering mechanisms contribute to determining this mean free path. The simplest of these mechanisms, and the one that can be varied for a given material at a fixed temperature, is the scattering of the acoustic phonons by isotopic mass fluctuations. This mechanism is best visualized by considering virtual-crystal phonons and how they collide with mass fluctuations at lattice sites where the masses are either higher or lower. This scattering is equivalent to Rayleigh scattering (of photons) at point defects. Within the Debye approximation, we find for phonons of frequency ω the contribution to τ_{ph}:

$$\tau_{ph}^{-1} = A\omega^4, \quad \text{with } A = \frac{g_2 V}{4\pi\langle v_{ph}\rangle^3}, \tag{4.2}$$

where V is the volume occupied by the isotopically mixed atom and the mass fluctuation parameter g_2 is given by

[7] $\tau_{ph}(T)$ is the phonon relaxation time.

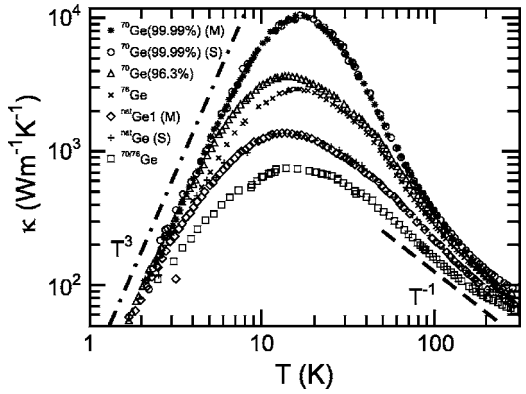

FIG. 11. Thermal conductivity vs temperature of five Ge samples with different isotopic compositions: ^{70}Ge(99.99%), ^{70}Ge(96.3%), ^{76}Ge(86%), ^{nat}Ge1, and $^{70/76}$Ge. Two of the samples, ^{70}Ge(99.99%) and ^{nat}Ge1, have been measured with two different experimental setups, in Stuttgart (*S*) and in Moscow (*M*). The dot-dashed line represents a T^3 law, expected for pure boundary scattering, while the dashed line shows a $1/T$ dependence, expected for phonon scattering at high temperatures. From Asen-Palmer *et al.*, 1997.

$$g_2 = \frac{\langle M^2\rangle - \langle M\rangle^2}{\langle M\rangle^2}. \tag{4.3}$$

In Eq. (4.3) the angular brackets represent averages over the isotopes of a given atom present in the crystal.

The isotope effect on the thermal conductivity was predicted by Pomeranchuk (1942). An early investigation of $\kappa(T)$ for LiF and its dependence on the g_2 of the lithium isotopes present can be found in the article of Berman and Brock (1965). We shall discuss here the results obtained for germanium (Geballe and Hull, 1958; Asen-Palmer *et al.*, 1997) and also mention data available for silicon (Ruf, Henn, *et al.*, 2000) and diamond (Wei *et al.*, 1993).

Figure 11 displays the thermal conductivity of several germanium samples with different isotopic compositions. (*M*) and (*S*) represent measurements performed on the same sample in Stuttgart (MPI) or at the Moscow Kurchatov Institute, respectively. The general behavior versus temperature of the curves in Fig. 11 is typical of most insulators and semiconductors, although the position of the maximum T_m and the corresponding absolute value of $\kappa(T_m)$ vary from material to material. T_m is, to a good approximation, independent of isotopic composition for a given material, whereas $\kappa(T_m)$ decreases strongly with increasing mass-fluctuation parameter g_2 (by as much as a factor of 13 in Fig. 11). This dependence of $\kappa(T_m)$ on g_2 is probably the strongest isotope mass effect observed in solids.

The curves in Fig. 11 exhibit three distinct regions:

(a) Below about 8 K they tend to the T^3 behavior expected from Eq. (4.1) if ℓ_{ph} is independent of T. This behavior arises from the proportionality of C_p to T^3.

(b) A maximum around $T_m \simeq 18$ K, which as already

mentioned, depends strongly on the isotopic mass fluctuation parameter g_2.

(c) Above 20 K, $\kappa(T)$ decreases rapidly with increasing T.

In region (a) $\ell_{\rm ph}$ is of the order of the sample dimensions and is basically determined by collisions with its walls. Although it is well defined for a given sample with a specific surface treatment, thermal conductivity as a material property is not uniquely defined. It depends on sample dimensions, shape, orientation, and, last but not least, surface treatment. Details for the samples of Fig. 11 are given in Table I of Asen-Palmer *et al.* (1997).

In region (b) κ is usually a well-defined property of the bulk material; $T_m \simeq 20$ K for Si whereas for diamond $T_m \simeq 80$ K (close to liquid-nitrogen temperature!). The high value of $\kappa(T_m)$ found for isotopically pure samples has suggested several applications to cases in which a large amount of heat is generated and must be carried away. Such applications have been implemented for isotopically pure diamond for which $\kappa(T_m)$ is three times higher than for the natural material (Berman *et al.*, 1993).

In region (c) anharmonic processes take over. These processes also operate in regions (a) and (b). In those regions, however, they do not contribute much to the thermal resistance since they mostly conserve crystal momentum and thus do not affect the heat flow. At sufficiently high temperatures, summation processes, in which two phonons combine into one with a crystal momentum outside the BZ, become possible. Bringing the phonon outside the BZ to a point inside (an umklapp process) reverses the sign of energy flow for this phonon and thus contributes to the thermal resistance. Since phonons of a sufficiently large energy must be present for the umklapp process to take place, these processes have an exponential dependence ($\sim e^{-C/T}$) on temperature.

We shall not delve into the details of the semiempirical calculations that lead to a description of the curves in Fig. 11. The resulting fits (see Fig. 4 of Asen-Palmer *et al.*, 1997) were performed using the same set of anharmonic scattering parameters and varying only the isotope scattering according to Eq. (4.2).

Thermal-conductivity measurements have also been performed for ^{28}Si and compared with those for natural samples (Ruf, Henn, *et al.*, 2000). $\kappa(T_m)$ was reported to be a factor of 6 larger in the ^{28}Si material. At 300 K an enhancement of about 60% was also reported. This enhancement suggested the use of ^{28}Si at room temperature for devices in which a lot of heat is generated and must be conducted away. Unfortunately, the measurements of the ^{28}Si sample were recently shown to be incorrect. New measurements showed reproducibly that the enhancement of $\kappa(T)$ for the ^{28}Si sample with respect to natural Si is only 10% (Kremer *et al.*, 2004). Nevertheless, an enhancement by about a factor of 2 at 77 K has been confirmed. This may still be of interest for components that operate at this temperature, such as mirrors and diffraction elements for use with synchrotron radiation (Berman *et al.*, 1993).

Until recently all theories on thermal conductivity had a strongly phenomenological flavor, making use of the relaxation-time approximation (see Asen-Palmer *et al.*, 1997, and references therein). In recent years, considerable progress towards an *ab initio* theory has been made by Omini and Sparavigna (1997) and by Sparavigna (2002, 2003). These authors used two- and three-body potentials obtained by fitting phonon dispersion relations and related the anharmonic properties with a single average Grüneisen parameter. In this manner they determined the third-order coupling coefficients for all possible three-phonon combinations. They then solved iteratively the Boltzmann equation for phonon transport without using the relaxation-time approximation. A scattering time must, however, still be used to describe boundary scattering in the lowest temperature region (a). In this manner they reproduced rather well the thermal conductivities of diamond, Ge, and Si, and the observed isotope effects.

B. Phonon self-energy due to the isotopic mass disorder

In Sec. IV.A we have discussed the effect of isotopic disorder on thermal conductivity. This effect is due to scattering of the acoustic phonons by mass fluctuations as represented by the parameter g_2. Here we discuss the equivalent effects on optic phonons, especially those that can be observed by Raman spectroscopy. These effects are represented by the Feynman diagrams (c) and (d) of Fig. 4. Diagram (c) vanishes if we adopt, for the unperturbed crystal, the virtual-crystal approximation. Restricting ourselves to these diagrams implies the use of perturbation theory up to second order, which is justified if the mass fluctuations (as measured by g_2) are small compared with the width of the relevant phonon band normalized to the phonon frequency. This is a reasonably good approximation for the semiconductors under consideration here (see Table II for the g_2's of elemental semiconductors and Fig. 1, typical for the bandwidths). Higher-order terms have nevertheless been discussed theoretically by Tamura (1983) and observed experimentally by Widulle *et al.* (2002). For molecular crystals, the phonon bands are rather narrow and perturbation theory may break down. In this case, localized vibrations (i.e., bound states) corresponding to the different isotopes can appear. Of particular interest is the case of the molecule C_{60} (fullerene), for which the virtual crystal provides a good approximation to the vibrations of a single molecule (e.g., either $^{12}C_{60}$ or $^{12}C_{59}$ $^{13}C_1$) but two molecules with different isotopes in crystalline form or in solution preserve their independent vibrational frequencies without averaging them (see Fig. 1 of Menéndez *et al.*, 1994).

Figure 4(d) shows a self-energy diagram similar to that of Fig. 4(a) but with the vertices corresponding to elastic scattering on a static mass fluctuation. The real and imaginary parts of the corresponding self-energy are given by expressions similar to Eqs. (3.14) and (3.15),

TABLE II. Isotopically mixed crystals of elemental semiconductors that have been used to determine the real (Δ_{0i}) and imaginary ($-\Gamma_{0i}/2$) parts of phonon self-energies due to isotopic disorder. The values of g_2 must be multiplied by 10^{-5}. For references see the text.

		Natural	$^{12}C_{0.85}{}^{13}C_{0.15}$	$^{12}C_{0.63}{}^{13}C_{0.37}$	$^{12}C_{0.53}{}^{13}C_{0.47}$	$^{12}C_{0.18}{}^{13}C_{0.82}$
Diamond	$\langle M\rangle$	12.01	12.15	12.37	12.47	12.82
	g_2	7	86	152	160	90
	Γ_{0i}	0	1.4	4.0	5.5	3.8
	Δ_{0i}	0	3	5	6	4
		Natural	$^{28}Si_{0.75}{}^{30}Si_{0.25}$	$^{28}Si_{0.50}{}^{30}Si_{0.50}$	$^{28}Si_{0.25}{}^{30}Si_{0.75}$	^{30}Si[a]
Si[a]	$\langle M\rangle$	28.1	28.5	28.8	29.5	29.7
	g_2	20	92	114	88	48
	Γ_{0i}	0	0.05	0.06	0.07	0.04
	Δ_{0i}	0.1	0.8	1.2	0.7	0.4
		Natural	$^{70}Ge_{0.5}{}^{76}Ge_{0.5}$			
Ge[b]	$\langle M\rangle$	72.6	72.8			
	g_2	59	153			
	Γ_{0i}	0.035	0.06			
	Δ_{0i}	0.34	1.06			
		Natural	$^{116}Sn_{0.5}{}^{124}Sn_{0.5}$	$^{112}Sn_{0.5}{}^{124}Sn_{0.5}$		
α-Sn	$\langle M\rangle$	118.7	120	118.1		
	g_2	33	110	258		
	Γ_{0i}	0	0.036	0.04		
	Δ_{0i}	0.02	0.7	1.8		

[a]The nominal ^{30}Si only has 87% of this isotope.
[b]The nominal ^{76}Ge only has 94% of this isotope.

with N_{d2} replaced by the one-phonon density of states N_{d1}. The anharmonic matrix element is replaced by the matrix element for the coupling to a mass difference (with respect to the virtual crystal), which must then be averaged for all possible lattice sites.[8] The resulting contribution to the linewidth is, for a cubic monatomic crystal (Tamura, 1983; Widulle *et al.*, 2002),

$$\Gamma_{0i} = \frac{\pi}{12} g_2 \omega^2 N_{d1}(\omega_0), \tag{4.4}$$

where N_{d1} is the density of one-phonon states at the frequency ω_0 of the phonon whose self-energy is being considered. The real part of the self-energy Δ_{0i}, corresponding to a frequency shift when inserted in Eq. (3.13), is given by

$$\Delta_{0i} = \frac{g_2 \omega_0^2}{24} \int_0^\infty \frac{\omega'}{\omega_0 - \omega'} N_{d1}(\omega') d\omega'. \tag{4.5}$$

[8]One must, however, keep in mind that the scattering involved in Figs. 4(c) and 4(d) is elastic, harmonic, and temperature independent, whereas that in Figs. 4(a) and 4(b) is inelastic, anharmonic, and temperature dependent.

Note that while only intermediate states which conserve the frequency ω_0 contribute to Eq. (4.4), all states ω' (i.e., virtual transitions) contribute Eq. (4.5). States such that $\omega' < \omega_0$ produce an upshift in frequency while those for which $\omega' > \omega_0$ give rise to a downshift and a certain degree of compensation takes place except for the highest-frequency phonons (the Raman phonons of Ge, Si, α-Sn) for which only upshift contributions occur. This is the reason for the relatively large values of Δ_{0i} listed in Table II in the cases of diamond, Si, Ge, and α-Sn. Note, however, that the values of Γ_{0i} in this table are rather small, except for diamond. This is illustrated in Fig. 12, where the Raman line shapes observed for silicon (a) and diamond (b) have been plotted for several isotopic compositions. Figure 12(b) shows a clear increase in the linewidth for the isotopically mixed samples with respect to the pure ones, whereas in Fig. 12(a) it is not possible to see such an increase with the naked eye. The observed widths are basically the anharmonic ones. A careful fit to the measured spectra, however, reveals mass disorder contribution of the order of 10% of the anharmonic one for Si, Ge, and α-Sn (see Fig. 5 and Table II), whereas for diamond the mass disorder contribution is even larger than the anharmonic one. This striking difference is related to the fact that ω_0

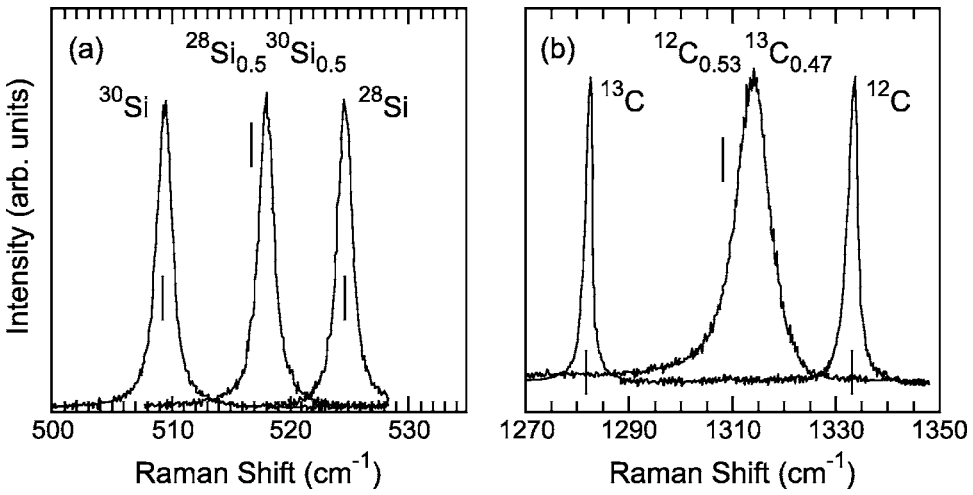

FIG. 12. Low-temperature Raman spectra of (a) silicon, with several isotopic concentrations. No broadening is apparent to the naked eye for the $^{28}Si_{0.5}$ $^{30}Si_{0.5}$ sample. (b) Diamond, with three different isotopic concentrations. Note the strong broadening for the isotopically disordered samples. The vertical lines indicate the peak positions expected in the absence of isotopic disorder. From Cardona and Ruf, 2001.

(corresponding to the center of the BZ) is the largest phonon frequency for Si, Ge, and α-Sn, but for diamond the highest frequency occurs away from the center of the BZ. In Eq. (4.4) N_{d1} vanishes when the Raman frequency is the largest one. No phonon states are present into which the Raman phonons can scatter elastically. For diamond, however, the highest phonon frequency lies away from the BZ center and elastic scattering of the Raman phonon becomes possible (see Fig. 13). The small values of Γ_{0i} listed in Table II for Si, Ge, and α-Sn are to be regarded as residual contributions that appear in higher-order perturbation theory. Anharmonicity broadens ω_0 and thus generates around it a finite N_{d1} into which the ω_0 phonon can scatter. The small values of Γ_{0i} given in Table II for Si, Ge, and α-Sn can thus be qualitatively understood as a higher-order perturbation effect involving anharmonicity and isotopic disorder (Fuchs *et al.*, 1993; Widulle *et al.*, 2001).

Even if Γ_{0i} is rather small, Δ_{0i} can be appreciably large because the contributions of all frequencies ω' to the integral in Eq. (4.4) are positive when the frequency ω_0 is the highest of all phonon frequencies. In the case of diamond there is a small region $\omega' > \omega_0$ that results in a negative contribution to Δ_{0i}. However, this contribution is small and a net positive shift results (see Table II). We show in Fig. 14 the measured frequency ω_0, including anharmonic and disorder effects, for $^{28}Si_x$ $^{30}Si_{1-x}$ crystals with six different values of x. The solid line represents the virtual-crystal behavior plus the anharmonic correction. The dashed line, drawn through the experimental points, includes the effect of mass disorder, which can be represented by (Widulle *et al.*, 2001)

$$\Delta_{0i} = 4.2x(1-x). \tag{4.6}$$

A calculation based on Eq. (4.4) gives the value 6 for the prefactor in Eq. (4.6). The shifts calculated with Eq. (4.4) for Ge, α-Sn, and diamond also agree reasonably well with the measured ones. *Ab initio* calculations of this effect, on the basis of vibrations of a large supercell containing several isotopes (i.e., without using perturbation theory), yield Δ_{0i}=1.1 cm^{-1} for $^{70}Ge_{0.5}$ $^{76}Ge_{0.5}$, in good agreement with the experimental data and with the results from Eq. (4.5) (Vast and Baroni, 2000).

We discuss next the mass-fluctuation effects in crystals with two different atoms per primitive cell (generalization to more than two different atoms is straightforward). In this case, we must introduce two different g_2 factors, one for the anion (g_{2a}) and one for the cation (g_{2c}). Equations (4.4) and (4.5) must be modified to take into account the separate effects of the two independent mass fluctuations. The modification must include the eigenvectors of the phonons under consideration at either the anion or the cation as well as those of the intermediate states. Equation (4.4) thus becomes

$$\Gamma_{0i} = \frac{\pi\omega_0^2}{6}[g_{2c}N_{d1c}(\omega_0)|\boldsymbol{e}_{0c}|^2 + g_{2a}N_{d1a}(\omega_0)|\boldsymbol{e}_{0a}|^2], \tag{4.7}$$

where $\boldsymbol{e}_{0c}$ and $\boldsymbol{e}_{0a}$ are the components of the eigenvector of the Raman phonon at either the cation or the anion, and N_{d1c}, N_{d1a} are the densities of states projected on the cation or anion, respectively [see Eq. (2.3)]. The latter include values of $|\boldsymbol{e}_c|^2$ and $|\boldsymbol{e}_a|^2$ for all phonons of frequency ω_0. A similar generalization of Eq. (4.5) to the diatomic crystal is straightforward.

The effect of mass disorder on the LO and TO phonons has been investigated for ZnSe and ZnS. No mass disorder-induced broadening is observed for the LO phonons, a fact that can also be related to the vanishing of the one-phonon density of states for the LO frequency, which is the highest in the phonon spectrum. However, a finite N_{d1} is present at the ω_{TO} frequency [Fig. 13(c)] and, correspondingly, a broadening due to mass disorder is found for the TO Raman phonons. For natural Zn and Se with a considerable isotopic mixture (see Table I), the measured contribution to Γ_i due to mass disorder of the TO Raman phonon is 1.4 cm^{-1}, in excellent agreement with the prediction of Eq. (4.7) (Göbel *et al.*, 1999). For these phonons, $\Delta_{0a} \simeq -0.5$ cm^{-1}. Note that the corresponding frequency shift is negative because of the large contribution of frequencies ω' larger than ω_{TO}. A strong effect of the oxygen mass disorder has been observed for the E_2^{high} phonons of Zn $^{16}O_{0.5}$ $^{18}O_{0.5}$ (see Fig. 7).

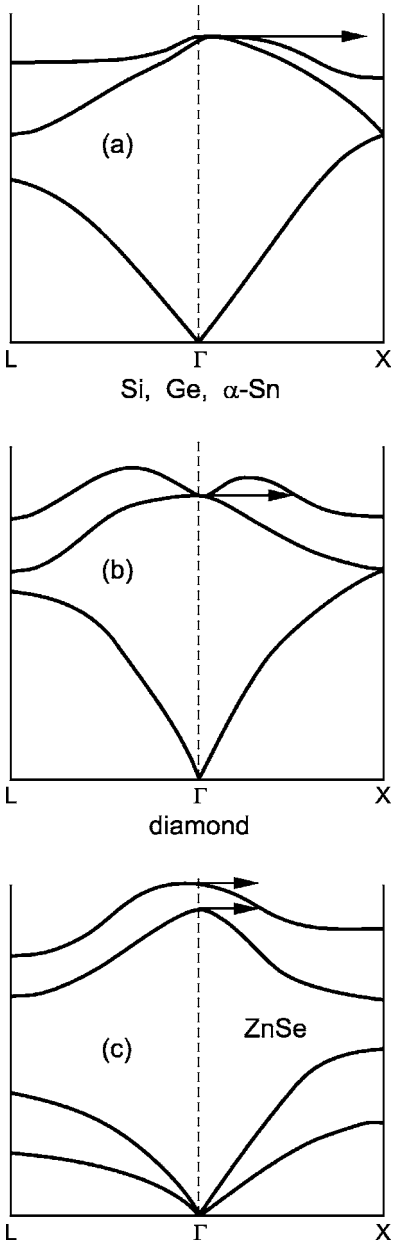

FIG. 13. Schematic diagrams of the processes that contribute to the mass disorder-induced broadening of the Raman phonons. (a) No elastic processes are possible for Si, Ge, and α-Sn. (b) Because of the reentrant dispersion relation at $\boldsymbol{q}=\mathbf{0}$, elastic processes are possible for diamond. (c) Typical example of an ionic material (ZnSe) in which the $\boldsymbol{q}=\mathbf{0}$ Raman phonons are split into longitudinal-optical (LO) and TO components. No elastic processes are possible for the LO component, whereas for TO phonons scattering into the LO band becomes possible.

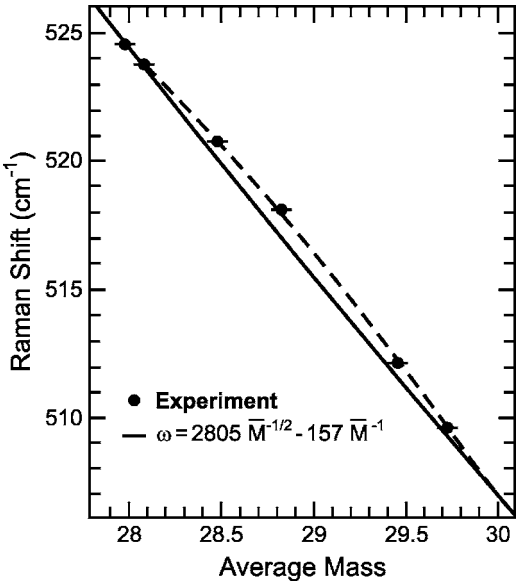

FIG. 14. Measured Raman shifts of the zone-center optic mode in silicon with various isotopic compositions. The solid line indicates the mass dependence expected for isotopically pure crystals, including anharmonic renormalization. Isotope mass fluctuation-induced deviations from this line for which a parabolic bowing (dashed line) is shown as a guide to the eye. From Widulle *et al.*, 2001, with permission from Elsevier.

Most of the isotopic work discussed so far for phonons has been confined to Raman phonons, i.e., those at the center of the BZ. A few publications have appeared dealing with more general points in the BZ. We have already mentioned the inelastic neutron-scattering work performed for Ge (Göbel, Wang, *et al.*, 1998). In Fig. 9 of Göbel, Wang, *et al.* (1998), mass disorder self-energies found for Ge throughout the 100–200-cm^{-1} frequency range are displayed and compared with calculations based on Eqs. (4.4) and (4.5). The experimental data were obtained by inelastic neutron scattering, second-order Raman and IR spectroscopy, and photoluminescence.

Because of its connection with the next section, we discuss briefly here the results of cathodoluminescence experiments on isotopically mixed diamonds (Cardona and Ruf, 2001). This luminescence results from recombination of electrons close to the X point of the BZ [$\boldsymbol{q}=(\mathbf{2}\pi/\boldsymbol{a})(0,0,0.76)$] and holes at the BZ center. It therefore involves the emission of phonons with a similar $\boldsymbol{q}$ vector. It was observed that the LO phonons with this $\boldsymbol{q}$ vector shift up with isotopic disorder whereas the corresponding TO phonons shift down. These shifts can be understood qualitatively on the basis of Eq. (4.5) and more quantitatively by using the more general coherent-potential approximation. Experimental and calculated results are displayed in Fig. 15.

C. Disorder-induced Raman scattering

It is usually believed that first-order Raman and IR spectra only reveal excitations near the center of the BZ ($q\simeq 0$). This is true if the crystals are perfect, not only from the point of view of the structure, but also from the isotopic point of view. Each constituent element must be isotopically pure. This is not the case for natural isotopic compositions of diamond, Si, Ge, and α-Sn. Therefore at least partial lifting of the $\boldsymbol{q}$-conservation rule is expected for these isotopically natural crystals and even more so for those with a 50% content of the higher and lower

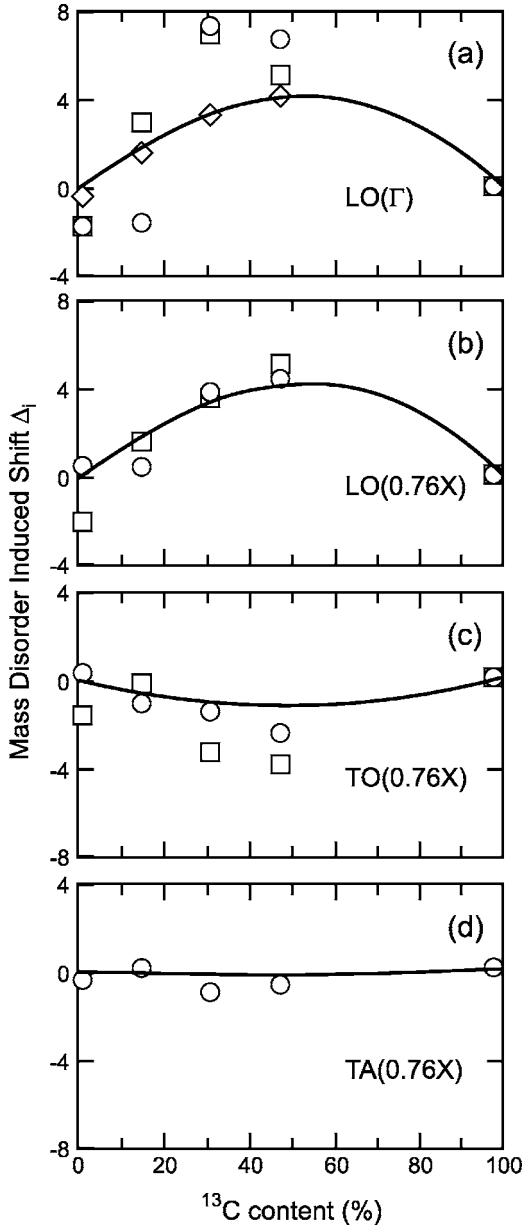

FIG. 15. Isotopic mass disorder contributions to phonon frequencies of diamond. (a) Raman-scattering data (lozenges) and cathodoluminescence data (circles and squares); (b)–(d) Data extracted from the cathodoluminescence spectra. The solid lines represent coherent-potential-approximation (CPA) calculations using *ab initio* lattice dynamics. From Cardona and Ruf, 2001.

isotopic masses (Table I). For these crystals, the Raman and IR spectra should, in principle, contain a broad component reflecting the density of states N_{d1}.[9]

Equations (3.13) and (4.4) provide a rather simple way to understand the origin of the disorder-induced density-of-states spectra. From Eq. (3.13) we obtain, for $\omega-\omega_{0j}-\Delta \gg \Gamma/2, \Delta$,

$$A_0 \simeq \frac{1}{\pi}\frac{\Gamma/2}{(\omega-\omega_0)^2}. \tag{4.8}$$

Substituting Eq. (4.4) into Eq. (4.8), after replacing ω_0 by ω, we find

$$A(\omega) \simeq \frac{1}{24} g_2 \frac{\omega^2 N_{d1}(\omega)}{(\omega-\omega_0)^2}. \tag{4.9}$$

To a good approximation, the line shape of the mass disorder-induced spectra should be given by Eq. (4.9). Note that the denominator in the right-hand side of this equation enhances the portions of $N_{d1}(\omega)$ for frequencies ω close to ω_0, i.e., the TO regions in $N_{d1}(\omega)$. The acoustic phonons are therefore very difficult to observe in disorder-induced spectra.

Spectra that correspond to Eq. (4.9), or to its more sophisticated coherent-potential-approximation version (Taylor, 1967; Widulle *et al.*, 2001), have been observed for isotopically mixed diamond (Spitzer *et al.*, 1993), Si [Widulle *et al.*, 2001; see Figs. 16(a) and 16(b)], germanium (Fuchs *et al.*, 1993), and α-Sn (Wang *et al.*, 1997).

D. Nuclear magnetic resonance

Isotopes with an odd atomic weight have a nuclear angular momentum (Table I) which can be used for nuclear magnetic resonance (NMR) investigations. Some low atomic number, even atomic weight, elements (e.g., ^{2}H, ^{10}B, ^{16}N) also have nuclear angular momentum $I \neq 0$. Each of the group-IV elements has at least one isotope with $I \neq 0$. The present ability to vary the concentration of nuclei with $I \neq 0$ in a crystal has inspired a number of NMR investigations involving diamond, Si, and Ge crystals. Considerable attention has been paid to ^{29}Si, whose nuclear spin states may find application as qubits in quantum computation (Ladd *et al.*, 2002). NMR investigations have been performed for diamond (Lefmann *et al.*, 1994), Si (Verhulst *et al.*, 2003), and ^{73}Ge (Verkhovskii *et al.*, 2000, 2003).

The magnetic isotopes ^{13}C and ^{29}Si have $I=\frac{1}{2}$ but their abundance is only a few percent in unenriched samples. Their value of I implies that electric quadrupole terms do not contribute to the NMR spectra. The NMR investigations performed for diamond and silicon crystals have therefore been confined to the effects of dipole-dipole interaction on the line shapes of the NMR spectra and the electron-lattice relaxation times, which are particularly large for ^{29}Si (>2 h). The perturbation Hamiltonian of the dipole-dipole interaction which contributes to the linewidths depends on the angle θ between the line connecting a given pair of dipoles and the magnetic field $\boldsymbol{H}$. This dependence is proportional to $1-3\cos^2\theta$. It thus vanishes at the magic angle $\theta=54.74°$, i.e., for nearest neighbors in tetrahedral semiconductors when $\boldsymbol{H}$ is along the [100] axis. For $\boldsymbol{H}\|[111]$ the dipole-dipole interaction effects reach a maximum that manifests itself as a spectral doublet corresponding to the bonds along [111] and those along $\{\bar{1}\bar{1}1\}$ (the Pake doublet; Pake,

[9]For the IR spectra this component has not been detected in group-IV crystals, a consequence of the homopolar nature of the bonds.

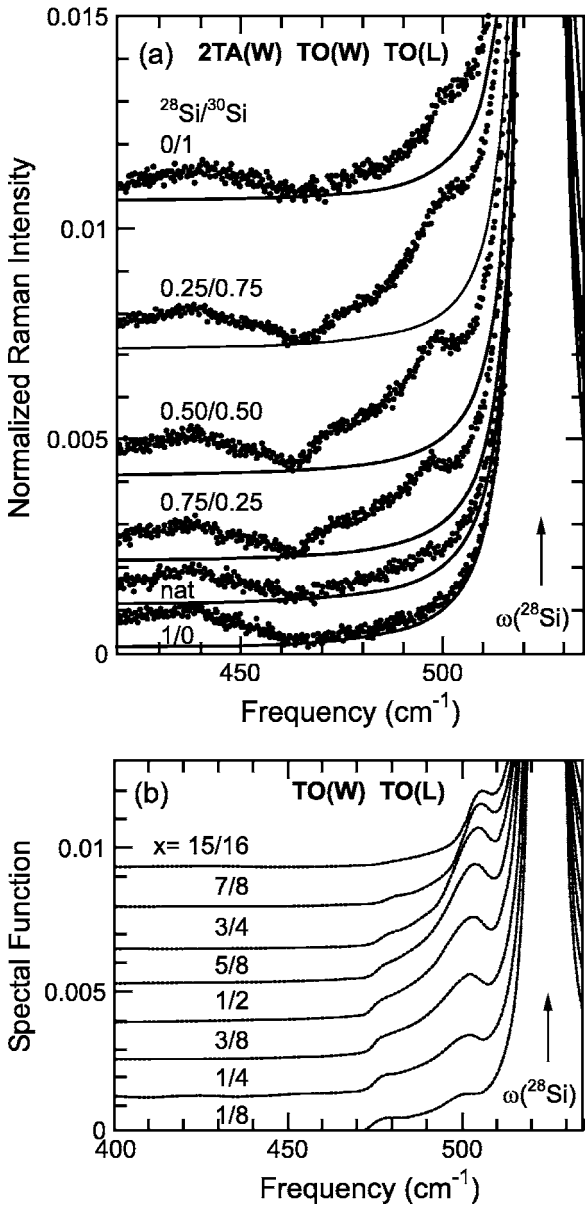

FIG. 16. (a) Spectra of six silicon crystals with several isotopic compositions, showing the disorder-induced density-of-states scattering in the 460–510-cm^{-1} region. The frequency scales have been shifted so as to cause the main Raman phonon peak to coincide for all samples. The height of this peak has been normalized to 1. The disorder-induced spectra show critical points of $N_{d1}(\omega)$ corresponding to TO (W) and TO (L). The 2TA band, centered at 440 cm^{-1}, is not disorder induced. (b) Isotope disorder-induced density-of-states spectra calculated with Eq. (3.13) using the frequency-dependent $\Gamma(\omega)$ and $\Delta(\omega)$. Note the similarity with the experimental results of Fig. 16(a). From Widulle *et al.*, 2001, with permission from Elsevier.

1948). The doublet splitting for $\boldsymbol{H}\|[111]$ has been measured to be 1.2 kHz in enriched (92%) ^{29}Si (Verhulst *et al.*, 2003) and 8 kHz for 99% ^{13}C diamond (Lefmann *et al.*, 1994).

The motivation for mentioning NMR in this section is provided by recent measurements performed for ^{73}Ge in crystals containing ^{73}Ge with $I=9/2$ (Verkhovskii *et al.*, 2003). In this case, nuclear quadrupole terms play an important role in determining the NMR line shape, especially in crystals with a low ^{73}Ge concentration: 0.1% for the crystals used by Verkhovskii *et al.* (2003). For these low concentrations, the effect of dipole-dipole interactions is rather small. Two types of crystals were used: one that was nearly isotopically pure (96% ^{70}Ge) and the other with 43% of ^{70}Ge and 48% of ^{76}Ge. The former can be considered as a nearly perfect cubic crystal for which the electric-field gradients at the ^{73}Ge nuclei vanish. Thus in the case of the nearly pure ^{70}Ge, the interaction of the electric-field gradient with the nuclear quadrupole moment is very small. In the ^{70}Ge-^{76}Ge mixed crystal, variations of the bond lengths around the randomly distributed isotopes, similar to those discussed in Sec. III.A.2, take place. They produce random strains as well as random variations of bond charges, which result in random electric-field gradients at the ^{73}Ge nuclei. These electric-field gradients, interacting with the nuclear quadrupole moments, lead to a broadening of the NMR spectra. Verkhovskii *et al.* (2003) have measured these broadenings and have calculated them using several parameters drawn from other experiments, e.g., the dependence of the lattice constant on isotopic mass (Sec. III.B.2). The observed inhomogeneously broadened line shapes are characterized by a linewidth parameter $\Delta\nu_Q$, which is proportional to $g_2^{1/2}$, not to g_2, as in most of the effects discussed so far. This proportionality is illustrated in Fig. 4 of Verkhovskii *et al.* (2003). We display in Fig. 17 the four NMR spectra measured by these authors for $^{70}Ge_{0.96}$ and $^{70}Ge_{0.43}$ $^{76}Ge_{0.48}$ with $\boldsymbol{H}\|[111]$ and $\boldsymbol{H}\|[100]$. The wings of the $^{70}Ge_{0.43}$ $^{76}Ge_{0.48}$ spectra are the signature of the mass disorder-induced quadrupole effects.

E. Local vibrational modes

We have, thus far, discussed the isotopic effects on the vibrations of chemically pure, but isotopically mixed, crystals. A related and very active research topic, with important scientific and technological applications, is the investigation of the local vibrational modes (LVMs) of chemical impurities in semiconductors, using either infrared absorption or Raman spectroscopy. An important aspect of these studies has involved changing the isotopic composition of the impurity species, and since only minute amounts of isotopically pure impurities are required, it started well before the current upsurge of work on host isotope effects, requiring the acquisition of macroscopic quantities of stable isotopes. As an example of early work see Hrostowski and Kaiser (1957). These authors used silicon doped with ^{18}O to demonstrate, on the basis of LVM spectroscopy, the structure of interstitial oxygen in Si (nonlinear Si-O-Si units). In view of the vast literature already extant for isotopic effects on LVMs, we shall confine this section to giving four references to review articles and a few specific references to recent original research, in particular, that in-

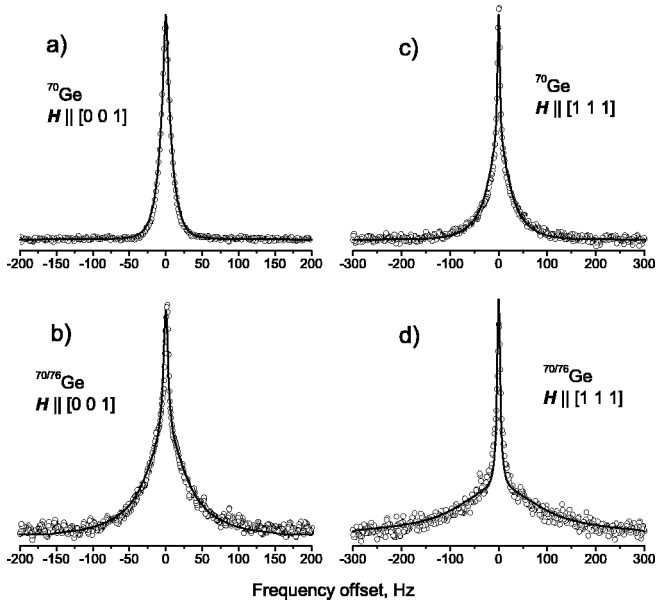

FIG. 17. NMR spectra of ^{73}Ge atoms in two Ge single crystals with different isotopic compositions. The experimental data are represented by circles. The solid lines correspond to calculations which take into account the quadrupole interaction induced by isotopic mass fluctuations. From Verkhovskii *et al.*, 2003.

volving host isotope effects, with some comments to the work they contain whenever appropriate.

The present understanding of the LVM of oxygen in Si was reviewed by Pajot (1994). This review also discussed effects of the natural isotopic abundances of three Si (host) isotopes on oxygen LVMs as well as isotopic effects of LVMs induced by carbon and hydrogen [for host effects on LVMs of oxygen in Si, see also the recent publication by Kato *et al.* (2003)]. A detailed account of LVMs of oxygen in Ge, including rotational effects and theoretical as well as experimental data, was given by Lassmann *et al.* (1999) and by Pajot *et al.* (1997, 2000). An analysis of the Ge-O-Ge vibrations using monoisotopic Ge as a host simplifies the interpretation of the LVMs (Mayur *et al.*, 1994). The interstitial oxygen vibrations in GaAs have been shown to be split due to the presence, as nearest neighbors, of the two Ga isotopes of the host (Schneider *et al.*, 1989). Similar topics, including the vibrations of substitutional impurities in II-VI compounds, were dealt with in a review by Stavola (1999). Another review article covering LVMs in GaAs, including substitutional impurities and impurity complexes (such as Si-Ge, Si-Cu, Si-Zn, Si-Li, Si-Li, and Si vacancy), also appeared in the series Semiconductors and Semimetals (Newman, 1993). An additional review covering most of the topics mentioned above has been authored by McCluskey (2000).

Recent work includes isotope effects on the LVM of O-Si:H in silicon (Bech-Nielsen *et al.*, 1997). We also mention an *ab initio* calculation of LVMs involving substitutional Se in ZnS and N in ZnSe, including all possible combinations of isotopes for the impurity and the nearest-neighbor host atom (resulting in 180 modes for nitrogen replacing Se in ZnSe; Petzke, 1999) and an experimental and theoretical study of the LVMs of protons placed interstitially in isotopically pure ^{28}Si, ^{29}Si, and ^{30}Si (Pereira *et al.*, 2003). We finally draw the reader's attention to work involving the lifetime and linewidth of LVMs (oxygen in Si and Ge) and its dependence on the isotopic mass of the impurity due to the shifts and change in overlap between the LVM energy and the density of states of the host phonons and their overtones (Sun *et al.*, 2004).

Davies *et al.* (2005) have compared a number of well-known impurity and defect-related LVMs between natural Si and ^{30}Si, and have developed an empirical model for the shifts of these transitions. Sennikov *et al.* (2005) have studied both the host-lattice modes and the carbon- and oxygen-related LVMs in ^{28}Si, ^{29}Si, and ^{30}Si, providing important information for the use of LVM-related spectroscopy in determining carbon and oxygen concentrations in isotopically modified silicon.

V. EFFECTS OF THE ELECTRON-PHONON INTERACTION ON THE FUNDAMENTAL OPTICAL SPECTRA

A. Introduction

1. The dielectric function

By *fundamental optical spectrum* of a solid we mean that which corresponds to optical transitions from occupied electronic states (the valence bands in the case of semiconductors or insulators) to empty states (the conduction bands in this case). In a perfect crystal these transitions must conserve the $\boldsymbol{k}$ vector (i.e., the crystal momentum of the electronic states). Since for photons in the optical range this vector is very small, the optical transitions must take place between valence and conduction states with the same $\boldsymbol{k}$ ($\boldsymbol{k}_c \simeq \boldsymbol{k}_v$, direct transitions). Semiconductors and insulators have the lowest transition energy above which direct transitions can occur. It is called the direct gap. In many cases the minimum energy difference between conduction and valence states corresponds to the direct gap (e.g., GaAs, ZnSe, CuCl). In others, however, transitions for which $\boldsymbol{k}_c \neq \boldsymbol{k}_v$ can take place below the direct gap. For optical excitation they require the contribution of a phonon or some kind of crystal disorder. These transitions are called indirect. The lowest gaps of some important semiconductors such as diamond, Ge, Si, and AlAs are indirect. For phonon-aided indirect transitions the observed optical absorption edge corresponds, at low T, to the electronic gap plus one phonon energy. Hence it depends on the isotopic mass through the relationship between phonon energy and mass (as we shall see later, the electronic energy difference between the band edges may also depend on $\langle M \rangle$). Such dependence has been investigated for diamond (Cardona and Ruf, 2001; see Fig. 15) and silicon (Karaiskaj *et al.*, 2002a).

The optical response of such crystals in the fundamental absorption region (and also below the gap) is de-

scribed by the complex dielectric function $\epsilon(\omega)=\epsilon_r(\omega)+i\epsilon_i(\omega)$. This function is usually a second-rank tensor since it connects two vectors, the electric field $\boldsymbol{E}$ and the displacement $\boldsymbol{D}$. We shall confine our discussion here, for simplicity, to cubic materials and neglect spatial dispersion effects [the dependence of $\epsilon(\omega)$ on photon wave vector; Yu and Cardona, 2005]. In this case $\epsilon(\omega)$ can be represented by a complex scalar function of ω. Its imaginary part is directly related to the joint density of states for interband transitions N_{cv} given by Eq. (2.1) with an additional factor of 2 to include spin degeneracy and $\omega=\omega_c(\boldsymbol{k})-\omega_v(\boldsymbol{k})$. The expression for $\epsilon_i(\omega)$ can thus be written to a good approximation (Cardona, 1969; Yu and Cardona, 1970), as

$$\epsilon_i(\omega)=\frac{4\pi^2}{\hbar}\left(\frac{e}{\omega m}\right)^2 P^2 N_{cv}(\omega), \tag{5.1}$$

where e (m) are the electron charge (mass), and P is an average matrix element of the linear momentum operator between valence and conduction states. The real part of $\epsilon(\omega)$ can be derived from $\epsilon_i(\omega)$ in a way similar to that used to derive Eq. (3.15) from Eq. (3.14), by employing the Kramers-Kronig relations (Yu and Cardona, 2005). We obtain

$$\epsilon_r(\omega)=\frac{8\pi}{\hbar}\left(\frac{e}{m}\right)^2\int_0^\infty \frac{N_{cv}(\omega')}{\omega'[(\omega')^2-\omega^2]}d\omega'. \tag{5.2}$$

Equations (5.1) and (5.2) will show van Hove singularities or critical points whenever $\nabla_{\boldsymbol{k}}(\omega_c-\omega_v)=0$ [see Eq. (2.1)]. These singularities have characteristic forms that have been discussed in detail by Yu and Cardona (2005). They are seen in the optical spectra, especially through the use of modulation spectroscopy (Cardona, 1969). An excellent technique for pinpointing such critical points and measuring their parameters is spectral ellipsometry followed by numerical differentiation of the $\epsilon_r(\omega)$ and $\epsilon_i(\omega)$ spectra obtained.

Figure 18 displays the electronic band structure of germanium. The vertical arrows indicate the critical points corresponding to direct transitions. The lowest direct critical point is labeled E_0. We note that about $\Delta_0=0.3$ eV higher in energy than E_0 there is another critical point, spin-orbit split from E_0, which is not explicitly labeled in Fig. 18. It is usually called $E_0+\Delta_0$ and corresponds to transitions between the Γ_7^+ states and the Γ_7^- states. The E_1 and $E_1+\Delta_1$ critical points, also spin-orbit split, will be discussed in Sec. V.B.1 in connection with isotopic effects.

Full experimental spectra of $\epsilon(\omega)$ appeared in the late 1950s and there was increasing activity in the field in the 1960s. The development of spectral ellipsometry in the 1970s led to renewed activity that has lasted until the present day (Aspnes and Studna, 1983; Aspnes, 2004). Soon after the first reliable spectra became available, theoretical efforts were begun to try to understand them on the basis of semiempirical theoretical band structures (the only kind available then). The first successful attempt seems to have been that of Brust *et al.* (1962).

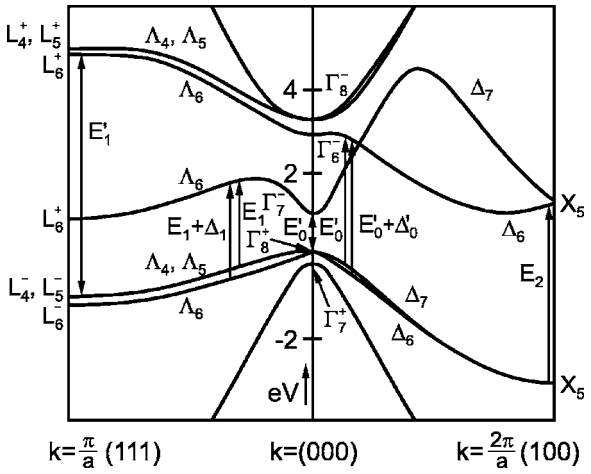

FIG. 18. Electronic band structure of germanium with the double-group (including spin) notation corresponding to high-symmetry points and directions. The vertical arrows indicate the direct interband transitions that dominate the fundamental optical spectra. The lowest gap is indirect, between Γ_8^+ and L_6^-. Adapted from Yu and Cardona, 2005, Fig. 6.13.

These authors calculated the $\epsilon_i(\omega)$ spectrum of Ge using Eq. (5.1) and treating P^2 as an adjustable parameter. The pseudopotential band structure used was similar to that of Fig. 18, except for the lack of spin-orbit coupling. Hence the splitting of the $E_1-(E_1+\Delta_1)$ critical points, observed experimentally, was not reproduced by the calculation.

2. *Ab initio* calculations

Soon after the work just mentioned, calculations including realistic, not average, matrix elements P and spin-orbit splittings appeared. For a review, see Cohen and Chelikowsky (1989).

The introduction of *ab initio* techniques based on the local-density approximation resulted, initially, in some disappointment. The calculated gaps, in particular the lowest one, were much too small. One soon realized that the local-density functional need not be the same for the crystal with either an electron in the conduction band or a hole in the valence band, a fact that could explain the discrepancy just mentioned (Perdew and Levy, 1983; Sham and Schluter, 1983).

This is the gap problem of the local-density approximation and can be rather striking. The lowest gap of germanium turns out to be negative (i.e., Ge would be a metal in a fully relativistic local-density-approximation calculation; Bachelet and Christensen, 1985). A number of attempts to solve this problem have been made. The most successful one is based on the *GW* approximation (Hybertsen and Louie, 1986). In this approach, the local-density exchange and correlation functional is replaced by a complex self-energy, whose calculation will be briefly discussed below. Hence the electrons and holes become quasiparticles. The real part of the self-energy effects a shift in their energy, whereas its imaginary part introduces a broadening in a way similar to the self-

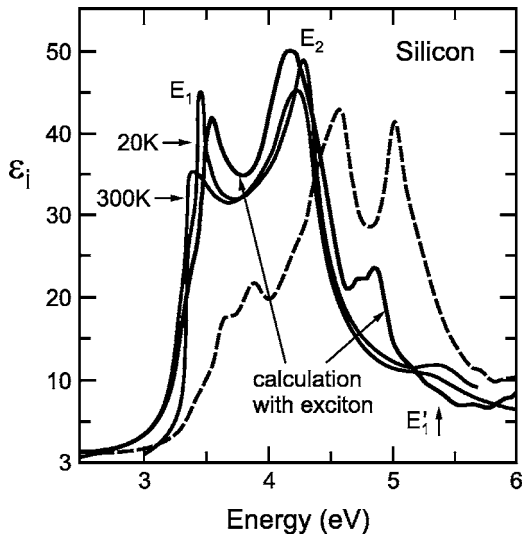

FIG. 19. Spectral dependence of the imaginary part of the dielectric function of silicon measured at 20 and 300 K. The dashed line represents the spectrum calculated *ab initio* without excitonic interaction. The thick solid line corresponds to such calculation including exciton effects. From Cardona *et al.*, 1999, and Albrecht *et al.*, 1998.

energies of phonons described in Secs. III.B.3 and IV.B. The self-energy is discontinuous at the lowest gap, thus introducing significant corrections to the gap energy, which for Ge ends up being 0.75 eV, in excellent agreement with the experimental value (0.74 eV at 0 K).

The self-energy is obtained by appropriately convoluting the bare single-particle Green's function with the screened Coulomb interaction (containing both direct and exchange contributions). This task reduces mainly to the determination of a manageable frequency and wave-vector-dependent dielectric screening matrix $\epsilon^{-1}(\omega,\boldsymbol{k})$, which has been described in detail by Hybertsen and Louie (1986). This *GW* procedure leads to correct energy gaps and single quasiparticle energies (including widths) for conduction electrons and valence holes. It still does not lead to a correct description of the two-particle excitation spectra as represented by $\epsilon_i(\omega)$ (Albrecht *et al.*, 1998). This is illustrated in Fig. 19 for silicon, where $\epsilon_i(\omega)$ spectra measured at 300 and 20 K are compared with calculations based on the quasiparticle band structure (dashed line). This comparison reveals a general trend for tetrahedral semiconductors. The calculated $\epsilon_i(\omega)$ is lower than the experimental one at the E_1 critical point, the missing spectral strength having been transferred to higher energies (between E_2 and E_1'). This problem is solved by considering that $\epsilon_i(\omega)$ is due to two-particle excitations, the excitons, consisting of a conduction electron and a valence hole. The experimental spectra are well reproduced (see solid curve labeled "calculation with exciton," Fig. 19). It is clear that the calculated spectrum agrees better with that measured at 20 K than with that for 300 K, especially around the E_1 critical point. With increasing temperature the spectrum is modified by the electron-phonon interaction, not included to date in any such calculations. Even measurements at the lowest possible temperatures are affected by the zero-point vibrations, as discussed in Sec. V.B.2.

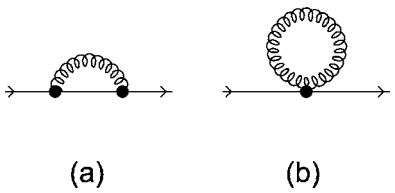

FIG. 20. Feynman diagrams representing the electron-phonon interaction that renormalizes the gap energies. (a) Self-energy diagram (also known as Fan diagram). (b) Debye-Waller (also known as Antončík or Yu-Brooks) terms. The former contribute a real and an imaginary part to the critical-point energy, the latter only a real part.

B. Electron-phonon interaction effects

1. Effect of the electron-phonon interaction on electronic states and interband transitions: Germanium and diamond

State-of-the-art calculations of critical-point energies in semiconductors, including *GW* self-energies and exciton interaction, are generally believed to reproduce the experimental data to better than 100 meV. Yet, they neglect the effect of electron-phonon interaction. As we shall see, the electron-phonon-interaction effects on the electronic band structure pose a rather formidable theoretical problem. Except for a calculation by King-Smith *et al.* (1989) based on an *ab initio* band structure, most calculations have been performed by combining a semiempirical phonon dispersion relation and the corresponding eigenvectors with a semiempirical band structure. We discuss next the general principles behind the effects of electron-phonon interaction on optical spectra and the corresponding calculations.

The Feynman diagrams that represent the renormalization of electronic states to second order in the phonon amplitude are shown in Fig. 20. The first-order terms cancel when taking the average over u in the harmonic approximation since $\langle u\rangle=0$. Note the similarity of this figure with Figs. 4(a) and 4(b). Figure 20(a) corresponds to the first-order electron-phonon interaction using second-order perturbation theory, whereas Fig. 20(b) represents the second-order electron-phonon interaction with first-order perturbation theory. Figure 20(a) is a self-energy diagram and effects a shift as well as a broadening of the corresponding electronic states. Figure 20(b), similar to Fig. 4(b), corresponds only to an energy shift. In order to have an imaginary part of the self-energy, $\Sigma_i(\omega)$, one must have an energy-conserving intermediate state in Fig. 20(a), i.e., the energy of the electronic state under consideration must equal that of the intermediate state plus or minus (for $T\neq 0$) the phonon energy. Note the similarity of these considerations with those made in connection with Figs. 4(a) and 4(b).

Both diagrams in Figs. 20(a) and 20(b) must be taken together since they correspond to effects proportional to $\langle u^2 \rangle$. Diagram 20(a) represents what are usually called the Fan terms and was taken as the only contribution to the electron-phonon renormalization of gaps in early work. Diagram 20(b) represents the Debye-Waller or Antončik (sometimes, inappropriately, Yu-Brooks) terms. Again, it was often taken to be the only contribution in some early publications, thus implying that the Fan and Antončik [Figs. 20(a) and 20(b)] terms represented different, alternative theories, instead of complementary terms to the same order in u and in T.

In a pseudopotential calculation, however, each of these terms is not uniquely defined, only their sum is. For a review see Cardona (2001a, 2001b) and Allen and Cardona (1981, 1983).

We have mentioned above that the first-order term in u vanishes in the harmonic approximation. It does not vanish in the presence of the anharmonic terms that are responsible for the thermal expansion and the zero-point renormalization of a_0 (Sec. III.B.2). Hence the additional thermal-expansion term

$$\Delta E_g^{\mathrm{te}} = \frac{\Delta a_0}{a_0}\left(\frac{\partial E_g}{\partial \ln a_0}\right)_T \tag{5.3}$$

must be added to the shifts corresponding to Figs. 20(a) and 20(b). In Eq. (5.3) $(\partial E_g/\partial \ln a_0)_T$ is the hydrostatic deformation potential of the critical point or gap E_g, which can be obtained from either an *ab initio* band-structure calculation or measured in an experiment performed under hydrostatic pressure. As discussed in Sec. III.B.2, this term can be represented by a Bose-Einstein function except at very low temperatures, at which one must take into account the nonmonotonic T dependence of $\Delta a_0/a_0$ if the gap measurements are sufficiently accurate (see Sec. VI).

We discuss next the terms in Figs. 20(a) and 20(b). The latter (Debye-Waller term) leads to an energy shift (for monatomic crystals):

$$\Delta E_g^{\mathrm{DW}} = \sum_{\boldsymbol{q},j} \frac{A^{\mathrm{DW}}(n,\boldsymbol{q})}{\omega_{\boldsymbol{q}j} M}[2n_B(\omega_{\boldsymbol{q}j}) + 1], \tag{5.4}$$

where A^{DW} is proportional to squared matrix elements of the electron–two-phonon interaction, M is the average isotopic mass, and $\omega_{\boldsymbol{q}j}$ the virtual-crystal frequency (if several isotopes are present). Figure 20(a) leads to a self-energy $\Sigma^{ep} = \Sigma_r + i\Sigma_i$ for direct electron-hole excitations[10] with an imaginary part that vanishes below the energy $E_{0,i} - \hbar\omega_{\boldsymbol{q}j}$, where $E_{0,i}$ represents the lowest gap, direct or indirect, as the case may be. This fact is very important at the indirect gap of silicon, as discussed in Sec. VI. Above the lowest gap, $-\Sigma_i$ soon reaches values of the order of 50 meV, close to or larger than the phonon frequencies. Because of this broadening, the phonon frequencies are usually neglected in the corresponding perturbation theoretical expression, but keep in mind that when dealing with transitions involving the lowest conduction or the highest valence states these frequencies must be restored in the corresponding expression, which for the imaginary part of Σ is

$$\Sigma_i^g = -\pi \sum_{\boldsymbol{q}j} [|V_{\boldsymbol{q}jc}^{ep}|^2 \delta(E_g^c - E_{\boldsymbol{q}j}) + |V_{\boldsymbol{q}jv}^{ep}|^2 \delta(E_g^v - E_{\boldsymbol{q}j})] \times [1 + 2n_B(\omega_{\boldsymbol{q}j})], \tag{5.5}$$

where $V_{\boldsymbol{q}jc}^{ep}$ and $V_{\boldsymbol{q}jv}^{ep}$ are the matrix elements of the electron-phonon Hamiltonian for energy-conserving transitions within the conduction and valence bands, respectively. In order to transform Eq. (5.5) into an expression containing the densities of conduction and valence states [similar to Eq. (3.14)], we must take $|V_{\boldsymbol{q}jc}^{ep}|^2[1 + 2n_B(\omega_{\boldsymbol{q}j})]$ and the corresponding equation for the valence band as averages out of the summation signs. Singularities in Σ_i^g will therefore appear at energies E_c and E_v for which there are singularities in the densities of states.

The real parts of Σ^g are obtained from the corresponding imaginary parts by application of the dispersion relations in a way similar to that used to convert Eq. (3.14) into Eq. (3.15). The δ functions in Eq. (5.5) are then replaced by energy denominators and all states, valence as well as conduction, contribute to Σ_r^g as virtual transition states. Those that are above E_g^c lower the gap, while those that are below raise the gap, whereas the opposite is true for E_g^v since $E_g = E_g^c - E_g^v$.

As in the cases of the temperature and mass dependence of phonon properties (see Secs. III.B.2 and III.B.3), the real self-energy effects [plus the thermal expansion and the effect of Eq. (5.4)] on critical-point energies, including the lowest indirect gaps of Si, Ge, and diamond, can be handled by replacing the Bose-Einstein factors by an average single oscillator. One must also keep in mind that the *e-p* matrix elements are proportional to $(\omega_{\boldsymbol{q}j}M)^{-1}$, i.e., to $M^{-1/2}$. Hence at low temperatures, all self-energy effects on the fundamental optical spectra should be proportional to $M^{-1/2}$ for monatomic crystals.

As discussed in connection with Eq. (3.8), the single-oscillator approximation cannot be used at very low temperatures if sufficient resolution (both instrumental and in terms of the natural linewidth) is available. The reason is the linear (Debye) dispersion relation of the acoustic phonons which cannot be approximated by a single oscillator. As in the case of Eq. (3.8), this leads to a T^4 dependence for Σ_r and also for the other two contributions to the shift of critical-point energies with temperature. Such effects have been observed for silicon and discussed in Sec. VI.

2. Dependence of gaps on temperature and isotopic mass: Typical examples

Before going into the description of the theoretical work on temperature and isotopic mass dependence of

[10]We neglect in the present discussion exciton effects. They can be, to a first approximation, introduced after *e-p* renormalization of the corresponding electron and hole states.

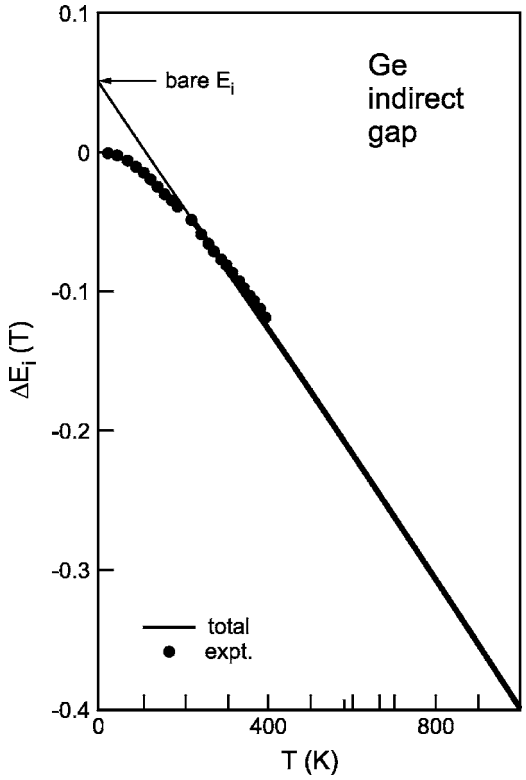

FIG. 21. Temperature dependence of the indirect gap measured for Ge (dots). The solid line (through the points and at higher temperatures) represents a fit with a single oscillator (see text). The thin line below 200 K represents the linear extrapolation of the single-oscillator fit to $T=0$, used to determine the zero-point renormalization of −53 meV.

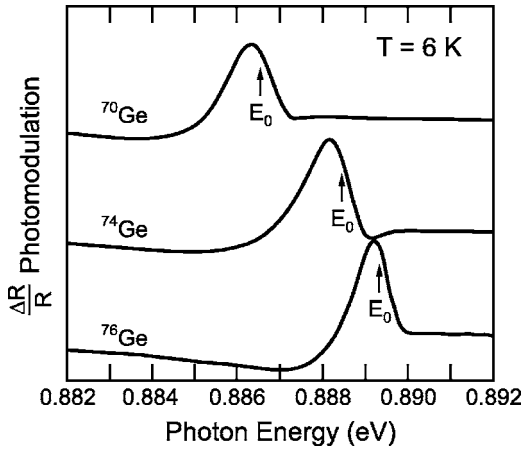

FIG. 22. Photomodulated reflectivity used to determine the E_0 direct gap of single crystals of ^{70}Ge, ^{74}Ge, and ^{76}Ge, at $T=6$ K. From Parks *et al.*, 1994.

critical-point energies, we give a few typical examples of single-oscillator fits to experimental data on the temperature dependence of gaps, and the consequences derived from them.

We plot in Fig. 21 the indirect gap of germanium measured versus temperature (dots) by Thurmond (1975). The continuous line through and above the dots represents the single-oscillator fit:

$$\Delta E_i(T) = 53(1 + 2[e^{235/T} - 1]^{-1}) \text{ meV}, \tag{5.6}$$

with T in K. Hence the single-oscillator frequency amounts to 235 K = 164 cm^{-1}, slightly more than half the Raman frequency of natural Ge (302 cm^{-1}). The fitted value of 164 cm^{-1} is thus reasonable as an average vibrational frequency of natural Ge. The gap E_i has been measured to shift up by 2.2 meV at low T from ^{70}Ge to ^{76}Ge (Etchegoin *et al.*, 1992). Using the $M^{-1/2}$ dependence of the zero-point mass renormalization we obtain

$$\Delta E_i(0) = -2 \times 2.2 \times \frac{M}{\Delta M} = -53.5 \text{ meV}, \tag{5.7}$$

in excellent agreement with the value obtained by the linear extrapolation method (−53 meV; see Fig. 21). In Ge it is also possible to measure rather accurately the lowest direct gap E_0 and its temperature dependence. The reason is that its energy is 0.90 eV at 4.2 K, only slightly above the lowest indirect gap (0.74 eV at 4.2 K). Actually, even the $E_0+\Delta_0$ gap and its dependence on isotopic mass can be measured (Parks *et al.*, 1994). The temperature dependence of E_0 for Ge has been already shown in Fig. 21. The extrapolation to $T=0$ of the linear dependence found at high temperature gives a zero-point renormalization of −60 meV, which is found to correspond, using Eq. (5.7), to an isotopic effect between ^{70}Ge and ^{76}Ge of 2.5 meV.

The value measured directly by Parks *et al.* (1994) is also 2.5 meV (see Fig. 22). The value of −370 meV found for the zero-point renormalization of E_i in diamond (see Fig. 23) can be used to obtain the dependence on isotopic mass by means of the $M^{-1/2}$ rule [Eq. (5.7)]. We find

$$\frac{dE_i(0)}{dM} = \frac{1}{2} \times 370 \times \frac{1}{13} = 14.2 \text{ meV/amu}. \tag{5.8}$$

This value of the isotope mass derivative agrees well with that determined by measuring the shifts of spectral features associated with E_i in diamond (13.6 meV/amu; Collins *et al.*, 1990).

3. Band-structure and lattice dynamical calculations of electron-phonon interaction effects

We have so far treated electron-phonon interaction effects with a phenomenological ansatz involving the approximation of the dispersion relations with a single Einstein oscillator whose frequency was a suitable average of all phonon frequencies. This ansatz turned out to be appropriate for describing the temperature dependence of the lowest gaps of diamond, silicon, and germanium, except for the indirect gap of silicon at very low temperatures ($T \leqslant 10$ K) where, because of the highly accurate data available, a T^4 dependence had to be used (Sec. VI). Through the simple device of linear extrapolation to $T=0$ of the dependence on T found at high temperatures, we have been able to obtain the zero-point renormalization of electronic states produced by

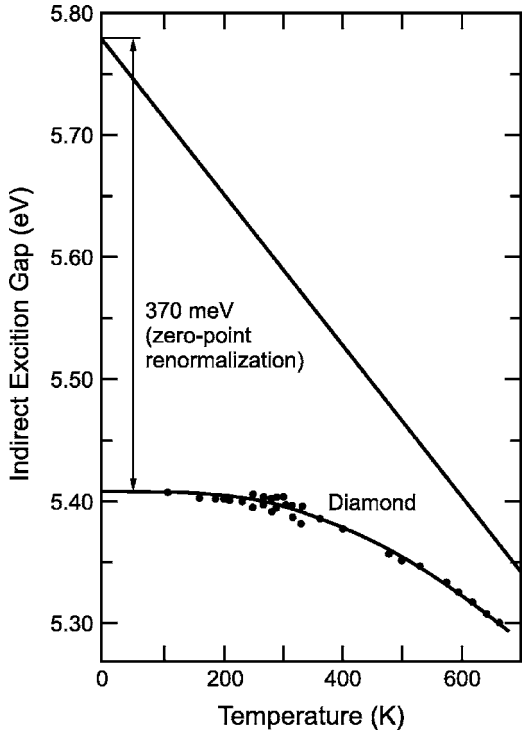

FIG. 23. Indirect exciton gap of diamond measured by Clark *et al.* (1964). The temperature range does not suffice to pinpoint the linear behavior expected at high temperatures, but a single-oscillator fit ($\langle\omega_{\rm ph}\rangle \simeq 1080\ {\rm cm}^{-1}$, see curve drawn through experimental points) helps (fit parameters from Pässler, 2001). The extrapolation of the linear behavior of the fitted curve at high T as a straight line to $T=0$ leads to a zero-point gap renormalization of −370 meV, much larger than the accuracy of 100 meV often claimed for full-blown *ab initio* calculations.

the electron-phonon interaction. In order to perform this extrapolation, fits to the experimental data versus T with any of several analytic expressions that reproduce the linear dependence at high T can be used. The single-oscillator Bose-Einstein factor is the simplest and physically most transparent of these expressions. As in the case of the specific heat (Nernst and Lindemann, 1911), two isolated oscillators can also be used to improve the quality of the fits to the temperature dependence of electronic gaps and critical points (Manoogian and Leclerc, 1979; Göbel, Ruf, *et al.*, 1998; Pässler, 2001). While the improvement achieved with the two-oscillator model for the group-IV semiconductors is not very significant, it may be in binary compounds, especially those in which the cation and anion masses are very different (Pässler, 2001). In semiconductors containing *d* electrons in the valence bands (e.g., the copper and silver halides and the corresponding chalcopyrites; Manoogian and Leclerc, 1979; Göbel, Ruf, *et al.* 1998; Serrano *et al.*, 2002), the contributions of the two oscillators in a two-oscillator fit turn out to have opposite signs!

Before discussing *ab initio* calculations of the effect of electron-phonon interaction on electronic states, we mention a few fully phenomenological expressions, without much physical content, which have been used to describe the temperature dependence of gaps. The most commonly used one is Varshni's expression (Varshni, 1967):

$$E_g(T) = E_g(0) - \frac{\alpha T^2}{\beta + T}. \tag{5.9}$$

This expression becomes linear in T at high T and thus can be used in the extrapolation procedure to determine unrenormalized gaps at $T=0$. It has, however, the problem of yielding a temperature dependence $\propto T^2$ at low T, instead of the T^4 predicted theoretically and observed experimentally for silicon (Sec. VI). This drawback has been illustrated for silicon in Fig. 4 of Cardona (2001b), where it was shown that in the case of silicon $E_i(T)$ below 50 K falls midway between the fit with Eq. (5.9) and the single-oscillator fit. In order to remedy this problem, Pässler (1999) proposed a number of other expressions, typically of the type

$$E_g(T) = E_g(0) - \frac{\alpha\Theta_p}{2}\left[\sqrt[p]{1+\left(\frac{2T}{\Theta_p}\right)^p} - 1\right], \tag{5.10}$$

with three adjustable parameters: α (units of meV K^{-1}), Θ_p (an average phonon temperature in units of K), and a dimensionless parameter p. For large T, Eq. (5.10) reproduces the linear temperature of the gap, whereas at low T it yields

$$E_g(T) \cong E_g(0) - \frac{\alpha\Theta}{2p}\left(\frac{2T}{\Theta}\right)^p. \tag{5.11}$$

Equation (5.11) reproduces the T^4 behavior for $p=4$. Pässler gave fitted values of p for 22 semiconductors (Table I of Pässler, 1999). They lie in the $2 \leqslant p \leqslant 3.3$ range. The reason why this value of p is lower than the expected value of 4 probably lies in the nature of the fit, which goes well beyond the T range of validity of the T^4 law.

Note that Eq. (5.10) leads to the following expression for the zero-point renormalization of E_g:

$$\Delta_g(0) = -\frac{\alpha\Theta_p}{2}. \tag{5.12}$$

From the values of α and Θ_p given in Table I of Pässler (1999) we find $\Delta_g(0) = 270$ meV for the indirect gap of diamond, 65 meV for that of Si, and 47 meV for that of Ge, in reasonable agreement with those given in Sec. V.B.2.

The only *ab initio* calculation of the temperature dependence of a gap (and, by extrapolation, of the zero-point electron-phonon renormalization) is that of King-Smith *et al.* (1989). For this calculation they used an approach rather different from that described by the diagrams of Fig. 20. They considered the energy of a solid in its ground state at a temperature T to be the electronic energy plus that of all phonons excited at that temperature. After exciting an electron-hole pair, the energy equals the electronic energy of the crystal with an electron missing at the top of the valence band, which

has been transferred to the bottom of the conduction band. To this energy one must add that of the corresponding phonons. The gap renormalization results from the fact that the phonon frequencies are not the same in the electronic ground state as in the state that contains an electron-hole excitations. The phonon frequencies actually decrease when the electron-hole pair is excited, a fact that results in a decrease of the gap with increasing temperature.

The *ab initio* calculation proceeds as follows. The electronic band structure is calculated with an *ab initio* pseudopotential using the local-density approximation. The harmonic frequencies of 60 phonons are then calculated using the frozen-phonon technique (Sec. II.C) and a large supercell (containing 16 atoms) in order to obtain phonons with $\boldsymbol{q}\neq\mathbf{0}$. This procedure is carried out twice: first for the electronic ground state and next for a state with 1% of valence electrons missing at the top of the valence band, which have been transferred to the bottom of the conduction band. The differences in the two frequencies, multiplied by the appropriate Bose-Einstein factors, give the temperature dependence of the gap after proper normalization to the crystal volume and one single excited pair (instead of 1% of the valence electrons).

The calculated temperature dependence is about two-thirds of the measured one, which is rather satisfactory when one considers that the calculation is *ab initio* and without adjustable parameters. The zero-point renormalization obtained with the linear extrapolation method from the calculated temperature dependence (see Fig. 2 of King-Smith *et al.*, 1989) is about 40 meV, somewhat smaller than estimates based on experimental data (see above and also Sec. VI). King-Smith *et al.* (1989) mentioned the interesting fact that all phonon branches contribute approximately an equal amount to the decrease in the indirect gap of Si with T.

All other available calculations of *e-p* renormalizations of electronic states evaluate the diagrams of Fig. 20 using several types of semiempirical band structures (e.g., pseudopotential, linear combination of atomic orbitals) and lattice dynamics (shell models, bond-charge models). The thermal-expansion effect is added separately. It is unfortunate that no such calculations are available for the Cu and Ag halides and related materials (Serrano *et al.*, 2002). For these materials, the vibrations of the copper (or silver) induce an increase in the gap with increasing temperature (and, correspondingly, a positive zero-point renormalization, as opposed to the vibrations of the anion, which lead to effects of the opposite sign).

The empirical linear-combination of atomic orbitals (also called tight-binding) method uses electronic band structures fitted to experimental data (Krishnamurty *et al.*, 1995). The atomic displacements associated with the various phonons and their eigenvectors induce changes in the matrix elements of the Hamiltonian corresponding to the overlap of wave functions of nearest-neighbor atoms (a sampling over the whole BZ is performed). This change is estimated with the conventional assumption that the matrix elements of the Hamiltonian are proportional to d^{-n}, where d is the bond length and n a number of the order of 2 (Olguin *et al.*, 2002). The perturbation Hamiltonian contains terms proportional to the first derivative of the overlap integrals with respect to d [corresponding to Fig. 20(a)] and also terms proportional to its second derivative [Fig. 20(b)]. For the exponent n the universal value $n=2$ has been proposed by Harrison (1989). More recent values of n, which differ somewhat from 2 depending on whether one considers *s-s*, *s-p*, or *p-p* overlap, have been used by Olguin *et al.* (2002). These authors calculated the temperature dependence of the lowest direct gaps of Ge, GaAs, InAs, ZnS, ZnSe, ZnTe, and CdTe and the corresponding dependence of the gap at $T=0$ on isotopic masses based on either the shell model or bond-charge-model lattice dynamics.

Figure 24 shows $E_0(T)$ calculated for GaAs with the shell model (solid curve) and the bond-charge model (dashed curve), including the effect of thermal expansion (dotted curve). The dots represent the experimental points, which follow rather closely the calculated curves. Olguin *et al.* (2002) also calculated $dE_0/dM_{\mathrm{Ga}}=0.35$ meV/amu (we give here the average of the two values obtained with the shell and bond-charge models), which agrees remarkably well with the experimental value of 0.39(6) meV/amu (Garro *et al.*, 1996). Although only one stable isotope of As exists, they also calculated $dE_0/dM_{\mathrm{As}}=0.37$ meV/amu. The dE_0/dM calculated for the direct gap of germanium (average bond-charge model and shell model) is 0.61 meV/amu, whereas the experimental one is 0.49 meV/amu (Parks *et al.*, 1994).

The band structure most commonly used for the calculation of electron-phonon effects in semiconductors is based on empirical pseudopotentials. The first and second derivatives of the pseudopotential are calculated on the basis of the rigid-ion model in which the crystal pseudopotential is constructed as a combination of atomic pseudopotential form factors $V_i(\boldsymbol{k})$ multiplied by the appropriate structure factors.

For a group-IV semiconductor we find the crystal pseudopotential $V(\boldsymbol{G})$:

$$V(\boldsymbol{G})=V_i(\boldsymbol{G})[e^{i\boldsymbol{G}\boldsymbol{\tau}}+e^{-i\boldsymbol{G}\boldsymbol{\tau}}], \tag{5.13}$$

where $\boldsymbol{G}$ are reciprocal-lattice vectors and $\boldsymbol{\tau}=(G_0/8)(111)$ for the undistorted crystal. One usually adjusts the magnitudes of the three shortest $\boldsymbol{G}$'s to experimental data (in general optical gaps) and then interpolates and extrapolates the three empirical values of $|\boldsymbol{G}|$ either with a spline or with a theoretical expression. When following this procedure, one must make a choice concerning the extrapolation of $V_i(\boldsymbol{G})$ to $|\boldsymbol{G}|=0$. Two types of ansatz are used, the respective results not being very different from each other: (a) $V_i(0)=0$ and (b) $V_i(0)=-2E_F/3$, where E_F is the Fermi energy of a metal with an electron density equal to the valence electron density (Allen and Cardona, 1983). The derivatives of $V(\boldsymbol{G})$ with respect to the phonon displacements (obtained from the corresponding

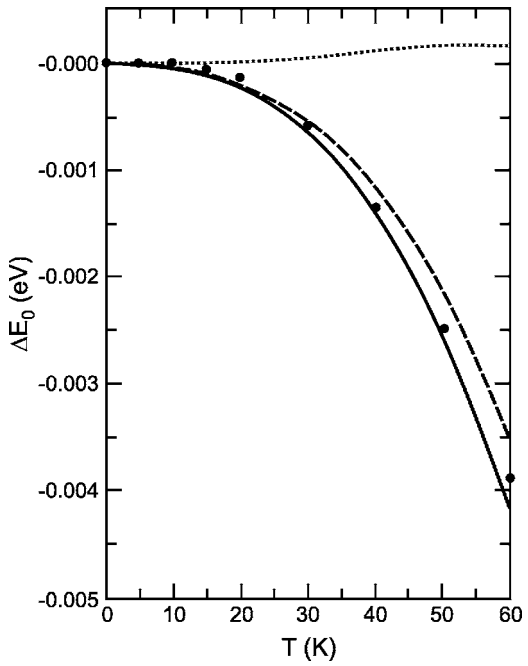

FIG. 24. Temperature dependence of the direct gap ΔE_0 for GaAs from low to room temperatures. The dots represent experimental data. The dotted line corresponds to the thermal-expansion term. The total contribution (thermal-expansion plus *e-p* terms) to ΔE_0 is represented by solid (shell model) and dashed (bond-charge model) lines. From Olguin *et al.*, 2002, with permission from Elsevier.

eigenvectors) are found after adding these displacements to $\boldsymbol{\tau}$ in Eq. (5.13).

The contribution of the diagram in Fig. 20(b) to the temperature dependence of an electronic state is obtained from the second derivative of Eq. (5.13) with respect to the displacement $\boldsymbol{u}$. This contribution can be evaluated in a rather simple way by replacing $V(\boldsymbol{G})$ in the band-structure calculation with $\tilde{V}(\boldsymbol{G})$:

$$\tilde{V}(\boldsymbol{G}) = V(\boldsymbol{G})\, e^{-(1/6)\langle u^2\rangle |\boldsymbol{G}|^2}, \tag{5.14}$$

where $\langle u^2\rangle$ is the average phonon displacement squared. The second factor on the right-hand side of Eq. (5.14) is the Debye-Waller factor which appears in many other fields of crystal physics.[11] The difference between the energy of a given electronic state obtained with Eq. (5.14) and that obtained with Eq. (5.13) gives the contribution of the diagram in Fig. 20(b) with the temperature effect under consideration. Note, however, that the exponential in Eq. (5.14) contains not only terms proportional to $\langle u^2\rangle$ (i.e., linear in T at high T) but all iterations of Fig. 20(b) terms to all orders in $\langle u^2\rangle$. Below the melting point, however, the higher-order terms can usually be neglected.

The simplicity of the calculation of the Debye-Waller terms resulted in its nearly exclusive use for calculating $E_g(T)$ while completely neglecting the Fan terms [Fig. 20(a); see Cohen and Chadi, 1980] until the early 1980s (Allen and Cardona, 1983; Lautenschlager, Allen, *et al.*, 1985).

The first articles in which both diagrams of Fig. 20 were evaluated presented electronic energies versus T without reporting explicitly the zero-point renormalization Δ. [It can nevertheless be extracted from $E(T)$ data by the linear extrapolation procedure.] The reason is that experimental determinations of Δ were not available due to the lack of isotopically modified crystals. As soon as such crystals became available (in the late 1980s), all calculations of $E(T)$ paid attention to zero-point renormalizations and the corresponding widths when finite.

We mention a rather exhaustive study of zero-point effects and temperature dependence of electronic states at high-symmetry points of the BZ performed for diamond and germanium using pseudopotential band structures and bond-charge-model lattice dynamics (Zollner *et al.*, 1992). For the indirect gap of diamond, a zero-point renormalization of −610 meV was calculated, even larger than the measured one (−340 meV, Cardona, 2001a; see also Sec. V.B.1 where the value of −370 meV is given). For the indirect gap of germanium the calculated zero-point renormalization was −56 meV, in rather good agreement with the experimental value (−53 meV; Parks *et al.*, 1994). The corresponding renormalization for the direct gap of Ge was calculated to be −62 meV, also in reasonable agreement with experimental data (−71 meV, Parks *et al.*, 1994). We note, however, that Parks *et al.* (1994) measured for the zero-point renormalization of the spin-orbit-split direct gap of Ge $(E_0+\Delta_0)$ the value −108 meV, which is hard to understand since one would expect this renormalization to be very similar to that of the E_0 gap.

The gap renormalization given above for diamond is nearly an order of magnitude larger than that found for germanium and silicon. This surprising result has been attributed to the lack of *p* electrons in the carbon cores (Cardona, 2005). It has also been related to the recent discovery of superconductivity in heavily boron-doped diamond (Ekimov *et al.*, 2004; Cardona, 2005).

A particularly interesting case is that of the lead chalcogenides (PbS, PbSe, PbTe) for which the lowest direct gap increases with increasing temperature (Paul and Jones, 1953; Laff, 1965). The thermal-expansion contribution also has an anomalous sign and accounts for about half of the measured temperature dependence of the gap. The Debye-Waller term of Fig. 20(b) was evaluated by Tsang and Cohen (1971) for PbTe. Together with the thermal-expansion contribution, it accounts rather well for the observed temperature dependence of the gap of PbTe up to ~400 K (see Fig. 3 of Cohen and Chadi, 1980). The available experimental data suggest a saturation of $E_0(T)$ above 400 K, which may be similar to the effect observed in CuCl (Göbel, Ruf, *et al.*, 1998) but requires additional confirmation. The isotopic mass derivatives of the lowest gaps and the corresponding

[11]Note that Eq. (5.14) is only valid for monatomic crystals. Generalization to the polyatomic case is straightforward.

zero-point mass renormalizations measured or calculated for a number of tetrahedral semiconductors are listed in Table III together with the linear temperature coefficients found at high T.

We discuss next the calculations of electron-phonon renormalization of the E_1 critical points that have been performed for germanium and silicon (Lautenschlager *et al.*, 1985) and compare them with experimental results. Since the E_1 interband critical points of Ge and Si overlap with the continuum of interband transitions, the corresponding self-energy has not only a real part but also an imaginary one (Lautenschlager *et al.*, 1986) which contributes to the measured Lorentzian width of the corresponding optical spectra. The calculation of the Fan and Debye-Waller terms of Fig. 20 must be performed not only at the edge of the BZ (see Fig. 18) but also for several Λ points along the Γ-L direction since they all contribute to the E_1 transitions. The existing calculations have not included spin-orbit coupling, which is clearly observed in the experimental spectra for Ge (E_1 and $E_1+\Delta_1$ critical points) but not for Si. This was done under the assumption, corroborated by the experiments, that Δ_1 is temperature independent, i.e., that E_1 and $E_1+\Delta_1$ behave the same way when the *e-p* interaction is included. We recall that the calculations attributed to E_1 and $E_1+\Delta_1$ (Zollner *et al.*, 1992) were performed only at an L point and may differ somewhat from more realistic calculations involving the whole Λ direction (Lautenschlager, Logothetidis, *et al.*, 1985, 1986).

The results of the calculation versus T of the real part of the self-energy, plus the contribution of the diagram in Fig. 20(b) and the thermal-expansion contribution, are compared with experimental data in Fig. 25. Although the experimental shifts of the E_1 gaps with T (dotted lines) are somewhat larger than the calculated ones (solid lines), the agreement is quite satisfactory. Extrapolation to $T=0$ of the calculated data, which can be performed either by hand (using Fig. 25) or with any of the fitting functions discussed earlier, leads to a zero-point renormalization of about $-90(20)$ meV for Ge and $-75(15)$ meV for Si. As can be seen in Fig. 25 the extrapolation of the experimental curves to $T=0$ leads to values of the zero-point renormalization that are only slightly higher than the theoretical ones.

The imaginary part of the self-energy corresponds to the Lorentzian half width at half maximum which will be designated here by Γ (note that in the case of phonon self-energies, Γ was taken to represent a FWHM). The Lorentzian Γ's are found by fitting the experimental $\epsilon_r(\omega)$ and $\epsilon_i(\omega)$ spectra with analytical expressions for the critical points of the type

$$\epsilon(\hbar\omega) \propto \varepsilon^{i\varphi}[\hbar\omega - E_g(T) + i\Gamma(T)]^{n/2}, \tag{5.15}$$

where n is an integer that represents the dimensionality of the critical point under consideration ($n=1$ for three-dimensional critical points; Yu and Cardona, 2005) and the phase φ represents the type of critical point (maximum, minimum, saddle point) and is sometimes used to include excitonic effects (Velický and Sak, 1966). The accuracy in the determination of the parameters of the fit with Eq. (5.15) is improved by fitting the second or third derivative of $\epsilon(\hbar\omega)$ versus ω to the corresponding derivative of Eq. (5.15). Because of experimental noise, the fit parameters, especially Γ, depend on the order of the derivative but usually they are already well converged when the second or third derivatives are used.

Figure 26 shows the calculated and measured dependence of Γ on T for the E_1 critical points of Si (a) and Ge (b). The experimental results for the $E_1+\Delta_1$ critical points of Ge have also been plotted so as to indicate that, while slightly broader, they depend on T in a manner similar to the calculated curve. It is interesting to note that $\Gamma(T)$ can be represented by a single-oscillator Bose-Einstein expression, which suggests that the zero-point width $\Gamma(0) \simeq 40$ meV results from the zero-point vibrations and other broadening mechanisms (impurities, imperfections, surfaces) can be excluded (see Sec. V.B.4).

The real and imaginary self-energies shown in Figs. 25 and 26 will be discussed further in the next subsection in connection with measurements for isotopically substituted samples.

4. E_1 gaps of germanium and silicon: Dependence on isotopic mass

Two investigations of the dependence of $\epsilon(\hbar\omega) = \epsilon_r(\hbar\omega) + i\epsilon_i(\hbar\omega)$ on isotopic mass for germanium and silicon covering the range of the E_1 and $E_1+\Delta_1$ critical points have been published (Rönnow *et al.*, 1998; Lastras-Martínez *et al.*, 2000).

In order to obtain information on zero-point renormalizations of critical points, the measurements were performed at low temperature ($\sim$30 K). The changes in E_1 and Γ_{E_1} induced by isotopic mass changes are rather small (a few meV) compared with the corresponding Lorentzian widths ($\sim$40 meV; see Fig. 26). Therefore the ellipsometric measurements of $\epsilon(\hbar\omega)$ must be performed very carefully and repeated several times in order to obtain meaningful data on their dependence on isotopic mass.

Lastras-Martínez *et al.* (2000) used a sophisticated method of data analysis based on a Fourier transform (Aspnes and Arwin, 1983) in the neighborhood of the critical points. Figure 27(a) shows the measured dependence of the E_1 and $E_1+\Delta_1$ gaps of Ge, and their difference Δ_1, on isotopic mass. The solid lines represent fits with the theoretical expression

$$E_{\boldsymbol{M}} = E_\infty + \frac{B}{\sqrt{M}}, \tag{5.16}$$

where E_∞ corresponds to the renormalized gap and B is a fit parameter. From the E_1 fit we obtain the gap renormalization for a natural Ge crystal $E_{72.6} - E_\infty = -132 \pm 28$ meV, which agrees with that given in the previous subsection. The renormalization of the $E_1+\Delta_1$ gap, however, is somewhat larger (-180 ± 30 meV) so that a marginal increase of Δ_1 with increasing mass seems to

TABLE III. Derivative with respect to the isotope masses of the lowest energy gaps E_0 for several elemental and binary semiconductors. Also, zero-temperature renormalization of these gaps $[-\Delta E_0(T=0)]$ as obtained from the mass derivatives (*) and from $E_0(T)$ (†, see text). The last column lists the linear T coefficients of $E_0(T)$ in the high-T limit. The listings are from experimental data and were extracted from Pässler (1999), Plekhanov (2001), Meyer *et al.* (2003), and the Landolt-Börnstein tables, unless otherwise indicated.

	$E_0(T\simeq 0)$ (eV)	dE_0/dM_c (meV/amu)	dE_0/dM_a (meV/amu)	$-\Delta E_0(T=0)$[a] (meV)	$-\Delta E_0(T=0)$[b] (meV)	$-(dE_0/dT)_{T\to\infty}$ (meV/K)
Diamond	5.48	14[c]	14[c]	364[d]	370[d]	0.54
Silicon	1.17	1.04[e]	1.0[e]	62[e]	64	0.32
Germanium	0.74	0.36	0.36	52	47	0.41
AlN	6.20				239	0.83
GaN	3.47	0.4[f]	4.2[f]	173[f]	173	0.60
InN	0.77[g]	0.025		178	68	0.21
AlP	2.5				23	0.35
GaP	2.34	0.19[h]	0.95[h]	86[h]	85	0.48
InP	1.42				48	0.39
AlAs	2.23				39	0.36
GaAs	1.52	0.39	0.34[i]	45[i]	54	0.47
InAs	0.41				20	0.28
AlSb	1.69				39	0.34
GaSb	0.81				33	0.38
InSb	0.23			16[i]	17	0.25
ZnO	3.44	0.39[j]	3.3[j]	164[j]	156[j]	0.57[j]
ZnS	3.84	0.31[k]	0.59[k]	105[k]	80[k]	0.53
ZnSe	2.82	0.21[i]	0.22[i]	50[i]	47	0.49
ZnTe	2.39	0.44[i]	0.10[i]	60[i]	33	0.45
CdS	2.58	0.06[h]	0.71[h]	62[h]	68[l]	0.40
CdSe	1.85				34	0.41
CdTe	1.61			24[i]	17	0.31
CuCl	3.40	−0.076[m,n]	0.36[m,n]	17[m,n]	31[h]	−0.089[o]
CuBr	3.07	−0.11[m,n]	0.12[m,n]	6[m,n]	5[m,n]	−0.087[n]
CuI	3.11	−0.53[m]			−9[m]	∼0.0[m]
PbS	0.29	+0.069[o]	−0.43[o]		∼0[o]	−0.45[o]
Cu_2O	2.17	0.22[p,d]	1.1	33[p,d]	33[p,d]	0.34[p,d]

[a]Obtained from the mass derivatives of the gaps.
[b]Obtained from the linear extrapolation of $E_0(T)$ to $T=0$.
[c]Collins *et al.* (1990).
[d]Cardona, Meyer, *et al.* (2004).
[e]Karaiskaj *et al.* (2002a).
[f]Manjón, Hernández-Fenollosa, *et al.* (2004).
[g]Yu and Cardona (2005).
[h]Meyer *et al.* (2003).
[i]Olguin *et al.* (2002).
[j]Manjón *et al.* (2003).
[k]Manjón, Moller, *et al.* (2004).
[l]Zhang, Ruf, *et al.* (1998).
[m]Serrano *et al.* (2002).
[n]Göbel, Ruf, *et al.* (1998).
[o]Thewalt and Cardona (unpublished).
[p]Fröhlich and Cardona (unpublished).

take place. It may be related to the increase in Δ_0 mentioned in Sec. V.B.2. The origin of this dependence of the spin-orbit splittings on mass is not known.

Figure 27(b) shows the dependence of the Lorentzian Γ (corresponding to a half width at half maximum) on isotope mass for Ge. The solid lines represent fits with the expression

$$\Gamma_{\boldsymbol{M}} = \Gamma_\infty + CM^{-1/2}, \tag{5.17}$$

where Γ_∞ and C are adjustable parameters. Γ_∞ should, in principle, represent any possible temperature-independent mechanisms and is expected to be small for high-quality crystals. From the fit to $\Gamma(E_1)$ one indeed finds $\Gamma_\infty = -4.6 \pm 11$ meV, a physically meaningless negative value which, however, is zero within the error bars. The zero-temperature width corresponding to the natural sample turns out to be 41 ± 11 meV and agrees remarkably well with the calculated value of 34 meV (Zollner *et al.*, 1992).

Similar measurements for silicon, described by Lastras-Martínez *et al.* (2000), yield at 30 K a shift of the E_1 gap of 3.7 ± 0.7 meV/amu, which corresponds to a

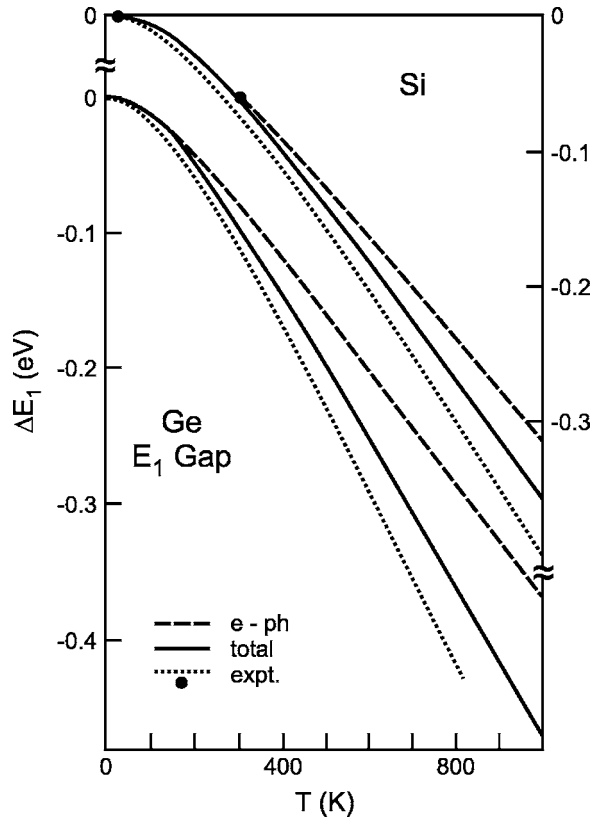

FIG. 25. Shift of the E_1 gap of Si and Ge vs temperature. Dashed line, shift due to electron-phonon interaction. Solid line, shift due to electron-phonon interaction plus thermal expansion. Dots, experimental points. From Lautenschlager, Allen, *et al.*, 1985.

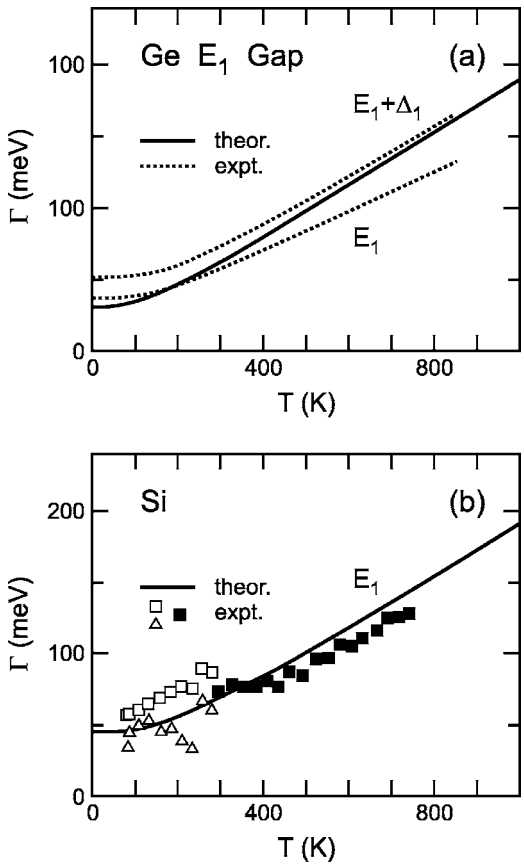

FIG. 26. Broadening of the E_1 gap for (a) Ge and (b) Si vs temperature. Solid lines, calculated phonon-induced broadenings. The symbols and dotted lines represent experimental data (for E_1 and $E_1+\Delta_1$ in the case of Ge). From Lautenschlager *et al.*, 1986.

zero-point renormalization of -118 ± 22 meV. Note that in Fig. 19 there is a shift of about -100 meV between the E_1 peak measured at 20 K and the calculated one. This difference may be due, at least in part, to not having included the electron-phonon interaction in the otherwise state-of-the-art calculation.

5. Low-frequency dielectric constant versus temperature and isotopic mass

An important parameter governing the optical response of crystals is the long-wavelength (i.e., low-frequency) dielectric function (usually called dielectric constant since the dispersion in this region is small). We consider here only cubic semiconductors, in which case this function $\epsilon(0)$ is real and a scalar. We discuss only nonpolar crystals so as to be able to neglect direct phonon-photon interaction. This interaction can, otherwise, be neglected above the frequency of all IR-active phonons. Our aim here is to discuss extant calculations and experimental data concerning the temperature and isotopic mass dependence of $\epsilon(0)$.

Like the case of other optical parameters, the temperature dependence (also called renormalization) of $\epsilon(0)$ contains two contributions: that of thermal expansion and that which results from the electron-phonon interaction, which is related to the effects of the diagrams in Fig. 20 as applied to all electronic intermediate states. The thermal-expansion effect can be obtained from the measured or calculated dependence of $\epsilon(0)$ on volume (at constant T) and the effect of thermal expansion on the lattice parameter $a_0(T)$ (Sec. III.B.2). An early calculation of the electron-phonon interaction effect on $\epsilon(0)$ (Yu and Cardona, 1970) included only Debye-Waller terms. It was based on the assumption of a single average gap, the Penn gap, with energy $\hbar\omega_{\mathrm{Penn}}$ which determines $\epsilon(0)$ through the expression

$$\epsilon(0) \simeq 1 + D\frac{\omega_p^2}{\omega_{\mathrm{Penn}}^2}. \tag{5.18}$$

In Eq. (5.18) ω_p is the plasma frequency of the valence electrons:

$$\omega_p^2 = \frac{4\pi N_v e^2}{m}, \tag{5.19}$$

where N_v is the number of valence electrons per unit volume and e,m the electron charge and mass, respectively.

Equation (5.18) can be used to calculate the dependence of $\epsilon(0)$ on volume provided the dependence of ω_{Penn} on volume and the effect of the e-p interaction is

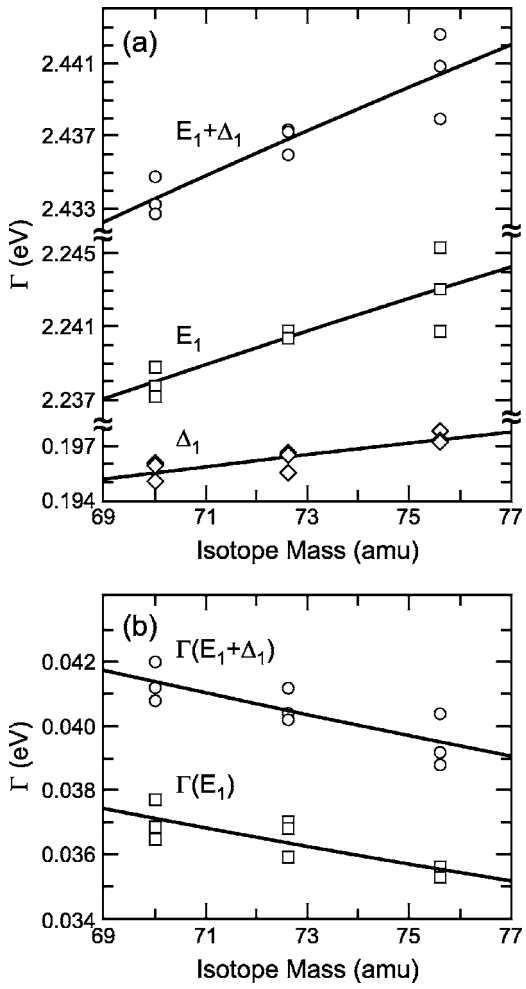

FIG. 27. (a) Energies of the E_1 and $E_1+\Delta_1$ critical points of germanium vs isotopic mass. Also shown is their difference, equal to the spin-orbit splitting Δ_1. The solid lines are fits to the experimental points with the expression $E_M=E_\infty+BM^{-1/2}$. (b) Lorentzian widths (half width at half maximum) of the E_1 and $E_1+\Delta_1$ critical points of germanium vs isotopic mass. The solid lines are fits with the expression $\Gamma_M=\Gamma_\infty+CM^{-1/2}$. From Rönnow *et al.*, 1998.

known. Yu and Cardona (1970) identify ω_{Penn} with the gap at the X point ($\approx$4.4 eV for Ge; see Fig. 18) and calculate the effect of the *e-p* interaction on ω_{Penn} using empirical pseudopotentials multiplied by temperature-dependent Debye-Waller factors, which corresponds to Fig. 20(b). A simple analytic calculation yields values of the high-temperature slope $d\epsilon(0)/dT$ that are in fairly good agreement with measurements for Si, Ge, GaAs, and other III-V compounds [see Table III of Yu and Cardona, 1970, where $d\ln n(0)/dT$ is given, $n(0)=\sqrt{\epsilon(0)}$ being the refractive index]. (For recent experimental results see McCaulley *et al.*, 1994.) Using a single-oscillator temperature dependence of $\epsilon(0)$, with $\langle\omega_{\mathrm{ph}}\rangle\simeq 430$ K, we estimate for silicon [$\epsilon(0)=12$] from the data in Table III of Yu and Cardona (1970) a zero-point *e-p* renormalization $\Delta\epsilon(0)\simeq+0.22$. A more elaborate calculation, including Debye-Waller and Fan terms (see Table I of Karch *et al.*, 1996), gives $\Delta\epsilon(0)=+0.14$.

The results of Yu and Cardona (1970) suggest that the Fan terms in the calculation of the corresponding temperature dependence of $\epsilon(0)$ are small. A hand-waving argument supporting this conclusion can be given as follows.

The conduction- and valence-band states involved in the transitions at the energy $\hbar\omega_{\mathrm{Penn}}$ occupy, on the average, the centers of the respective valence and conduction bands. The corresponding self-energy diagrams [Fig. 20(a)] have intermediate states above and below those involved in the Penn gap. The corresponding $\Sigma_r(\omega_{\mathrm{Penn}})$ for these two groups of states are negative and positive, respectively. They therefore approximately cancel each other. The imaginary part $\Sigma_i(\omega_{\mathrm{Penn}})$, of course, does not vanish and contributes to the broadening of the corresponding critical points but such broadening, to a first approximation, does not contribute to $\Delta\epsilon(0)$.

Taking the usual $M^{-1/2}$ dependence for $\epsilon(0)$, we find for silicon

$$\frac{d\epsilon(0)}{dM}=-\frac{1}{2}\frac{\Delta\epsilon(0)}{M}\simeq-\frac{1}{2}\frac{0.14}{29}=-2.4\times10^{-3}\ (\mathrm{amu})^{-1}. \tag{5.20}$$

The isotope mass derivative in Eq. (5.20) is rather small, corresponding to $d\ln n(0)/dM=1\times10^{-4}$ (amu)$^{-1}$. This is the reason why, to date, there are no direct experimental determinations of the dependence of $\epsilon(0)$ on isotope mass.

The points in Fig. 28 represent measurements of the temperature dependence of the refractive index of diamond $n(0,T)$. The solid curve through the points corresponds to the single-oscillator fit (Ruf, Henn, *et al.*, 2000):

$$n(0,T)=n_0+A\left[n_B(\hbar\langle\omega\rangle/kT)+\frac{1}{2}\right], \tag{5.21}$$

where $\langle\omega\rangle\simeq 711$ cm^{-1}, $A=0.019(7)$, and $n_0=2.377(3)$. The straight line in Fig. 28 represents the asymptotic behavior corresponding to Eq. (5.21), whose intercept with the vertical axis yields a zero-point renormalization $n(0,0)-n_0=A/2=+0.0095$, which corresponds to $\Delta\epsilon(0)=0.045$; this value is three times smaller than that calculated by Karch *et al.* (1996). In order to clarify this discrepancy, it would be interesting to measure directly the dependence of $\epsilon(0)$ on isotopic mass. The value expected on the basis of the $M^{-1/2}$ behavior [Eq. (5.20)] is, however, too small to justify the expense involved in the production of two suitable diamonds.

6. Donor and acceptor states

The discovery of discrete infrared absorption transitions between the ground state and various bound excited states of the shallow acceptor impurity B in Si by Burstein *et al.* (1953) provided an important new tool for the advancement of semiconductor physics. The rapid progress of this field, with ever-increasing spectral resolution and sensitivity coupled with increasingly sophisti-

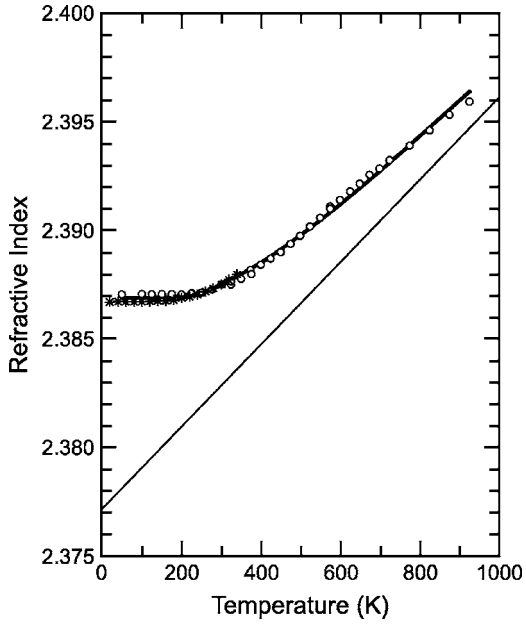

FIG. 28. Temperature dependence of the refractive index of diamond. The open circles and asterisks represent experimental data. The thick solid line represents the fit of Eq. (5.21) to these data. The thin solid line extrapolates the high-temperature limit of the fit to the data. From Ruf, Cardona, *et al.*, 2000.

cated theoretical treatments of the ground- and excited-state binding energies, is covered in the excellent review by Ramdas and Rodriguez (1981).

The common analogy between impurity states and the states of the hydrogen atom is most directly applicable to the case of shallow donor impurities in direct-gap semiconductors, where the electron effective mass m^* is a scalar and small compared to the free-electron mass m_0. Thus the spectrum of bound states is simply a scaled version of the hydrogen spectrum, with binding energy for states of principal quantum number n ($n=1$ being the ground state) of

$$E_B^n = 13.6\frac{m^*}{n^2\epsilon_0^2}\ (\text{eV}), \tag{5.22}$$

where 13.6 eV is the hydrogen Rydberg, m^* the effective mass of the bound carrier (in units of the free-electron mass), and ϵ_0 the dielectric constant of the host material (the static ϵ in nonpolar semiconductors). Calculations for donor states in indirect band-gap semiconductors such as Si and Ge are rendered somewhat more complicated by the existence of multiple, degenerate conduction-band minima, together with the fact that for each minimum the constant-energy surfaces are ellipsoids of revolution, requiring characterization by two effective masses, labeled longitudinal and transverse. The calculation of acceptor levels is complicated by the degeneracy of the valence bands at the center of the BZ and the resulting warping of the constant-energy surfaces, which makes the definition of a simple effective-mass tensor for bound holes impossible. Baldereschi and Lipari (1973, 1974)) introduced a powerful method, rewriting the Luttinger Hamiltonian in terms of spherical tensors and separating terms having cubic and spherical symmetry, with the properties of the valence-band edge characterized by the dimensionless Luttinger parameters γ_1, γ_2, and γ_3. For further details on the theory of impurity states and their binding energies the reader is again referred to the review by Ramdas and Rodriguez (1981) and to Yu and Cardona (2005, Chap. 4).

Another complication that we have not yet discussed is the deviation from the simple screened Coulomb potential seen by the bound carrier when it approaches near the impurity ion—the so-called central-cell effects. These are, of course, most significant for states whose wave functions have significant amplitudes near the impurity ion: *S*-like states, and in particular the ground state. They are almost always negligible for excited states having odd symmetry and thus wave functions with nodes at the impurity-ion core.

The most general of these effects is the reduced screening of the Coulomb potential near the impurity ion, which requires the use of a spatially dependent, or nonlocal dielectric constant, leading to an increase in the ground-state binding energy as compared to the simple hydrogenic approximation. A technologically important effect is the chemical shift, which results from the existence of potentials other than the simple Coulomb potential when the bound particle is near the impurity-ion core, leading to different ground-state binding energies for different chemical impurity species. The chemical shift is smallest for isocoric impurities, whose nuclear charge differs only by ±1 from the replaced host atom (for Si, the isocoric acceptor is Al, and the isocoric donor P). These chemical shifts also affect, to a lesser extent, the even-parity impurity excited-state binding energies, but are generally negligible for the odd-parity excited states.

An interesting central-cell effect seen in a few cases is the small dependence of the impurity ground-state binding energy on the isotopic mass of the impurity species. Since this effect is outside the scope of this review, it will be discussed only briefly. It was first reported by Dingle (1959) for the Cu acceptor in ZnO. It was later observed for a number of other impurities in a variety of semiconductors as reviewed in the theoretical paper by Heine and Henry (1975), who following Morgan (1968) interpreted the energy shift as resulting from the change of the (mass-dependent) zero-point vibrational energy of the impurity due to the change in the charge distribution near the impurity ion between the electronic ground and excited (or ionized) states. Since the ground-state charge distribution very near the impurity ion is central to this effect, it is expected to be significant only for rather deep impurities and traps, as summarized by Heine and Henry (1975), but recent results for the shallow acceptor B in Si discussed in the next section would seem to challenge this assumption.

The first report of a host isotope dependence of an impurity binding energy was for the B acceptor in diamond (Kim *et al.*, 1997, 1998). In Fig. 29 the ground-state

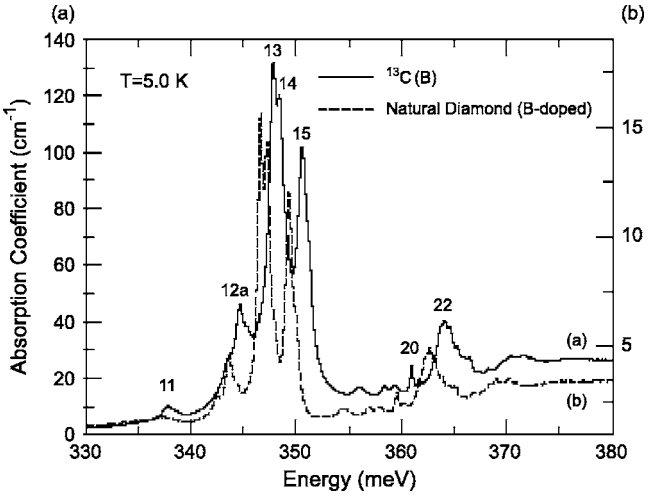

FIG. 29. Comparison of the absorption spectrum of the boron acceptor in diamond of natural isotopic composition (99 % ^{12}C) and ^{13}C diamond. From Kim *et al.*, 1998.

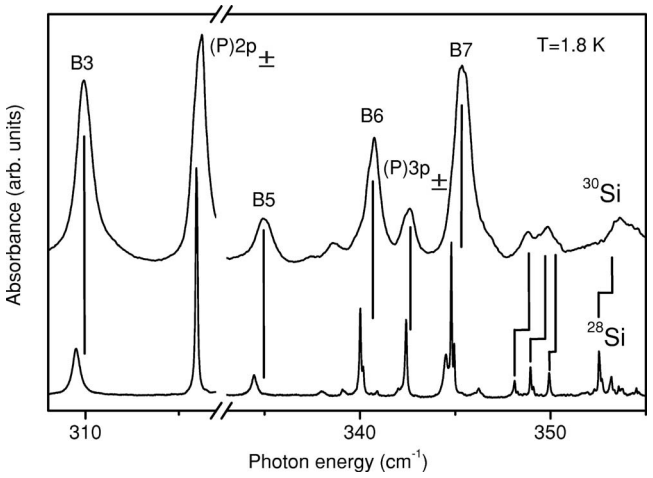

FIG. 30. Comparison of several of the infrared absorption lines of the acceptor boron and the donor phosphorus between ^{28}Si and ^{30}Si. From Karaiskaj, Thewalt, *et al.*, 2003.

to excited-state absorption spectrum for B in natural diamond (~99 % ^{12}C) is compared to that in a ~99% ^{13}C diamond. Clearly the B ground-state binding energy is ~1.5 meV larger in ^{13}C than in ^{12}C. A closer examination also reveals that the isotopic shift is not constant for the different transitions, but increases somewhat as the relevant excited-state binding energy decreases. Kim *et al.* (1997, 1998) considered a number of possible mechanisms for the observed shift, concluding, for example, that the host isotope dependence of ϵ_0 would be much too small to account for it, but were unable to provide any quantitative explanation.

Cardona (2002) similarly concluded that the change in ϵ_0 was much too small to account for the observed shifts, but introduced a simple explanation in terms of the host isotope dependence of the valence-band effective masses, which reproduced the observed result. In general, band-edge effective masses as determined via $\boldsymbol{k}\cdot\boldsymbol{p}$ perturbation theory are to a good approximation proportional to the relevant interband gap energy (Yu and Cardona, 2005). Since the host isotope dependence of many of the gap energies have already been determined, one can then calculate the expected change in carrier effective mass (or valence-band Luttinger parameters) with isotopic composition, and substitute these into Eq. (5.22) or a more sophisticated binding-energy calculation, and obtain the host isotope shift of the impurity ground- and excited-state binding energies. For the case of diamond, Cardona (2002) used the simple one spherical band approximation for the acceptor binding energy in which the binding energies are given by Eq. (5.22) with the simple substitution $m^* = \gamma_1$, which can be justified by the dominance of γ_1 for diamond. Taking $\gamma_1 \propto (E_0')^{-1}$, where E_0' is the lowest direct gap, m^* was found to increase by 0.37% in going from ^{12}C to ^{13}C, producing the same relative increase in the ground-state binding energy, in good agreement with experiment. While not discussed explicitly by Cardona (2002), this simple model clearly predicts that the excited-state binding energies will also increase by the same factor, explaining qualitatively the observation of Kim *et al.* (1997, 1998) that the energy differences between the transitions in ^{12}C and ^{13}C increased with increasing transition energy.

Similar host isotope shifts of the binding energy of the shallow donor P and the shallow acceptor B have been observed between ^{28}Si and ^{30}Si by Karaiskaj, Thewalt, *et al.* (2003), as shown in Fig. 30. As for diamond, the impurity binding energies are seen to increase with increasing host mass, and the shift between transitions in ^{28}Si and ^{30}Si is seen to increase for increasing transition energy (smaller final-state binding energy). In Si these shifts were found to be much less than for B in diamond, both due to the small relative mass change and to the much lower impurity binding energies. An accurate determination of the shifts was further hampered by the relatively low quality of the ^{30}Si sample, resulting in broad and slightly split transitions due to heavy doping effects and the presence of random strain fields, possibly from C contamination. Karaiskaj, Thewalt, *et al.* (2003) concluded that between ^{28}Si and ^{30}Si the ground-state binding energy for the B acceptor increased by 0.73 cm^{-1}, and that of the P donor by 0.32 cm^{-1}, in good agreement with theoretical estimates based on the host isotope dependence of ϵ_0 and m^*.

VI. NEW RESULTS FOR ^{28}Si: EFFECTS OF ISOTOPIC RANDOMNESS ON ELECTRONIC PROPERTIES AND TRANSITIONS

A. Introduction

As discussed in Sec. IV, the isotopic randomness present in semiconductor crystals having the natural isotopic composition, or in crystals having a modified but mixed isotopic composition, can have important effects on many aspects of the vibrational properties of the material and on the spectroscopy of its phonons. In particu-

lar, the isotopic randomness has a dramatic influence on the thermal conductivity, especially at low temperatures, as reviewed in Sec. IV.A. However, until the recent results for highly enriched ^{28}Si appeared, the subject of this section, studies of isotopic effects on the electronic properties of semiconductors, focusing mainly on the dependence of electronic band-gap energies on average isotopic mass $\langle M \rangle$ as reviewed in Sec. V.B, provided no evidence for the possible effects of isotopic randomness. In other words, they dealt with isotopic effects only within the virtual-crystal approximation. The lack of any experimental evidence for the broadening of electronic transitions due to isotopic randomness in the numerous previous studies of other semiconductors summarized in Table III likely resulted from the rather small effects of isotopic composition on band gaps and electronic transition energies. In semiconductors other than Si unrelated inhomogeneous broadening mechanisms dominated the observed linewidths.

The various dramatic demonstrations of the importance of the isotopic randomness present in natural Si reviewed in this section are a testament to the highly developed state of Si materials science and technology. Indeed, the importance of inhomogeneous isotope broadening effects in setting many of the spectroscopic limits in natural Si is at first surprising given that natural Si is close to monoisotopic, consisting of 92.23% ^{28}Si +4.67% ^{29}Si+3.10% ^{30}Si. It is now routine to produce natural Si samples via the floating-zone method and dislocation-free growth, which have sufficiently low concentrations of both electrically active impurities (donors and acceptors) and electrically inactive impurities such as O and C (which can nevertheless introduce inhomogeneous random strain fields) so as to leave the inhomogeneous isotope broadening as the dominant broadening mechanism for many transitions. Of course, the demonstration of this also requires the growth of isotopically enriched samples that are dislocation-free and have sufficient chemical purity so that their transitions are narrower than those seen in natural Si. While this has been achieved for ^{28}Si, the chemical purity of these samples still lags considerably behind what is available for natural Si. Consequently, while many transitions are found to be narrower in ^{28}Si than in natural Si, and sometimes dramatically so, the question of the ultimate linewidths, and what mechanisms determine them, remains open at this time.

B. Linewidths of shallow donor and acceptor bound-exciton transitions in isotopically enriched Si

1. The spectroscopic challenge presented by ^{28}Si

The spectroscopy of electronic transitions in isotopically enriched ^{28}Si held, and no doubt still holds, many surprises, as became evident in the first comparison of the photoluminescence (PL) spectra of ^{28}Si and natural Si (Karaiskaj *et al.*, 2001). High-resolution PL spectroscopy had been carried out for a number of years on high-quality samples of natural Si doped with a variety of impurities, using the improved resolution available with Fourier transform techniques based on commercially available Michelson interferometers (Thewalt *et al.*, 1990; Karasyuk *et al.*, 1992, 1993, 1994). The maximum instrumental resolution of $\sim$0.014 cm^{-1} available with such instruments (Bomem DA8) at the Si photoluminescence energy region was more than adequate to resolve the narrowest line observed in natural Si, the no-phonon transition of the P bound exciton, which exhibited a FWHM of 0.041 cm^{-1}. It should be emphasized that identical linewidths and BE structure were seen in all high-quality samples of natural Si, where high quality can be defined as dislocation-free with very low concentrations of C and O (less than $\sim 10^{16}$ cm^{-3}) and donor and acceptor concentrations below $\sim 10^{15}$ cm^{-3}, and in fact usually well below that. Note that P and B are the most widely studied shallow donor and acceptor impurities in Si, since their residual concentrations of $\sim 10^{11}$ cm^{-3} in even the purest natural Si are readily observed in the bound-exciton PL spectrum.

The no-phonon PL transitions of the bound excitons (BE) associated with the shallow donor P and the shallow acceptor B are shown for natural Si as the top spectrum in Fig. 31. Note that the donor BE transition α^1_{NP} is expected to be a single unsplit line (in the absence of magnetic or strain fields) from the shell model of BE and bound multiexciton complexes in Si (Kirczenow, 1977). The nine components of the B bound exciton evident in natural Si spectra, when using a PL apparatus having sufficient spectral resolution, can be understood at a simplified level as arising from two separate threefold splittings of the acceptor BE ground state. First, the 12-fold degenerate (including spin) 1*s*-like electron state in Si is split by the valley-orbit interaction into three states having symmetry Γ_1, Γ_3, and Γ_5, just as for the donor ground state, and second, the two 1*s*-like Γ_8 holes in the acceptor BE interact, and this hole-hole interaction splits the coupled two-hole state into three components ($\{\Gamma_8 \times \Gamma_8\} = \Gamma_1 + \Gamma_3 + \Gamma_5$). In reality, the B bound-exciton ground state is even more complicated, as shown by detailed studies of the splitting of these PL transitions in natural Si under uniaxial stress (Karasyuk *et al.*, 1992) and magnetic fields (Karasyuk *et al.*, 1993). The predicted location of 18 BE ground-state components in the absence of perturbations, based on fitting to the uniaxial stress results (Karasyuk *et al.*, 1992), are shown as the vertical dashes at the bottom of Fig. 31, but again only nine distinct components can be resolved in the PL spectrum of B in natural Si.

The no-phonon region of the PL spectrum of ^{28}Si (enriched to 99.9%), shifted so as to compensate for the 0.92 cm^{-1} decrease in band-gap energy relative to natural Si, is shown at the bottom of Fig. 31. It is immediately obvious that the lines are much sharper in the ^{28}Si sample than in natural Si, even though the ^{28}Si was of only moderate chemical purity, with a B concentration of 7×10^{14} cm^{-3} and a P concentration of 7×10^{13} cm^{-3}. Note that the new structure for the B bound exciton revealed in the ^{28}Si spectrum agrees well with the pre-

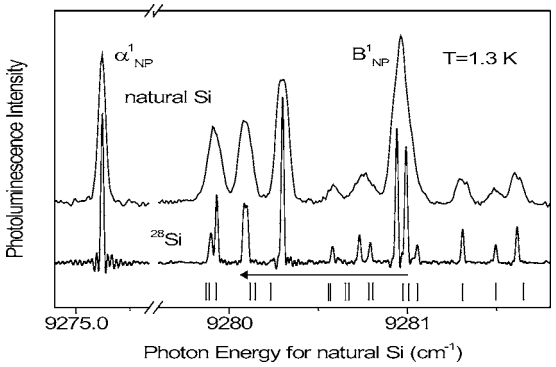

FIG. 31. Photoluminescence spectra at the maximum instrumental resolution of 0.014 cm^{-1} FWHM, comparing the no-phonon P bound-exciton (BE) (α^1_{NP}) and B bound-exciton transitions in natural Si (top) and ^{28}Si (bottom). The ^{28}Si spectrum has been shifted up in energy by the change in band-gap energy (0.92 cm^{-1}, the length of the horizontal arrow) so as to align the transitions. From Karaiskaj *et al.*, 2001.

dicted location of the components indicated along the bottom. The observed linewidth of the P bound exciton line was 0.014 cm^{-1} FWHM, essentially identical to the measured instrumental resolution. The inability of our instrument to resolve the linewidths of the BE transitions in the ^{28}Si sample is further evidenced by the structure at the base of the P bound-exciton line in the bottom spectrum of Fig. 31—it results from taking the Fourier transform, with no apodization so as to maximize the resolution, of an interferogram that is still strongly modulated at the maximum optical path difference achievable by the instrument. On the basis of these results, Karaiskaj *et al.* (2001) could only set an upper limit of 0.005 cm^{-1} on the true FWHM of the P bound exciton in ^{28}Si. No instrument capable of collecting PL spectra at such high resolution at this photon energy was commercially available, resulting in a spectroscopic challenge. A solution to this challenge will be discussed in the next subsection.

In hindsight, the importance of inhomogeneous isotope broadening for the no-phonon bound-exciton PL transitions, which have been studied in natural Si for many years, is readily understood. It is nonetheless remarkable that so little attention was paid in the past to the issue of how narrow these transitions might be, and what processes determined their widths. A simple calculation combining the observed shift of the band-gap energy in Si with average isotopic mass with the statistical fluctuations of the isotopic composition expected for natural Si within an effective BE volume of radius ~3.5 nm produces a broadening in good agreement with the observed FWHM of 0.041 cm^{-1} for the P bound exciton in natural Si. Dramatic reductions of the BE no-phonon linewidths were also observed for the deeper acceptors Al, Ga, and In in ^{28}Si, as discussed in Sec. VI.C, although for the acceptor BE the broadening may be better modeled as arising predominantly from a broadening of the acceptor ground state, the final state of the BE transition. This is because the randomness of the isotopic composition has a greater effect on the valence-band edge than on the conduction-band edge, as discussed in Sec. VI.C, and also because the impurity ground-state wave function is spatially more compact than either the electron or hole wave functions of the BE, resulting in larger statistical fluctuations around the average composition within the effective volume of the ground-state wave function.

Thus the first investigation of bound-exciton PL in isotopically enriched Si (Karaiskaj *et al.*, 2001) left us with a spectroscopic challenge. The BE linewidths in ^{28}Si were narrower than the instrumental resolution available with a Fourier transform PL apparatus having the highest resolution available in that spectral region of any commercially available system. One possible approach would be to construct a PL apparatus having higher resolution, either a custom-made Michelson interferometer or a system based on Fabry-Perot interferometers. We decided against both of these possibilities, the first because constructing a Michelson interferometer having more than a modest increase in resolution over existing systems would be time consuming and financially prohibitive, and the second since it lacked the spectroscopic flexibility we had become accustomed to in Fourier transform PL, and also because it was not clear that it would provide the sensitivity needed to study the weak Si PL signals at the required resolution.

2. Meeting the ^{28}Si challenge: Photoluminescence excitation spectroscopy

Instead we adopted an approach capable of an enormous increase in spectral resolution: photoluminescence excitation spectroscopy, using a tunable single-frequency laser source whose sub-MHz linewidth (~40 kHz) would be more than adequate to resolve the BE linewidths even if they were at their fundamental lifetime limit [shallow BE lifetimes in Si are in the 100 ns–1 μs range (Schmid, 1977)]. In photoluminescence excitation spectroscopy, the laser source is scanned across the BE no-phonon transitions, and the very weak absorption in which BE are created is monitored by observing the resulting PL in the relatively strong transverse-optical (TO) wave-vector-conserving-phonon replica, which is well separated in energy from the no-phonon region simplifying the rejection of the strong scattered laser light. We had earlier demonstrated the feasibility of studying shallow BE no-phonon transitions in natural Si at moderate resolution using a multimode Ti-sapphire laser source (Karasyuk *et al.*, 1994). The new photoluminescence excitation apparatus, which has been described briefly elsewhere (Cardona, Meyer, and Thewalt, 2004; Thewalt *et al.*, 2004), is based on a temperature-tunable distributed feedback Yb-doped fiber laser, followed by an Yb-doped fiber amplifier providing up to 600 mW of tunable single-frequency laser excitation spanning the Si no-phonon BE energy region. The transverse-optical wave-vector-conserving-phonon replica BE photoluminescence signal is separated from the scattered laser radiation using a 3/4 m double monochromator, and

detected by a liquid-nitrogen–cooled InGaAs photodetector. While the details of the photoluminescence excitation spectroscopy of ^{28}Si will be published elsewhere, we give a brief summary of the results here.

In Fig. 32, the photoluminescence excitation spectra of two subcomponents of the B bound-exciton no-phonon spectrum, which are seen as single lines in the PL spectrum at the bottom of Fig. 31, are compared for two samples of ^{28}Si, both enriched to 99.9% but having somewhat different impurity content (in comparing transition energies, note that the ^{28}Si spectrum in Fig. 31 has been shifted up by 0.92 cm^{-1}). Linewidths as narrow as 0.0025 cm^{-1} are observed for the ^{28}Si sample 1, but there is good reason to believe that this is still not the fundamental limit for BE linewidths in isotopically enriched Si. As seen in Fig. 32, the spectrum of sample 1 in the region near 9280.00 cm^{-1} is considerably sharper than that of sample 2, while the transitions near 9279.37 cm^{-1} show an additional splitting, which is larger for sample 2 than it is for sample 1. We believe that this sample-dependent splitting, and the extra broadening seen for sample 2, both result from residual random strain fields in the samples, which are evidently larger for sample 2. Note that the splitting of some of the B bound-exciton components and the broadening of others can be understood in terms of the different responses of the various BE ground-state components to strain fields (Karasyuk *et al.*, 1992). The presence of random internal strain fields is also demonstrated in the photoluminescence excitation spectrum of the P bound exciton in both samples, which is expected to be a single line, but is in fact split with sample 2 again showing the larger splitting.

The origin of these random internal strain fields is quite likely unintentional C impurities, which at higher concentrations have been shown (Safonov, Davies, and Lightowlers, 1996) to produce readily observable splittings of the P bound-exciton no-phonon PL line in natural Si. The photoluminescence excitation spectroscopy of ^{28}Si thus appears to be sample limited at the present time, and the determination of the ultimate shallow BE linewidths must await the availability of samples having higher chemical purity and perfection.

Another aspect of the photoluminescence excitation spectra shown in Fig. 32 remains to be discussed: the splitting of each of the components into doublets, with identical splitting energies of ~0.011 cm^{-1} and intensity ratios of ~80/20. In fact, all of the components of the B bound exciton observed in the photoluminescence excitation spectra show this doublet splitting. It is interpreted as a shift of the B bound-exciton localization energy with B isotopic species, since natural B consists of ^{11}B and ^{10}B with an abundance ratio of ~80/20. While shifts of BE energies with the isotopic mass of the binding center have been previously observed for much deeper BE in other semiconductors (Heine and Henry, 1975), this is the first observation of an impurity isotope shift for such a shallow BE, and its observation results directly from the dramatic improvement in BE linewidth

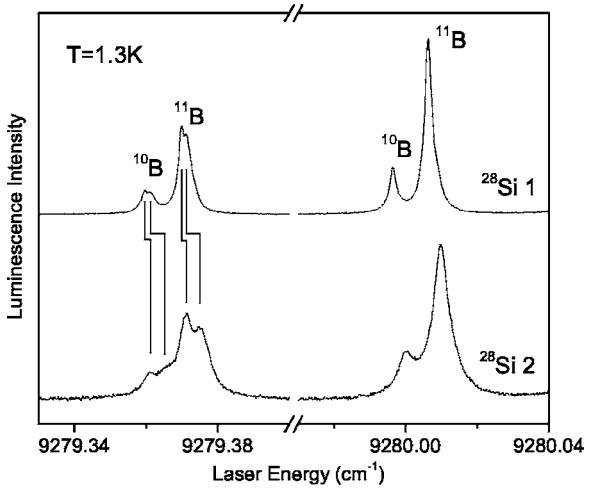

FIG. 32. Photoluminescence excitation (PLE) spectra of two of the B BE no-phonon components revealed in the bottom spectrum of Fig. 31 compared for the two best available samples of ^{28}Si. In comparing energies with Fig. 31, the 0.92-cm^{-1} shift applied there to the ^{28}Si spectrum must be taken into account. The narrowest component of sample 1 has a FWHM of 0.0025 cm^{-1}. Note that both samples show an identical doublet splitting for all B BE components of 0.011 cm^{-1}, which is interpreted as a splitting between the BE associated with ^{10}B and ^{11}B. Differences between the spectra for samples 1 and 2 are discussed in the text.

realized in ^{28}Si. Confirmation of the B isotope shift in Si has been obtained from high-resolution midinfrared absorption spectroscopy of the B acceptor in ^{28}Si, as discussed in Sec. VI.D.

3. Applications of ultrahigh-resolution photoluminescence excitation spectroscopy in ^{28}Si: The temperature dependence of gap energies as $T \rightarrow 0$

As discussed in Secs. V.B.1 and V.B.2, the temperature dependence of band-gap energies in semiconductors has received much attention, both theoretically and experimentally. In the past, the observed temperature dependences have been fitted with empirical expressions such as Eq. (5.9) suggested by Varshni (1967), which predicts a T^2 dependence as $T \rightarrow 0$, and more general forms such as Eq. (5.10), proposed by Pässler (1999), which in the low-T limit varies as T^p where p is a fitting parameter ranging from 2 to 3.3 for various semiconductors. However, because of the limited spectral resolution available in all of the previous studies, reliable data were not available in the true $T \rightarrow 0$ limit, and the fits are in fact dominated by the intermediate to high-T behavior. It has already been argued in Secs. V.B.1 and V.B.2 that the true, universal low-T behavior of gap energies should go as T^4, but this argument appeared only very recently in our study (Cardona, Meyer, *et al.*, 2004) of the temperature shift of BE transitions in ^{28}Si covering the liquid-He temperature region.

That study made use of the remarkably narrow BE linewidths discussed above in the photoluminescence ex-

citation spectra of shallow BE in ^{28}Si, having $E/\Delta E \approx 4 \times 10^6$. The temperature shift of the band gap, which is barely observable between 4.2 and 1.3 K when using standard PL spectroscopy at the maximum instrumental resolution of 0.014 cm^{-1}, was revealed by locking the photoluminescence excitation laser source to the strongest B bound-exciton transition and monitoring the laser frequency with a wave meter, using averaging to increase the precision. In this way, changes of E_G ($\sim$278.2 THz in frequency units) as small as 2 MHz could be detected, giving a resolving power of greater than 10^8. While the raw data of BE energy versus temperature already gave a good fit to T^4, it was realized that the actual temperature dependence was only a small part of the observed shift. In all of these ultrahigh-resolution measurements, the sample sits freely in the liquid-He bath and the temperature is changed by pumping on the He gas, reducing the vapor pressure and thus the temperature. Thus the hydrostatic pressure changes as well as the temperature and it could be demonstrated that this pressure effect was, in fact, larger than the temperature effect and that the hydrostatic pressure coefficient of the Si band gap measured at He temperature and $\sim$1 bar agreed well with the known coefficient, measured using much higher pressures (Cardona, Meyer, and Thewalt, 2004).

After carefully accounting for these hydrostatic pressure effects, the remaining temperature component of the Si band-gap shift was in very good agreement with the predicted T^4 behavior, as shown in Fig. 33. While these results for the indirect gap of ^{28}Si are at present the only clear confirmation of the behavior, the prediction is expected to apply quite generally to the gaps and critical-point energies of all semiconductors and insulators in the $T \rightarrow 0$ limit.

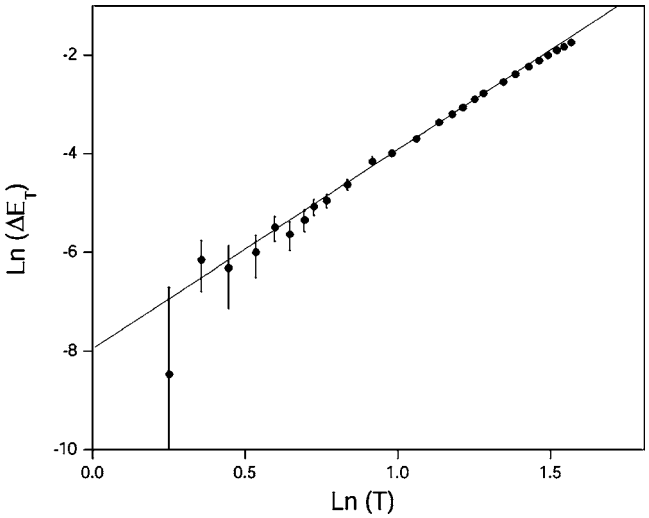

FIG. 33. The natural logarithm of ΔE_T, the temperature-dependent component of the observed shift in band-gap energy (in GHz) relative to the asymptotic $T=0$ value, is plotted vs the natural logarithm of the temperature (in K). The straight line has a slope of exactly 4. From Cardona, Meyer, *et al.*, 2004.

C. Origin of the intrinsic acceptor ground-state splitting in Si: Isotopic randomness

A discussion of the literature on the intrinsic or residual acceptor ground-state splitting, which has been studied in Si using a wide array of experimental techniques for over 25 years, is beyond the scope of this review, but a short summary has been given by Karaiskaj, Thewalt, *et al.* (2002b, 2003). These diverse studies demonstrated a small doublet splitting (or, to be more precise, a distribution of small splittings) of the neutral acceptor (A^0) ground state, which was expected to be a fourfold degenerate $1S\,\Gamma_8$ level in the absence of perturbations reducing the crystal symmetry. The most probable splitting increases with increasing acceptor binding energy, and the distribution for a given acceptor species is reproducible between all samples of sufficiently high quality. This splitting is discussed here due to a method of detecting it optically in the no-phonon PL and photoluminescence excitation spectra of BE associated with these shallow acceptors in natural Si (Karasyuk *et al.*, 1994). Indeed, the initial investigation in isotopically enriched Si was based on the expectation that the use of ^{28}Si to eliminate the inhomogeneous isotope broadening inherent in natural Si, as discussed in Sec. VI.B.1 for the P and B bound excitons, would lead to better resolved spectra of the A^0 splitting. The result, as shown for the Al bound exciton in Fig. 34, was much more surprising—not only were the lines much sharper, but all evidence of the A^0 splitting disappeared in the spectra using ^{28}Si (Karaiskaj *et al.*, 2002b). The same dramatic sharpening of the spectra, and disappearance of the A^0 splitting, were also observed for the Ga and In bound excitons (Karaiskaj *et al.*, 2002b; Thewalt *et al.*, 2003). The best available spectrum of the In bound-exciton no-phonon spectrum from ^{28}Si is compared to the natural Si spectrum in Fig. 35, revealing a dramatic sharpening of the transitions. While the A^0 ground-state splitting in natural Si is less evident in the In bound-exciton spectrum than for the Al bound exciton, it is clearly absent in the ^{28}Si spectrum.

The obvious conclusion is that the intrinsic A^0 ground-state splitting is actually a result of the randomness inherent in the isotopic distribution of natural Si and hence the same in all high-quality samples of natural Si. In hindsight, this is a rather obvious solution to the problem of the origin of the splitting since the random distribution of Si isotopes surrounding a given acceptor impurity in natural Si reduces the local symmetry and can therefore lift the degeneracy of the $1S\,\Gamma_8$ A^0 ground state. The reason why this was not put forward as a possible explanation of the A^0 splitting long ago is that it was difficult to see how an effect as subtle as the isotopic randomness present in natural Si could produce such a relatively large splitting. A related effect—the splitting of the A^0 ground state by compositional fluctuations in semiconductor alloys—was analyzed earlier by Benoit à laGuillaume (1983), but that formalism, together with the Schechter (1962) wave functions for A^0 and any rea-

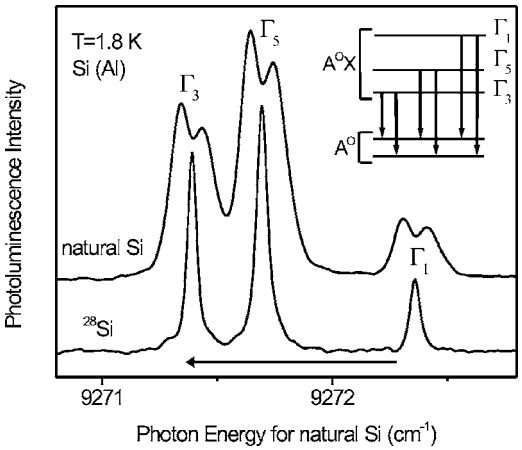

FIG. 34. High-resolution no-phonon photoluminescence (PL) spectra of the Al BE in natural Si and ^{28}Si compared, after shifting the ^{28}Si spectrum up by the band-gap shift of 0.92 cm^{-1}, as indicated by the arrow at the bottom. Inset: The origin of the six components seen in natural Si as a result of the threefold BE (A^0X) splitting together with the A^0 ground-state splitting, which is found to be absent in ^{28}Si.

sonable estimation of the fields produced by the isotopic fluctuations, would predict a splitting far smaller than the observed intrinsic splitting of A^0.

However, Karaiskaj, Kirczenow, *et al.* (2003) were able to quantitatively account for the isotopic origin of the acceptor ground-state splitting in natural Si using the observed shift of the band gap between ^{28}Si, ^{29}Si, and ^{30}Si, together with highly accurate variational wave functions for the acceptor ground state (Buczko and Bassani, 1992). A simple calculation, based on the results of Cardona and Gopalan (1989), provided an estimate that the changes in band-gap energy were mainly (75%) due to changes in the valence-band edge energy with isotopic composition. It was assumed that the A^0 ground-state binding energy was identical in ^{28}Si, ^{29}Si, and ^{30}Si, a good approximation as seen in Sec. V.B.6. Finally, the effects of a specific distribution (having the same average isotopic ratios as natural Si) of the Si isotopes surrounding the acceptor site were evaluated using the variational wave functions for the acceptor ground state and diagonalizing the Hamiltonian discretized onto the lattice sites, where an additional potential of 0, ΔE^{29}, or ΔE^{30} is placed at each site for, respectively, ^{28}Si, ^{29}Si, and ^{30}Si. ΔE^{29} and ΔE^{30} ($\approx 2\Delta E^{29}$) are simply the valence-band edge shifts (75% of the band-gap shifts) between ^{29}Si and ^{30}Si, and ^{28}Si, which is taken as the reference point. These random perturbations can both lift the degeneracy of the A^0 ground state and shift the center-of-mass of the resulting doublet, where the average shift is equal to the shift in the valence-band edge energy between ^{28}Si and natural Si, or, in other words, 75% of the observed band-gap shift. For each acceptor species, this procedure was repeated for 40 000 different random distributions of Si isotopes around the acceptor site. The resulting distributions of A^0 ground-state splittings for B, Al, Ga, and In acceptors in natural Si are shown in Fig. 36. The most probable splitting and the overall shape of the splitting distributions are in excellent agreement with the known intrinsic ground-state splitting distributions, as reviewed by Karaiskaj, Kirczenow, *et al.* (2003).

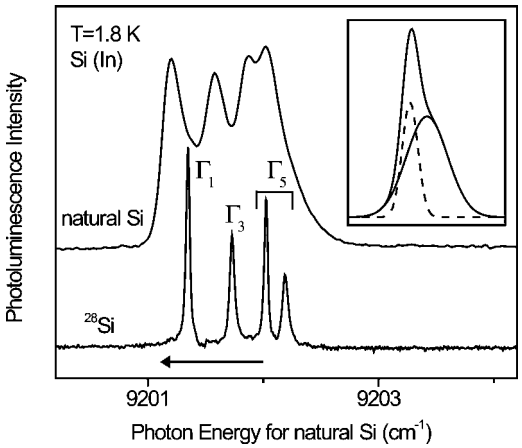

FIG. 35. High-resolution no-phonon PL spectra for In BE compared for natural Si and ^{28}Si, as in Fig. 34. Inset: The doublet splitting of the A^0 ground state obtained by fitting the natural Si spectrum. For In, the Γ_5 BE state is further split by spin-orbit coupling. From Thewalt *et al.*, 2003.

Before leaving the discussion of the acceptor ground-state splitting, it is interesting to note that a similar small splitting of the B acceptor ground state in diamond has been observed using electronic Raman scattering [Kim *et al.* (1999)] and explained in terms of a Jahn-Teller distortion. Such distortion had also been postulated as an explanation for the splittings in Si by Karasyuk *et al.* (1994) before the isotopic origin of the effect in Si was demonstrated by Karaiskaj *et al.* (2002b). Diamonds made from natural C are isotopically mixed, with the nominal composition being 98.9% ^{12}C+1.1% ^{13}C. While the isotopic randomness is thus less in natural diamond than in natural Si, it must be remembered that the binding energy of B in diamond is much larger than that of any of the shallow acceptors in Si, resulting in a very compact ground-state wave function with the smaller effective volume accentuating any effect of statistical fluctuations in the isotopic composition. The band-gap shift for a 1 amu change in isotopic mass is also much larger for diamond than for Si, as shown in Table III. The B ground-state splitting was reported to be "observably smaller" in a ^{13}C diamond sample (Kim *et al.*, 1999), but that sample had comparable isotopic randomness to natural diamond since it contained approximately 1% ^{12}C. If the B ground-state splitting in diamond has an isotopic origin, as is the case in Si, then it should vanish for a B-doped enriched ^{12}C (or pure ^{13}C) diamond, a possibility that should be investigated.

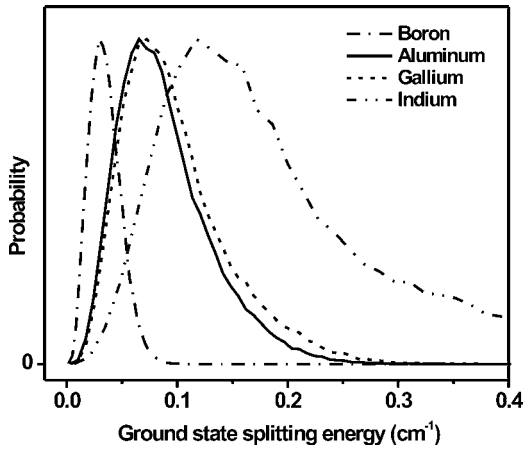

FIG. 36. The calculated statistical distribution of the B, Al, Ga, and In acceptor ground-state splittings for 40 000 configurations of random distributions of the Si isotopes, with average abundances equal to those of natural Si, around the acceptor site. From Karaiskaj, Kirczenow, *et al.*, 2003.

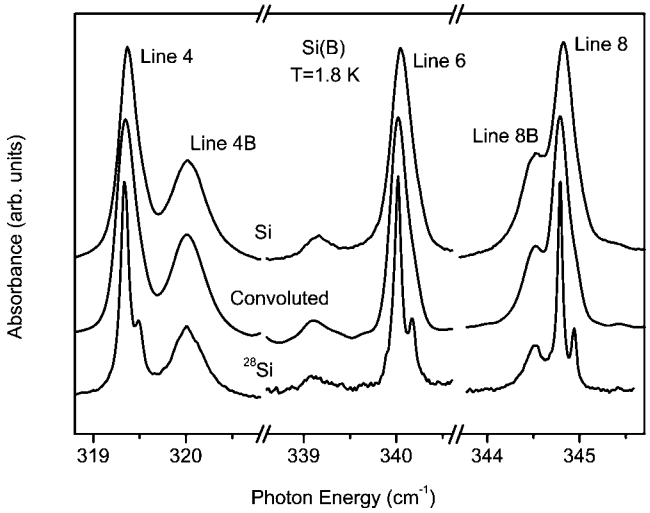

FIG. 37. Absorption lines of the B acceptor compared between natural Si (top) and ^{28}Si (bottom). Lines 4, 6, and 8 are significantly sharper in ^{28}Si than ever before seen in natural Si, revealing a doublet structure with a splitting of 0.15 cm^{-1}, explained in the text as a B isotope splitting. The middle spectra, which are seen to accurately reproduce the observed spectra for natural Si, were obtained by convolving the ^{28}Si spectra with the distribution of ground-state broadenings calculated for B in natural Si. From Karaiskaj, Stotz, *et al.*, 2003.

D. Importance of inhomogeneous isotope broadening in the midinfrared absorption spectroscopy of shallow donors and acceptors in Si

The study of the infrared absorption resulting from transitions between the electronic ground state of neutral donor and acceptor impurities and their bound excited states is one of the oldest (Kohn, 1957) and most well developed of semiconductor spectroscopies. Initially, the widths of these transitions were dominated by inhomogeneous fields and interimpurity interactions resulting from relatively high impurity concentrations and a lack of crystalline perfection present in early Si. As the field progressed, together with the development of Si technology, there came a point when the linewidth of a given transition in high-quality dislocation-free samples grown using the floating-zone method ceased to improve when the sample purity increased. This naturally suggested that the linewidth had reached a fundamental limit, and that all sources of inhomogeneous broadening had been eliminated. A suitable fundamental limit, in reasonable agreement with the observed linewidths, was provided with the theory of Barrie and Nishikawa (1963), which treated the lifetime broadening of the impurity excited states resulting from phonon-assisted transitions to other near-lying states. While these calculations were not exact, the agreement with the observed ultimate linewidths was sufficiently close that it became generally assumed that all of the observed linewidths in high-quality Si samples were in fact determined by this process. As we shall see, this may be true for some of the absorption transitions in natural Si, but it is far from being true in general. The mechanism proposed by Barrie and Nishikawa (1963) will provide an ultimate limit to the linewidth once all inhomogeneous broadenings have been rendered negligible.

The importance of the isotopic randomness present in natural Si was demonstrated by Karaiskaj, Stotz, *et al.* (2003) in comparison of the infrared absorption spectra of shallow donor and acceptor impurities between natural Si and ^{28}Si. We begin by considering the results for the shallow acceptor B, since the origin of the inhomogeneous isotope broadening follows from model calculations of the broadening and splitting of the acceptor ground state (Karaiskaj, Kirczenow, *et al.*, 2003) described in the preceding section. In Fig. 37, we see a comparison of several of the well-known B absorption transitions, labeled according to the convention of Ramdas and Rodriguez (1981), between natural Si (top) and ^{28}Si (bottom). Some of the B transitions, such as line 4B seen in the figure, appear identical (and broad) in both natural Si and ^{28}Si, and we can therefore conclude that for the excited states involved in such transitions the lifetime broadening mechanism proposed by Barrie and Nishikawa (1963) dominates over the inhomogeneous isotope broadening. However, lines 4 and 6 in Fig. 37, and five other B transitions studied by Karaiskaj, Stotz, *et al.* (2003), show a dramatic narrowing in ^{28}Si as compared to natural Si. For these transitions, the inhomogeneous isotope broadening must dominate over the lifetime broadening in natural Si. For these seven transitions, the lines in ^{28}Si resolve into very similar doublets, as seen for lines 4, 6, and 8 in Fig. 37, with a splitting of 0.15 cm^{-1} and an intensity ratio of 80/20, with the weaker component lying at higher energy.

As in Sec. VI.B.2 and Fig. 32, this doublet is explained as arising from a B isotope effect, since natural B contains ^{11}B and ^{10}B in an 80/20 ratio. The binding energy of ^{10}B is seen to be larger than that of ^{11}B (by 0.15 cm^{-1}), as expected from the work of Heine and Henry (1975). Note that in Fig. 32 the ^{10}B transition lies

at lower energy than that of ^{11}B, rather than higher as in Fig. 37. This is simply because a larger impurity binding energy results in a larger BE localization energy for that impurity, thus producing PL at a lower energy. Indeed, this relationship between the impurity binding energy and the associated BE localization energy, known as the Haynes rule (Haynes, 1960), also explains the difference in the splitting energy observed in the IR absorption spectra and the BE PL spectra. For shallow impurities in Si, the Haynes rule produces a BE localization energy that is approximately 10% of the impurity binding energy, hence the 0.011-cm^{-1} splitting seen in the BE spectrum and the 0.15-cm^{-1} splitting seen in the IR absorption spectrum are entirely consistent. At present, the size of the B isotope splitting, which is quite large for such a shallow impurity, remains to be explained.

The inhomogeneous isotopic broadening of the shallow impurity infrared absorption transitions in natural Si was explained by Karaiskaj, Stotz, *et al.* (2003) in terms of the effects of isotopic randomness on the impurity ground-state energy. Changes of the ground-state binding energy within the virtual-crystal approximation, or, in other words, the differences in binding energy between pure ^{28}Si, ^{29}Si, and, ^{30}Si discussed in Sec. V.B.6, were ignored. This seems a reasonable approximation, given the very small expected size of this shift between natural Si and ^{28}Si, based on the difference between ^{28}Si and ^{30}Si. Instead, the broadening may be understood in terms of the model used in Sec. VI.C to calculate the splitting and broadening of the acceptor ground state observed in the acceptor bound-exciton PL spectrum. In this model, the deviation of the actual isotopic composition away from the average composition within the volume of the rather compact acceptor ground-state wave function produces a local shift in the valence-band energy from the value expected within the virtual-crystal approximation. As summarized in Sec. VI.C, the virtual-crystal-approximation shift of the valence band, relative to the energy in ^{28}Si, should be approximately 75% of the shift in band-gap energy between natural Si and ^{28}Si. The acceptor ground-state energy is assumed to shift rigidly with this local shift in valence-band energy. Since the excited states are much more extended than the ground state, the excited-state wave functions sample an isotopic composition much closer to the average composition of natural Si. The ground-state binding energy, which is equal to the absorption transition energy in the limit of the excited final-state binding energy tending to zero, is thus modified for each acceptor by the difference between the average composition and the detailed isotopic environment as sampled by its ground-state wave function. Thus in natural Si all of the absorption transitions would be expected to be broadened by essentially the same amount—the ground-state broadening.

Since these acceptor ground-state distributions were already calculated by Karaiskaj, Kirczenow, *et al.* (2003) in explaining the bound-exciton PL spectra, it can be demonstrated that they also account for the inhomogeneous isotope broadening of the IR absorption transitions in natural Si. The middle spectra in Fig. 37 are the observed spectra for B in ^{28}Si convolved with the broadening of the B ground state in natural Si calculated by Karaiskaj, Kirczenow, *et al.* (2003). The result is seen to be in excellent agreement with the observed spectra in natural Si. It would be interesting to compare the absorption spectra of deeper acceptors in ^{28}Si and natural Si, since for the deeper acceptors, with their more compact ground-state wave functions, an even larger inhomogeneous isotope broadening would be expected in natural Si. To a good approximation, the inhomogeneous ground-state broadening present in natural Si for the deeper acceptors Al and In may be estimated by comparing the observed sharpening of their bound-exciton PL spectra as shown in Figs. 34 and 35.

Karaiskaj, Stotz, *et al.* (2003) reported similar reductions for the linewidths of many shallow donor IR absorption transitions in ^{28}Si as compared to natural Si. As seen in Fig. 38(a), the $2p_0$ absorption line of the P donor in ^{28}Si had a FWHM of only 0.034 cm^{-1}, five times narrower than the narrowest reported measurement of the same line in natural Si! The P $2p_\pm$ and $3p_\pm$ transitions in the ^{28}Si sample were also narrower than in natural Si, but less dramatically so since for the higher excited states the broadening due to interimpurity interactions (concentration broadening) inherent in the relatively heavily doped and compensated ^{28}Si sample became more important. Still, the dramatically sharpened P $2p_0$ line sets a new record for the narrowest linewidth of an impurity absorption transition. Similarly, as shown in Figs. 38(b)–38(d), the transitions to the lower-lying excited states of the Li donor, inadvertently introduced in some samples during annealing, were also considerably sharper in ^{28}Si revealing new structure which was interpreted as resulting from the splitting between the Γ_3 and Γ_5 valley-orbit components of the Li 1*s* ground states (Karaiskaj, Stotz, *et al.* 2003). Samples of ^{28}Si having much higher chemical purity will be needed to observe the true linewidths of transitions to higher-lying excited states and to verify that the removal of the inhomogeneous ground-state broadening sharpens all donor transitions. Indeed, if ^{28}Si samples of higher chemical purity can be produced, it seems likely that new records for narrow linewidths may be set for some of these transitions to higher-lying excited states. The explanation of inhomogeneous isotope broadening of the shallow donor IR absorption transitions in natural Si is identical to that offered above for the acceptors, differing only in scale, since the conduction-band shift with changing isotopic composition is only approximately one-third that of the valence band. It should be possible to quantitatively account for donor ground-state broadenings in natural Si using calculations similar to those described for acceptors in Sec. VI.C and accurate wave functions for the ground state of specific donor species.

Hayama, Davies, and Ito (2004) and Hayama, Davies, Tan, *et al.* (2004) have recently reported studies of deep photoluminescence centers in ^{30}Si, showing that the energy shifts as compared to natural Si could be under-

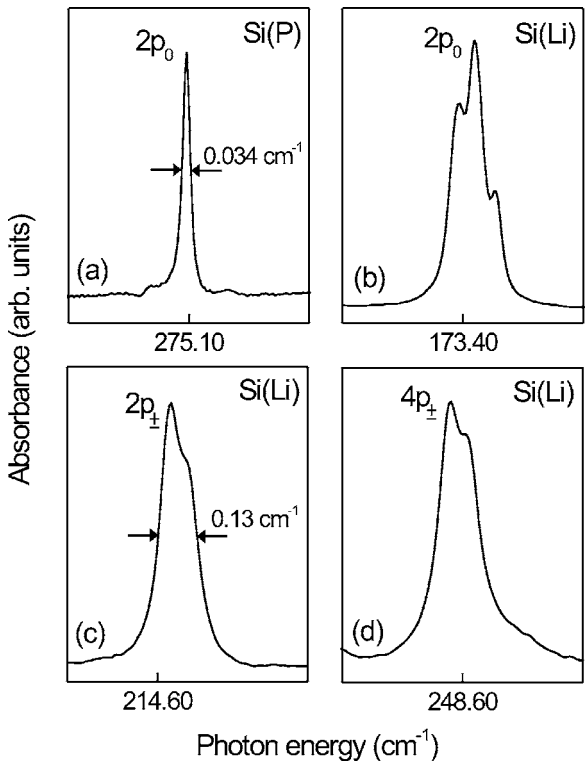

FIG. 38. Four representative absorption lines are shown for the shallow donors (a) P and (b)–(d) Li in a sample of ^{28}Si at a temperature of 1.8 K, with an instrumental resolution of 0.014 cm^{-1} FWHM. From Karaiskaj, Stotz, *et al.*, 2003.

stood on the basis of a simple empirical relationship, but there have as yet been no observations of reduced linewidths for deep transitions in isotopically enriched semiconductors.

E. The elimination of inhomogeneous isotope broadening: Future prospects

As outlined above, much has already been accomplished. The limits of BE spectroscopy and impurity absorption spectroscopy in isotopically enriched Si have already been shown to lie far beyond what were commonly assumed to be the limits based on the study of natural Si, in some cases by more than an order of magnitude. As a result of the improvements in spectral resolution, new effects have been discovered such as the T^4 dependence of E_G in the limit of $T \rightarrow 0$ and the isotope splitting between the shallow acceptors ^{10}B and ^{11}B. However, at present we are in much the same situation that studies using natural Si were at several decades ago—the ultimate linewidths of many of the transitions are presently limited by the chemical purity and crystalline perfection of the available ^{28}Si samples. In particular, the rather high concentrations of electrically active impurities in the presently available ^{28}Si makes the investigation of the very weakly bound impurity excited states impossible, and it is there that some of the truly narrow transitions may yet be discovered. Not only must the concentrations of electrically active impurities such as B and P be reduced, but also the concentration of electrically inactive species such as C and O, which can introduce inhomogeneous broadening due to random strain fields.

Even more dramatic improvements of the linewidths of absorption transitions associated with deeper impurities can be expected, even in the presently available ^{28}Si, due to their more compact ground-state wave functions, and these should be actively investigated. Similar dramatic improvements in the emission linewidths of deeper BE centers can also be expected in ^{28}Si. Moving further afield, the discovery that the intrinsic acceptor ground-state splitting is an isotopic effect that vanishes in enriched ^{28}Si suggests that the electron-spin-resonance spectra of the neutral acceptor ground state should be reinvestigated in ^{28}Si, from which improved results may be expected. Also, as discussed above, the B acceptor ground state should be investigated in ^{12}C diamond to determine whether the origin of the observed splitting is isotopic or due to a Jahn-Teller effect now that the isotopic origin of the analogous splitting in Si has been discovered. Such samples would also allow for a comparison of the B bound-exciton linewidths and infrared absorption linewidths in natural and ^{12}C diamond, for investigating whether inhomogeneous isotope broadening is significant in natural diamond. Related to this, diamond, and perhaps in particular ^{12}C diamond (depending on the outcome of the linewidth comparison), may be a suitable material for further investigating the newly discovered T^4 dependence of the band-gap energy in the low-temperature limit.

Given the very high perfection and chemical purity now possible in the growth of epitaxial GaAs using molecular beam epitaxy, it would be interesting to investigate the effects of the elimination of the rather large isotopic randomness present due to the use of natural Ga, which consists of ^{69}Ga and ^{71}Ga in a 60/40 ratio. This could begin with high-resolution photoluminescence spectroscopy, but the effects of the elimination of isotopic randomness may not be limited to optical properties. Given the remarkable low-temperature electron mobilities achievable in remotely doped two-dimensional electron gases, one wonders what bounds isotopic randomness scattering may place on such properties.

In conclusion, while much has been discovered regarding the spectroscopy of isotopically enriched semiconductors, and particularly Si, very little is yet complete, and what we have learned so far suggests many new possibilities for further discoveries both in Si and in other semiconductors.

VII. CONCLUSIONS

We have discussed the effects of isotopic substitution on the physical properties of semiconductor crystals and possible applications to the investigation and characterization of these technologically important materials. With few exceptions (Al, P, As, I), the constituent atoms

of tetrahedral semiconductors have several stable isotopes and single crystals can be grown with custom-made concentrations provided budgetary considerations allow it. Three types of effects have been identified: effects corresponding to the average isotopic mass, effects corresponding to the random distribution of the isotopic masses, and, in a few cases, effects due to the nuclear spins. We have discussed first the effects on macroscopic thermomechanical properties, including the effect of the average isotopic mass on the specific heat and thermal expansion. In the case of thermal expansion, we have emphasized the zero-point renormalization of the crystal dimensions, which is strongly affected by the average isotopic mass. For thermal conductivity, we discussed the effect of isotopic mass disorder, which is particularly important at low temperatures. As an example of effects related to nuclear spins we discussed the nuclear resonance of ^{73}Ge, whose spectral linewidth is strongly affected by the random distribution of other Ge isotopes present. We next discussed the direct effect of average isotopic masses and their random distribution on specific phonons and phonon dispersion relations. The harmonic approximation must be modified to include anharmonicity (which depends on the average isotopic masses of each of the constituent elements) and spatial distribution of such isotopes, random or otherwise. These effects have been characterized by complex self-energies, with real parts which represent temperature-dependent frequency shifts (including zero-point renormalizations) and imaginary parts which describe linewidths of phonons and, correspondingly, their lifetimes. Theoretical predictions have been compared with available experimental data.

Isotopic effects have also played an important role in the investigation and structural assignment of local vibrational modes. Because of space limitations and the availability of extensive reviews, we have not discussed them here in detail. We have simply mentioned some of the salient problems and given appropriate-literature references.

Average isotopic compositions and their spatial distribution also affect the energies and widths of electronic states and corresponding spectroscopic transitions. We discussed isotopic effects on the lowest (fundamental) energy gap of several semiconductors, which in some cases, such as diamond, silicon, and germanium, is indirect (phonon or defect-aided transitions), whereas in others (GaAs, GaN, ZnO) it is direct. The observed effects, including zero-point renormalizations, have been attributed to thermal expansion and to electron-phonon interaction. Particularly interesting is the case of diamond, for which the zero-point gap renormalization is an order of magnitude larger than that for germanium and silicon. It has been suggested that the correspondingly large electron-phonon interaction is of the essence to the superconductivity recently reported for boron-doped diamond.

The electronic effects discussed are related to the average isotopic mass $\langle M \rangle$. In fact, they are proportional to $\langle M \rangle^{-1/2}$ for elemental semiconductors. They can be described, at the lowest absorption edge, by real self-energies which gain an imaginary component (corresponding to a broadening or a lifetime) for higher gaps. The last section of this review discusses effects of the isotopic disorder on electronic excitations in silicon. Paramount among these effects is the broadening of the photoluminescence spectra of excitons bound to electrically active impurities. Contrary to the homogeneous broadenings described earlier, this broadening is inhomogeneous. It is related to fluctuations in the isotopic abundance within the sphere determined by the radius of the bound exciton. It has been shown that this phenomenon determines the linewidth of the corresponding luminescence spectra of natural silicon. Isotopically pure ^{28}Si samples exhibit extremely sharp bound-exciton luminescence lines that can be used to precisely determine the temperature dependence of the indirect band gap of Si in the very-low-temperature region (2–6 K). In this manner, the theoretically predicted T^4 dependence has been confirmed. Related effects observed for transitions between acceptor impurity levels, in particular the splitting of the acceptor ground state, have also been attributed to the random distribution of the three isotopes present in natural silicon.

A very recent issue of *Solid State Communications* [**133**, 691–747 (2005)] is fully devoted to isotope effects in semiconductors.

This review has been confined to basic isotope effects on phonons and electrons in semiconductors. In doing so, and because of space limitations, we have omitted rather important related topics of applied interest. Among them we mention here the doping by nuclear transmutation. This technique, first proposed by Lark-Horovitz (1951), is being applied commercially for the *n*-type doping of silicon. It makes use of the natural abundance of ^{30}Si which is transmuted into ^{31}Si upon neutron capture. The unstable ^{31}Si decays into the stable donor ^{31}P [see Jagannath *et al.* (1979)]. For the doping by nuclear transmutation of Ge, see Itoh *et al.* (1993). Another important topic which lies beyond the scope of the present review concerns the application of isotopic superlattices for investigating self-diffusion in semiconductors. The interested reader should consult the review by Haller (2005). While some of the future prospects which originate from the elimination of the inhomogeneous isotope broadening present in silicon (and also in all other semiconductors) have been discussed in Sec. VI.E, it is worth underlining that this is at present a very new and exciting field, which may have quite unexpected impacts. One of these may be on quantum computing. Fu *et al.* (2004) have recently described an optical detection technique for the phosphorus nuclear spin in highly enriched ^{28}Si using the hyperfine splitting of the donor ground state, which they conclude may be observable based on the sharpening of the shallow donor bound-exciton transitions in ^{28}Si described in Sec. VI.B. Another possibility, based on the elimination of the inhomogeneous broadening of the donor and acceptor transitions described in Sec. VI.D, is the expectation

that transitions to the higher excited states of these centers in highly enriched ^{28}Si may become extremely narrow once the chemical purity of the samples has been improved sufficiently to eliminate concentration broadening, perhaps allowing for spectroscopy similar to that involving the Rydberg states of atomic systems.

Finally, we mention an application of highly pure ^{28}Si which is now in progress as part of an international collaboration (Becker, 2003). This work is motivated by the fact that nearly all fundamental units (meter, second, ohm, etc.) can nowadays be based on atomic properties, the only exception being the kilogram (kg). The kg can be derived from atomic units through Avogadro's number N_A, which is the number of atoms in a mole of ^{28}Si (27.976 927 g in the present units of mass). For the purpose of redefining the unit of mass in terms of the atomic mass, an extremely perfect sphere of approximately 1 kg weight is being made out of highly pure ^{28}Si. The number of atoms in such a sphere will then be determined by x-ray techniques. This will fix the mass of the sphere in atomic mass units. Avogadro's number will then lead to the mass of the sphere in kg.

ACKNOWLEDGMENTS

M.C. thanks many graduate students and associates he has had during the past 15 years. Most of them appear explicitly as authors in the references. Nevertheless, he would like to express his gratitude to his most recent collaborators: A. Cantarero, A. Göbel, F.J. Manjón, A.K. Ramdas, T. Ruf, J. Serrano, B.A. Weinstein, and F. Widulle. M.L.W.T. gratefully acknowledges the major contributions on silicon work made by a number of graduate students, first and foremost, Denis Karaiskaj, as well as Thomas Meyer, and James Stotz, Albion Yang, and Haijun Lian, and also important discussions and collaborations with Eugene Haller, Joel Ager, Hans-Joachim Pohl, George Kirczenow, and Ryszard Buczko. M.L.W.T. also gratefully acknowledges the support of NSERC and thanks the Canada Council for the award of the Killam Research Fellowship. Last, but not least, both authors are indebted to Renée Stotz for her expert help in bridging the Atlantic divide. They also thank A.K. Ramdas and E.E. Haller for a critical reading of the manuscript.

REFERENCES

Albrecht, S., L. Reining, R. Del Sole, and G. Onida, 1998, "*Ab initio* calculations of excitonic effects in the optical spectra of semiconductors," Phys. Rev. Lett. **80**, 4510–4513.

Allen, P. B., 1994, "Zero-point and isotope shifts: Relation to thermal shifts," Philos. Mag. B **70**, 527–534.

Allen, P. B., and M. Cardona, 1981, "Theory of the temperature dependence of the direct gap of germanium," Phys. Rev. B **23**, 1495–1505.

Allen, P. B., and M. Cardona, 1983, "Temperature dependence of the direct gap of Si and Ge," Phys. Rev. B **27**, 4760–4769.

Asen-Palmer, M., K. Bartkowski, E. Gmelin, M. Cardona, A. P. Zhernov, V. I. Ozhogin, A. V. Inyushkin, A. Taldenkov, K. Itoh, and E. E. Haller, 1997, "Thermal conductivity of germanium crystals with different isotopic compositions," Phys. Rev. B **56**, 9431–9447.

Aspnes, D. E., 2004, "Expanding horizons: new developments in ellipsometry and polarimetry," Thin Solid Films **455**, 3–13.

Aspnes, D. E., and H. Arwin, 1983, "Analysis of optical-spectra by Fourier methods: Filtering and least-squares regression in reciprocal space," J. Opt. Soc. Am. **73**, 1759–1764.

Aspnes, D. E., and A. A. Studna, 1983, "Dielectric functions and optical parameters of Si, Ge, GaP, GaAs, GaSb, InP, InAs, and InSb from 1.5 to 6.0 eV," Phys. Rev. B **27**, 985–1009.

Aston, F. W., 1920, "Isotopes and atomic weights," Nature (London) **105**, 617–619.

Bachelet, G. B., and N. E. Christensen, 1985, "Relativistic and core-relaxation effects on the energy bands of gallium arsenide and germanium," Phys. Rev. B **31**, 879–887.

Baldereschi, A., and N. O. Lipari, 1973, "Spherical model of shallow acceptor states in semiconductors," Phys. Rev. B **8**, 2697–2709.

Baldereschi, A., and N. O. Lipari, 1974, "Cubic contributions to the spherical model of shallow acceptor states," Phys. Rev. B **9**, 1525–1539.

Baroni, S., S. de Gironcoli, and A. dal Corso, 2001, "Phonons and related crystal properties from density-functional perturbation theory," Rev. Mod. Phys. **73**, 515–562.

Barrie, R., and K. Nishikawa, 1963, "Phonon broadening of impurity spectral lines II. Application to silicon," Can. J. Phys. **41**, 1823–1835.

Barron, T. H. K., and M. Klein, 1974, in *Perturbation Theory of Anharmonic Crystals*, edited by G. K. Horton and A. A. Maradudin, Vol. 1 of Dynamical Properties of Solids (North-Holland, Amsterdam), Chap. 7, pp. 391–449.

Bech-Nielsen, B., K. Tanderup, M. Budde, K. Bonde-Nielsen, J. L. Lindström, R. Jones, S. Öberg, B. Hourahine, and P. Briddon, 1997, "Local vibrational modes of weakly bound O-H complexes in Si," Mater. Sci. Forum **258-263**, 391–398.

Beck, O., *et al.*, 1998, "Nondestructive determination of the C-13 content in isotopic diamond by nuclear resonance fluorescence," J. Appl. Phys. **83**, 5484–5488.

Becker, P., 2003, "Tracing the definition of the kilogram to the Avogadro constant using a silicon single crystal," Metrologia **40**, 366–375.

Benoit à laGuillaume, C., 1983, "Splitting of the acceptor ground state in zincblende semiconductor alloys," Solid State Commun. **48**, 513–516.

Berman, L. E., J. B. Hastings, D. P. Siddons, M. Koike, V. Stojanoff, and M. Hart, 1993, "Diamond crystal x-ray optics for high-power-density in synchrotron radiation beams," Nucl. Instrum. Methods Phys. Res. A **329**, 555–563.

Berman, R., and J. C. F. Brock, 1965, "Effect of isotopes on the lattice heat conductivity. 1. Lithium fluoride," Proc. R. Soc. London, Ser. A **289**, 46–65.

Bienenstock, A., 1964, "A calculation of the expansion coefficient of germanium," Philos. Mag. **9**, 755–766.

Born, M., and K. Huang, 1956, *Dynamical Theory of Crystal Lattices* (Oxford University, Oxford).

Born, M., and T. von Kármán, 1912, "On vibrations in space lattices," Phys. Z. **13**, 297–309 (in German).

Brockhouse, B. M., and P. K. Iyengar, 1958, "Normal modes of germanium by neutron spectrometry," Phys. Rev. **111**, 747–754.

Brust, D., F. Bassani, and J. L. Phillips, 1962, "Critical points

and ultraviolet reflectivity of semiconductors," Phys. Rev. Lett. **9**, 94–97.
Buchenauer, C. J., M. Cardona, and F. H. Pollak, 1971, "Raman scattering in grey tin," Phys. Rev. B **3**, 1243–1244.
Buczko, R., and F. Bassani, 1992, "Shallow acceptor resonant states in Si and Ge," Phys. Rev. B **45**, 5838–5847.
Bulanov, A. D., 2000, "The highly isotopic enriched (99.99%), highly-pure Si-28 single crystal," Cryst. Res. Technol. **35**, 1023–1026.
Burstein, E., E. E. Bell, J. W. Davisson, and M. Lax, 1953, "Optical investigation of impurity levels in silicon," J. Phys. Chem. **57**, 849–852.
Buschert, R. C., A. E. Merlini, S. Pace, S. Rodriguez, and M. H. Grimsditch, 1988, "Effect of the isotope concentration on the lattice parameters of germanium perfect crystals," Phys. Rev. B **38**, 5219–5221.
Cardona, M., 1969, *Modulation Spectroscopy* (Academic, New York).
Cardona, M., 2001a, "Renormalization of the optical response of semiconductors by electron-phonon interaction," Phys. Status Solidi A **188**, 1209–1232.
Cardona, M., 2001b, *Effects of Electron-Phonon Interaction on the Optical Response of Semiconductors* (Scuola Normale Superiore, Pisa), Chap. 3, Electrons and Phonons in Solids, pp. 25–47.
Cardona, M., 2002, "Dependence of the excitation energies of boron in diamond on isotopic mass," Solid State Commun. **121**, 7–8.
Cardona, M., 2005, "Electron-phonon interaction in tetrahedral semiconductors," Solid State Commun. **133**, 3–18.
Cardona, M., and S. Gopalan, 1989, *Progress in Electronic Properties of Solids* (Kluwer, Dordrecht), Chap. 1, pp. 51–64.
Cardona, M., R. K. Kremer, M. Sanati, S. K. Estreicher, and T. R. Anthony, 2005, "Measurements of the heat capacity of diamond with different isotopic compositions," Solid State Commun. **133**, 465–468.
Cardona, M., L. F. Lastras-Martínez, and D. E. Aspnes, 1999, "Comment on '*Ab initio* calculation of excitonic effects in the optical spectra of semiconductors,' " Phys. Rev. Lett. **83**, 3970.
Cardona, M., T. A. Meyer, and M. L. W. Thewalt, 2004, "Temperature dependence of the energy gap of semiconductors in the low-temperature limit," Phys. Rev. Lett. **92**, 196403.
Cardona, M., and T. Ruf, 2001, "Phonon self-energies in semiconductors: Anharmonic and isotopic contributions," Solid State Commun. **117**, 201–212.
Clark, C. D., P. J. Dean, and P. V. Harris, 1964, "Intrinsic edge absorption in diamond," Proc. R. Soc. London, Ser. A **277**, 312–329.
Cohen, M. L., and D. J. Chadi, 1980, in *Handbook of Semiconductors*, edited by M. Balkanski (North-Holland, Amsterdam), Vol. 2, pp. 155–179.
Cohen, M. L., and J. R. Chelikowsky, 1989, *Electronic Structure and Optical Properties of Semiconductors*, 2nd ed. (Springer, Berlin).
Collins, A. T., S. C. Lawson, G. Davies, and H. Kanda, 1990, "Indirect energy gap of ^{13}C diamond," Phys. Rev. Lett. **65**, 891–894.
Colombo, L., and P. Gianozzi, 1995, "First-principles derived parametrization of the adiabatic bond charge model," Solid State Commun. **96**, 49–52.
Davies, G., S. Hayama, S. Hao, B. Bech-Nielsen, J. Coutinho, M. Sanati, S. Estreicher, and K. Itoh, 2005, "Host isotope effects on midinfrared optical transitions in silicon," Phys. Rev. B **71**, 115212.
Debernardi, A., 2000, "Anharmonic effects in the phonons of III-V semiconductors: First-principles calculations," Solid State Commun. **113**, 1–10.
Debernardi, A., S. Baroni, and E. Molinari, 1995, "Anharmonic phonon lifetimes in semiconductors by density functional perturbation theory," Phys. Rev. Lett. **75**, 1819–1822.
Debernardi, A., and M. Cardona, 1996, "Isotopic effects on the lattice constant in compound semiconductors by perturbation theory: An *ab initio* calculation," Phys. Rev. B **54**, 11305–11310.
Debernardi, A., N. M. Pyka, A. Göbel, R. Lauck, S. Kramp, and M. Cardona, 1997, "Lattice dynamics of wurtzite CdS: Neutron scattering and *ab initio* calculations," Solid State Commun. **103**, 297–301.
Debye, P., 1912, "On the theory of specific heats," Ann. Phys. **39**, 789–839 (in German).
Dingle, R., 1959, "Luminescent transitions associated with divalent copper impurities and the green emission from semiconducting zinc oxide," Phys. Rev. Lett. **23**, 579–581.
Einstein, A., 1907, "The quantum theory of radiation and the theory of the specific heat,"Ann. Phys. **22**, 180–190 (in German).
Ekimov, E., V. A. Sidorov, E. D. Bauer, N. Mel'nik, N. Curro, J. Thompson, and S. Stiskov, 2004, "Superconductivity in diamond," Nature (London) **428**, 542–545.
Emsley, J., 1990, *The Elements* (Oxford University, Oxford).
Etchegoin, P., J. Weber, and M. Cardona, 1992, "Isotope effect in Ge: A photoluminescence study," Solid State Commun. **83**, 843–848.
Fu, K.-M. C., T. Ladd, C. Santori, and Y. Yamamoto, 2004, "Optical detection of the spin state of a single nucleus in silicon," Phys. Rev. B **69**, 125306.
Fuchs, H. D., P. Etchegoin, M. Cardona, K. Itoh, and E. E. Haller, 1993, "Vibrational band modes in germanium: Isotopic disorder-induced Raman scattering," Phys. Rev. Lett. **70**, 1715–1718.
Garro, N., A. Cantarero, M. Cardona, A. Göbel, T. Ruf, and K. Eberl, 1996, "Dependence of the lattice parameters and the energy gap of zincblende-type semiconductors on isotopic masses," Phys. Rev. B **54**, 4732–4740.
Geballe, T., and G. Hull, 1958, "Isotopic and other types of thermal resistance in germanium," Phys. Rev. **110**, 773–775.
Giannozzi, P. S., S. de Gironcoli, P. Pavone, and S. Baroni, 1991, "*Ab initio* calculation of phonon dispersions in semiconductors," Phys. Rev. B **43**, 7231–7242.
Gibin, A., G. Devyatykh, A. Gusev, R. Kremer, M. Cardona, and H.-J. Pohl, 2005, "Heat capacity of isotopically enriched ^{28}Si and ^{30}Si in the temperature range $4\ \mathrm{K} < T < 100\ \mathrm{K}$," Solid State Commun. **133**, 569–572.
Göbel, A., T. Ruf, M. Cardona, C. T. Lin, J. Wrzeskinski, M. Steube, K. Reimann, J.-C. Merle, and M. Joucla, 1998, "Effects of the isotopic composition on the fundamental gap of CuCl," Phys. Rev. B **57**, 15183–15190.
Göbel, A., T. Ruf, C. T. Lin, M. Cardona, J. C. Merle, and M. Joucla, 1997, "Effects of isotopic composition on the lattice dynamics of CuCl," Phys. Rev. B **56**, 210–220.
Göbel, A., T. Ruf, J. M. Zhang, R. Lauck, and M. Cardona, 1999, "Phonons and fundamental gap in ZnSe: Effects of the isotopic composition," Phys. Rev. B **59**, 2749–2759.
Göbel, A., D. T. Wang, M. Cardona, L. Pintschovius, W. Reichardt, J. Kulda, N. M. Pyka, K. Itoh, and E. E. Haller, 1998,

"Effects of isotope disorder on energies and lifetimes of phonons in germanium," Phys. Rev. B **58**, 10510–10522.

Gonze, X., *et al.*, 2002, "First-principles computation of materials properties: The ABINIT software project," Comput. Mater. Sci. **25**, 478–492.

Haller, E., 2005, "Isotopically controlled semiconductors," Solid State Commun. **133**, 693–707.

Harrison, W. A., 1989, *Electronic Structure and the Properties of Solids* (Dover, New York).

Hass, K. C., M. C. Tamor, T. R. Anthony, and W. F. Banholzer, 1992, "Lattice dynamics and Raman spectra of isotopically mixed diamond," Phys. Rev. B **45**, 7171–7182.

Hayama, S., G. Davies, and K. Itoh, 2004, "Photoluminescence studies of implantation damage centers in ^{30}Si," J. Appl. Phys. **96**, 1754–1756.

Hayama, S., G. Davies, J. Tan, J. Coutinho, R. Jones, and K. Itoh, 2004, "Lattice isotope effects on optical transitions in silicon," Phys. Rev. B **70**, 035202.

Haynes, J. R., 1960, "Experimental proof of the existence of a new electronic complex in silicon," Phys. Rev. Lett. **4**, 361–363.

Heine, V., and C. H. Henry, 1975, "Theory of the isotope shift for zero-phonon optical transitions at traps in semiconductors," Phys. Rev. B **11**, 3795–3803.

Henn, R., T. Strach, E. Schönherr, and M. Cardona, 1997, "Isotope effects in the optical phonons of $YBa_2Cu_3O_7$: Eigenvector and infrared charge determination," Phys. Rev. B **55**, 3285–3296.

Herchen, H., and M. A. Capelli, 1981, "First-order Raman spectra of diamond at high temperature," Phys. Rev. B **43**, 11740–11744.

Herman, F., 1959, "Lattice vibrational spectrum of germanium," J. Phys. Chem. Solids **8**, 405–418.

Hohenberg, P., and W. Kohn, 1964, "Inhomogeneous electron gas," Phys. Rev. **136**, B864–B871.

Holloway, H., K. C. Hass, M. A. Tamar, T. R. Anthony, and W. F. Banholzer, 1991, "Isotopic dependence of the lattice constant of diamond," Phys. Rev. B **44**, 7123–7126.

Hrostowski, H. J., and R. H. Kaiser, 1957, "Infrared absorption of oxygen in silicon," Phys. Rev. **107**, 966–972.

Hu, M., *et al.*, 2003, "Effect of isotopic composition on the lattice parameter of germanium measured by x-ray backscattering," Phys. Rev. B **67**, 113306.

Hybertsen, M. S., and S. G. Louie, 1986, "Electron correlation in semiconductors and insulators: Band gaps and quasiparticle energies," Phys. Rev. B **34**, 5390–5413.

Itoh, K., W. L. Hansen, E. E. Haller, J. W. Farmer, V. I. Ozhogin, A. I. Rudnev, and A. I. Tikhomirov, 1993, "High purity isotopically enriched ^{70}Ge and ^{74}Ge single crystals: Isotope separation, purification and growth," J. Mater. Res. **8**, 1341–1347.

Jagannath, C., Z. Grabowski, and A. Ramdas, 1979, "A high resolution study of the excitation spectrum of phosphorus donors introduced in silicon by neutron transmutation," Solid State Commun. **29**, 355–359.

Karaiskaj, D., G. Kirczenow, M. L. W. Thewalt, R. Buczko, and M. Cardona, 2003, "Origin of the residual acceptor ground-state splitting in silicon," Phys. Rev. Lett. **90**, 016404.

Karaiskaj, D., J. A. H. Stotz, T. Meyer, M. L. W. Thewalt, and M. Cardona, 2003, "Impurity absorption spectroscopy in ^{28}Si: The importance of inhomogeneous isotope broadening," Phys. Rev. Lett. **90**, 186402.

Karaiskaj, D., M. L. W. Thewalt, T. Ruf, and M. Cardona, 2003, "Dependence of the ionization energy of shallow donors and acceptors in silicon on the host isotopic mass," Phys. Rev. B **68**, 121201.

Karaiskaj, D., M. L. W. Thewalt, T. Ruf, M. Cardona, and M. Konuma, 2002a, "Photoluminescence studies of isotopically-enriched silicon: Isotopic effects on indirect electronic band gap and phonon energies," Solid State Commun. **123**, 87–92.

Karaiskaj, D., M. L. W. Thewalt, T. Ruf, M. Cardona, and M. Konuma, 2002b, "'Intrinsic' acceptor ground state splitting in silicon: An isotopic effect," Phys. Rev. Lett. **89**, 016401.

Karaiskaj, D., M. L. W. Thewalt, T. Ruf, M. Cardona, H.-J. Pohl, G. G. Deviatych, P. Sennikov, and H. Riemann, 2001, "Photoluminescence of isotopically purified silicon: How sharp are bound exciton transitions?," Phys. Rev. Lett. **86**, 6010–6013.

Karasyuk, V. A., D. M. Brake, and M. L. W. Thewalt, 1993, "Ultrahigh-resolution photoluminescence studies of excitons bound to boron in silicon in magnetic fields," Phys. Rev. B **47**, 9354–9360.

Karasyuk, V. A., D. M. Brake, and M. L. W. Thewalt, 1994, "Intrinsic splitting of the acceptor ground state in silicon," Phys. Rev. Lett. **73**, 2340–2343.

Karasyuk, V. A., A. G. Steele, A. Mainwood, E. C. Lightowlers, G. Davies, D. M. Brake, and M. L. W. Thewalt, 1992, "Ultrahigh-resolution photoluminescence studies of excitons bound to boron in silicon under uniaxial stress," Phys. Rev. B **45**, 11736–11743.

Karch, K., T. Dietrich, W. Windl, P. Pavone, A. P. Mayer, and D. Strauch, 1996, "Contribution of quantum and thermal fluctuations to the elastic moduli and dielectric constants of covalent semiconductors," Phys. Rev. B **53**, 7259–7266.

Kato, J., M. K. Itoh, H. Yamada-Kaneta, and H. Pohl, 2003, "Host isotope effect on the localized vibrational modes of oxygen in isotopically enriched ^{28}Si, ^{29}Si, and ^{30}Si single crystals," Phys. Rev. B **68**, 035205.

Kim, H., A. K. Ramdas, and S. Rodriguez, 1997, "Electronic transitions of holes bound to boron acceptors in isotopically controlled diamonds," Solid State Commun. **102**, 861–865.

Kim, H., A. K. Ramdas, S. Rodriguez, M. Grimsditch, and T. R. Anthony, 1999, "Spontaneous symmetry breaking of acceptors in 'blue' diamonds," Phys. Rev. Lett. **83**, 4140–4143.

Kim, H., R. Vogelgesang, A. K. Ramdas, S. Rodriguez, M. Grimsditch, and T. R. Anthony, 1998, "Electronic Raman and infrared spectra of acceptors in isotopically controlled diamonds," Phys. Rev. B **57**, 15315–15327.

King-Smith, R. D., R. J. Needs, V. Heine, and M. J. Hodgson, 1989, "A first-principles calculation of the temperature dependence of the indirect band gap of silicon," Europhys. Lett. **10**, 569–574.

Kirczenow, G., 1977, "A new model for bound multiexciton complexes," Solid State Commun. **21**, 713–715.

Kohn, W., 1957, *Shallow Impurity States in Silicon and Germanium*, Vol. 5 of Solid State Physics (Academic Press, New York), Chap. 1, pp. 257–320.

Kohn, W., and L. J. Sham, 1965, "Self-consistent equations including exchange and correlation effects," Phys. Rev. **140**, A1133–A1138.

Krautzman, M., R. M. Pick, H. Poulet, G. Hamel, and B. Prevot, 1974, "Raman detection of one-phonon-two-phonon interactions in CuCl," Phys. Rev. Lett. **33**, 528–530.

Kremer, R. K., K. Graf, M. Cardona, G. G. Devyatykh, A. V. Gusev, A. M. Gibin, A. V. Inyushkin, A. Taldenkov, and H.-J. Pohl, 2004, "Thermal conductivity of isotopically-enriched

^{28}Si: Revisited," Solid State Commun. **131**, 499–503.
Krishnamurty, S., A. B. Chen, and M. V. Schilfgaarde, 1995, "Temperature dependence of band-gaps in Hg-CdTe and other semiconductors," J. Electron. Mater. **24**, 1121–1125.
Kulda, J., A. Debernardi, M. Cardona, F. D. Geuser, and E. E. Haller, 2003, "Self-energy of zone boundary phonons in semiconductors: *Ab initio* calculations vs. neutron spin echo measurements," Phys. Rev. B **69**, 045209.
Kunc, K., and R. M. Martin, 1982, "*Ab initio* force constants of GaAs: A new approach to calculations of phonons and adiabatic properties," Phys. Rev. Lett. **48**, 406–409.
Ladd, T. D., J. R. Goldman, Y. Yamaguchi, E. Abe, and K. M. Itoh, 2002, "All-silicon quantum computer," Phys. Rev. Lett. **89**, 017901.
Laff, R. A., 1965, "Photoeffects in lead telluride *p-n* junctions," J. Appl. Phys. **36**, 3324–3329.
Lang, G., K. Karch, M. Schmitt, P. Pavone, A. P. Mayer, R. K. Wehner, and D. Strauch, 1999, "Anharmonic line shift and linewidth of the Raman mode in covalent semiconductors," Phys. Rev. B **59**, 6182–6188.
Lark-Horovitz, K., 1951, *Nucleon-Bombarded Semiconductors, Semiconducting Materials* (Butterworths, London), pp. 47–69.
Lassmann, K., C. Linsenmaier, F. Maier, F. Zeller, E. Haller, K. Itoh, L. Khirunenko, B. Pajot, and H. Müssig, 1999, "Isotopic shifts of the low-energy excitations of interstitial oxygen in germanium," Physica B **263-264**, 384–387.
Lastras-Martínez, L. F., T. Ruf, M. Konuma, M. Cardona, and D. E. Aspnes, 2000, "Isotopic effects on the dielectric response of Si around the E_1 gap," Phys. Rev. B **61**, 12946–12951.
Lautenschlager, P., P. B. Allen, and M. Cardona, 1985, "Temperature dependence of band gaps in Si and Ge," Phys. Rev. B **31**, 2163–2171.
Lautenschlager, P., P. B. Allen, and M. Cardona, 1986, "Phonon-induced lifetime broadenings of electronic states and critical points in Si and Ge," Phys. Rev. B **33**, 5501–5511.
Lautenschlager, P., S. Logothetidis, L. Viña, and M. Cardona, 1985, "Ellipsometric studies of the dielectric function of $Cd_{1-x}Mn_xTe$ alloys," Phys. Rev. B **32**, 3811–3818.
Lefmann, K., B. Buras, E. J. Petersen, E. Shabanova, P. A. Thorsen, and F. B. Rasmussen, 1994, "NMR spectra of pure ^{13}C diamond," Phys. Rev. B **50**, 15623–15627.
London, H., 1958, "The difference in the molecular volume of isotopes," Z. Phys. Chem. (Munich) **16**, 302–309.
Love, L. O., 1973, "Electromagnetic separation of isotopes at Oak Ridge," Science **182**, 343–352.
Manjon, J., M. A. Hernández-Fenollosa, B. Marí, S. F. Li, C. D. Poweleit, A. Bell, J. Menéndez, and M. Cardona, 2004, "Effect of N-isotopic mass on photoluminescence and cathodoluminescence spectra of Gallium Nitride," Eur. Phys. J. B **40**, 453–458.
Manjon, J., M. Mollar, M. A. Hernández-Fenollosa, B. Marí, R. Lauck, and M. Cardona, 2003, "Effect of isotopic mass on photoluminescence spectra of zinc oxide," Solid State Commun. **128**, 35–39.
Manjón, J., M. Mollar, B. Mari, N. Garro, A. Cantarero, R. Lauck, and M. Cardona, 2004, "Effect of isotopic mass on photoluminescence spectra of β-Zinc sulfide," Solid State Commun. **133**, 253–258.
Manjón, J., J. Serrano, I. Loa, K. Syassen, C. T. Lin, and M. Cardona, 2001, "Effect of pressure on the anomalous Raman spectrum of CuBr," Phys. Status Solidi B **223**, 331–336.
Manoogian, A., and A. Leclerc, 1979, "Determination of the dilation and vibrational contributions to the indirect energy-band gap of diamond semiconductor," Can. J. Phys. **57**, 1766–1769.
Manuel, O., 2001, *Origins of Elements in the Solar System* (Kluwer/Academic/Plenum, New York).
Martin, R., 1969, "Dielectric screening model for lattice vibrations of diamond structure crystals," Phys. Rev. **186**, 871–884.
Mason, S. F., 1991, *Chemical Evolution* (Clarendon, Oxford, UK).
Mayur, A. J., M. D. Sciacca, M. K. Udo, and A. K. Ramdas, 1994, "Fine structure of the asymmetric stretching vibration of dispersed oxygen in monoisotopic germanium," Phys. Rev. B **49**, 16293–16299.
McCaulley, J. A., V. M. Donnelly, M. Vernon, and I. Taha, 1994, "Temperature dependence of the near-infrared refractive index of silicon, galium arsenide and indium phosphide," Phys. Rev. B **49**, 7408–7417.
McCluskey, M. D., 2000, "Local vibrational modes of impurities in semiconductors," J. Appl. Phys. **87**, 3593–3617.
Menéndez, J., and M. Cardona, 1984, "Temperature dependence of the first-order Raman scattering by phonons in Si, Ge, and α-Sn: Anharmonic effects," Phys. Rev. B **29**, 2051–2059.
Menéndez, J., J. B. Page, and S. Guha, 1994, "The isotope effect of the Raman spectrum of molecular C_{60}," Philos. Mag. B **70**, 651–659.
Meyer, T. A., D. Karaiskaj, M. L. W. Thewalt, and M. Cardona, 2003, "Effect of isotopic mass of gallium on the indirect gap of GaP," Solid State Commun. **126**, 119–123.
Morgan, T. N., 1968, "Optical properties of Cd-O and Zn-O complexes in GaP," Phys. Rev. **166**, 751–753.
Nelin, G., and G. Nilsson, 1972, "Phonon density of states in germanium at 8 K measured by neutron spectroscopy," Phys. Rev. B **5**, 3151–3160.
Nelin, G., and G. Nilsson, 1974, "Phonon anharmonicity of germanium in the temperature range 80–880 K," Phys. Rev. B **10**, 612–620.
Nernst, W., and F. A. Lindemann, 1911, "Specific heat and quantum theory," Z. Elektrochem. Angew. Phys. Chem. **18**, 817–827 (in German).
Newman, R., 1993, *Imperfections in III-V Materials* (Academic, Boston), Vol. 38, Chap. 4, pp. 117–187.
Nilsson, G., and G. Nelin, 1971, "Dispersion relations in germanium at 80 K," Phys. Rev. B **3**, 364–369.
Olander, D. R., 1978, "The gas centrifuge," Sci. Am. **239**, 27–33.
Olguin, D., M. Cardona, and A. Cantarero, 2002, "Electron-phonon effects on the direct band gap in semiconductors: LCAO calculations," Solid State Commun. **122**, 575–589.
Omini, M., and A. Sparavigna, 1997, "Thermal conductivity of dielectric solids with diamond structure," Nuovo Cimento D **19**, 1537–1563.
Pajot, B., 1994, "Some atomic configurations of oxygen," in *Semiconductors and Semimetals*, edited by F. Shimura (Academic, San Diego, CA), Vol. 42, Chap. 6, pp. 191–249.
Pajot, B., E. Artacho, L. Khirunenko, K. Itoh, and E. Haller, 1997, "Isotope shift of a vibrational mode of interstitial oxygen in germanium," Mater. Sci. Forum **258**, 41–46.
Pajot, B., P. Clauws, J. L. Lindstrom, and E. Artacho, 2000, "Oxygen isotope effects and vibration-rotation lines of interstitial oxygen in germanium," Phys. Rev. B **62**, 10165–10172.
Pake, G., 1948, "Nuclear resonance absorption in hydrated crystals—Fine structure of the proton line," J. Chem. Phys.

16, 327–336.
Parks, C., A. K. Ramdas, S. Rodriguez, K. M. Itoh, and E. E. Haller, 1994, "Electronic band structure of isotopically pure germanium: Modulated transmission and reflectivity study," Phys. Rev. B **49**, 14244–14250.
Pässler, R., 1999, "Parameter sets due to fittings of the temperature dependencies of fundamental bandgaps in semiconductors," Phys. Status Solidi B **216**, 975–1007.
Pässler, R., 2001, "Temperature dependence of fundamental band gaps in group IV, III-V, and II-VI materials via a two-oscillator model," J. Appl. Phys. **89**, 6235–6240.
Paul, W., and R. V. Jones, 1953, "Absorption spectrum of lead sulphide at different temperatures," Proc. Phys. Soc. London, Sect. B **66**, 194–200.
Pavone, P., and S. Baroni, 1994, "Dependence of the crystal-lattice constant on isotopic composition: Theory and *ab initio* calculations for C, Si and Ge," Solid State Commun. **90**, 295–297.
Perdew, J. P., and M. Levy, 1983, "Physical content of the Kohn-Sham orbital energies: Band gaps and derivative discontinuities," Phys. Rev. Lett. **51**, 1884–1887.
Pereira, R. N., T. Ohya, K. M. Itoh, and B. B. Nielsen, 2003, "Local vibrational modes of bond-centered H in ^{28}Si, ^{29}Si and ^{30}Si crystals," Physica B **340-342**, 697–700.
Petzke, K., 1999, "*Ab initio* study of local vibrational modes in II-VI semiconductors: ZnS:Se and ZnSe:N," Physica B **273-274**, 866–869.
Plekhanov, V. G., 2001, *Isotope Effects in Solid State Physics*, Semiconductors and Semimetals, Vol. 68 (Academic, San Diego).
Pomeranchuk, I. Y., 1942, "On the thermal conductivity of dielectrics at temperatures lower than that of Debye," J. Phys. (Moscow) **6**, 237–255.
Ramdas, A. K., and S. Rodriguez, 1981, "Spectroscopy of the solid-state analogues of the hydrogen atom: Donors and acceptors in semiconductors," Rep. Prog. Phys. **44**, 1297–1387.
Reeber, R. R., and K. Wang, 1996, "Thermal expansion, nuclear volume, and specific heat of diamond from 0 to 3000 K," J. Electron. Mater. **25**, 63–67.
Rönnow, D., L. F. Lastras-Martínez, and M. Cardona, 1998, "Isotope effects on the electronic critical points of germanium: Ellipsometric investigation of the E_1 and $E_1+\Delta_1$ transitions," Eur. Phys. J. B **5**, 29–35.
Rowe, J. M., R. M. Nicklow, D. L. Price, and K. Zanio, 1974, "Lattice-dynamics of cadmium telluride," Phys. Rev. B **10**, 671–675.
Ruf, T., M. Cardona, C. Pickles, and R. Sussmann, 2000, "Temperature dependence of 925 K of the refractive index in diamond," Phys. Rev. B **62**, 16578–16581.
Ruf, T., R. W. Henn, M. Asen-Palmer, E. Gmelin, M. Cardona, H.-J. Pohl, G. G. Devyatych, and P. G. Sennikov, 2000, "Thermal conductivity of isotopically-enriched silicon," Solid State Commun. **115**, 243–247; **127**, 257(E) (2003).
Ruf, T., J. Serrano, M. Cardona, P. Pavone, M. Pabst, M. Krisch, M. D'Astuto, T. Suski, I. Grzegory, and M. Leszczynski, 2001a, "Phonon dispersion curves in wurtzite-structure GaN determined by inelastic x-ray scattering," Phys. Rev. Lett. **86**, 906–909.
Ruf, T., J. Serrano, M. Cardona, P. Pavone, M. Pabst, M. Krisch, M. D'Astuto, T. Suski, I. Grzegory, M. Leszczynski, and T. R. Anthony, 2001b, in *25th International Conference on Physics of Semiconductors*, edited by N. Miura and T. Ando (Springer, Heidelberg), 87, pp. 1531–1532.
Safonov, A. N., G. Davies, and E. C. Lightowlers, 1996, "Lineshape of the no-phonon luminescence of excitons bound to phosphorus in carbon-doped silicon," Phys. Rev. B **54**, 4409–4412.
Sanati, M., and S. K. Estreicher, 2003, "Defects in silicon: The role of vibrational entropy," Solid State Commun. **128**, 181–185.
Sanati, M., S. K. Estreicher, and M. Cardona, 2004,"Isotopic dependence of the heat capacity of c-C, Si and Ge: An *ab initio* calculation," Solid State Commun. **131**, 229–233.
Savrasov, S. Y., 1996, "Linear response theory and lattice dynamics: A muffin tin orbital approach," Phys. Rev. B **54**, 16470–16486.
Schechter, D., 1962, "Theory of shallow acceptor states in Si and Ge," J. Phys. Chem. Solids **23**, 237–247.
Schmid, W., 1977, "Auger lifetimes for excitons bound to neutral donors and acceptors in Si," Phys. Status Solidi B **84**, 529–540.
Schneider, J., B. Dischler, H. Seelewind, P. Mooney, J. Lagowski, M. Matsui, D. R. Beard, and R. Newman, 1989, "Assessment of oxygen in gallium arsenide by infrared local vibrational mode spectroscopy," Appl. Phys. Lett. **54**, 1442–1444.
Schnelle, W., and E. Gmelin, 2001, "Heat capacity of germanium crystals with various isotopic compositions," J. Phys.: Condens. Matter **13**, 6087–6094.
Sennikov, P., T. Kotereva, A. Kurganov, B. Andreev, H. Niemann, D. Schiel, V. Emtsev, and H.-J. Pohl, 2005, "Spectroscopic parameters of the absorption bands related to local vibrational modes of carbon and oxygen impurities in silicon enriched with ^{28}Si, ^{29}Si and ^{30}Si isotopes," Semiconductors **39**, 300–307.
Serrano, J., F. J. Manjón, F. Widulle, A. H. Romero, R. Lauck, and M. Cardona, 2003, "Dispersive phonon linewidths: The E_2 phonons of ZnO," Phys. Rev. Lett. **90**, 055510.
Serrano, J., T. Ruf, F. Widulle, C. T. Lin, and M. Cardona, 2001, "Isotopic investigation of lattice dynamics in CuBr," Phys. Rev. B **64**, 045201.
Serrano, J., Ch. Schweizer, C. T. Lin, K. Reimann, M. Cardona, and D. Fröhlich, 2002, "Electron-phonon renormalization of the absorption edge of the cuprous halides," Phys. Rev. B **65**, 125110.
Serrano, J., F. Widulle, A. H. Romero, A. Rubio, R. Lauck, and M. Cardona, 2003, "Dependence of phonon widths on pressure and isotopic mass: ZnO," Phys. Status Solidi B **235**, 260–266.
Sham, L. J., 1974, in *Covalent Crystals*, edited by C. K. Horton and A. A. Maradudin, Dynamical Properties of Solids Vol. 1 (North-Holland, Amsterdam), Chap. 5, pp. 301–342.
Sham, L. J., and M. Schluter, 1983, "Density-functional theory of the energy gap," Phys. Rev. Lett. **51**, 1888–1891.
Singh, H. P., 1968, "Determination of thermal expansion of germanium, rhodium and iridium by x-rays," Acta Crystallogr., Sect. A: Cryst. Phys., Diffr., Theor. Gen. Crystallogr. **A24**, 469–471.
Soddy, F., 1913, "Intra-atomic charge," Nature (London) **92**, 399–400.
Sozontov, E., L. X. Cao, A. Kazimirov, V. Kohn, M. Konuma, and J. Zegenhagen, 2001, "X-ray standing wave analysis of the effect of isotopic composition on the lattice constants of Si and Ge," Phys. Rev. Lett. **86**, 5329–5332.
Sparavigna, A., 2002, "Influence of isotope scattering on the thermal conductivity of diamond," Phys. Rev. B **65**, 064305.

Sparavigna, A., 2003, "Role of nonpairwise interactions on phonon thermal transport," Phys. Rev. B **67**, 144305.

Spitzer, J., P. Etchegoin, M. Cardona, T. R. Anthony, and W. F. Banholzer, 1993, "Isotopic-disorder-induced Raman scattering in diamond," Solid State Commun. **88**, 509–514.

Srivastava, G. P., 1990, *The Physics of Phonons* (Hilger, Bristol).

Stavola, M., 1999, *Identification of Defects in Semiconductors*, Semiconductors and Semimetals (Academic Press, Boston), Vol. 51B, Chap. 3, pp. 153–224.

Strauch, D., and B. Dorner, 1986, "Phonon eigenvector determination in GaAs by inelastic neutron-scattering," J. Phys. C **19**, 2853–2864.

Strauch, D., A. P. Mayer, and B. Dorner, 1990, "Phonon eigenvectors in Si determined by inelastic neutron-scattering," Z. Phys. B: Condens. Matter **78**, 405–410.

Suess, H. E., and H. C. Urey, 1956, "Abundances of the elements," Rev. Mod. Phys. **28**, 53–74.

Sun, B., Q. Yang, R. C. Newman, B. Pajot, N. H. Tolk, L. C. Feldman, and G. Lüpke, 2004, "Vibrational lifetimes and isotope effects of interstitial oxygen in silicon and germanium," Phys. Rev. Lett. **92**, 185503.

Tallman, R., T. M. Ritter, B. A. Weinstein, A. Cantarero, J. Serrano, R. Lauck, and M. Cardona, 2004, "Pressure measurements of TO-phonon anharmonicity in isotopic ZnS," Phys. Status Solidi B **241**, 491–494.

Tamura, S., 1983, "Isotope scattering of dispersive phonons in Ge," Phys. Rev. B **27**, 858–866.

Taylor, D. W., 1967, "Vibrational properties of imperfect crystals with large defect concentrations," Phys. Rev. **156**, 1017–1029.

Thewalt, M. L. W., D. Karaiskaj, T. Ruf, and M. Cardona, 2003, in *Proceedings of the 26th International Conference on the Physics of Semiconductors 2002*, edited by A. R. Long and J. H. Davies (Institute of Physics, Bristol, Edinburgh, UK), Vol. 171, pp. 101–108.

Thewalt, M. L. W., T. A. Meyer, D. Karaiskaj, M. Cardona, E. E. Haller, J. W. Ager, and H. Riemann, 2004, in *Proceedings of the 27th International Conference on the Physics of Semiconductors*, edited by J. Menendez (AIP, Melville, NY), pp. 67–68.

Thewalt, M. L. W., N. K. Nissen, D. J. S. Beckett, and K. R. Lundgren, 1990, "High-performance photoluminescence spectroscopy using Fourier transform interferometry," in *Impurities, Defects and Diffusion in Semiconductors: Bulk and Layered Structures*, edited by D. J. Wolford, J. Bernholc, and E. E. Haller, MRS Symposia Proceedings No. 163 (Materials Research Society, Pittsburgh), pp. 221–231.

Thomson, J. J., 1913, "On the appearance of helium and neon in vacuum tubes," Nature (London) **90**, 645–647.

Thurmond, C. D., 1975, "Standard thermodynamic functions for formation of electrons and holes in Ge, Si, GaAs, and GaP," J. Electrochem. Soc. **122**, 1133–1141.

Tsang, Y. W., and M. L. Cohen, 1971, "Calculation of the temperature dependence of the energy gaps in PbTe and SnTe," Phys. Rev. B **3**, 1254–1261.

Ulrich, C., E. Anastassakis, K. Syassen, A. Debernardi, and M. Cardona, 1997, "Lifetime of phonons in semiconductors under pressure," Phys. Rev. Lett. **78**, 1283–1286.

Ulrich, C., A. Göbel, K. Syassen, and M. Cardona, 1999, "Pressure-induced disappearance of the Raman anomaly in CuCl," Phys. Rev. Lett. **82**, 351–354.

Vanderbilt, D., S. G. Louie, and M. L. Cohen, 1984, "Calculation of phonon-phonon interactions and the absence of 2-phonon bound states in diamond," Phys. Rev. Lett. **53**, 1477–1480.

Varslini, Y. P., 1967, "Temperature dependence of energy gaps in semiconductors," Physica (Amsterdam) **34**, 149–151.

Vast, N., and S. Baroni, 2000, "Effects of isotopic disorder on the Raman frequencies of crystals: Theory and *ab initio* calculations for diamond and germanium," Phys. Rev. B **61**, 9387–9392.

Velický, B., and J. Sak, 1966, "Excitonic effects in interaband absorption of semiconductors," Phys. Status Solidi **16**, 147–157.

Verhulst, A. S., D. Maryenko, Y. Yamamoto, and K. M. Itoh, 2003, "Double and single peaks in NMR spectra of natural and ^{29}Si-enriched single-crystal silicon," Phys. Rev. B **68**, 054105.

Verkhovskii, S. V., B. Z. Malkin, A. Trokiner, A. Y. Yakubovsky, E. Haller, A. Ananyev, A. Gerashenko, Y. Piskunov, S. Saikin, A. Tikhomirov, and V. I. Ozhogin, 2000, "Quadrupole effects on ^{73}Ge NMR spectra in isotopically controlled Ge single crystals," Z. Naturforsch., A: Phys. Sci. **55a**, 105–110.

Verkhovskii, S. V., A. Y. Yakubovsky, B. Z. Malkin, S. K. Saikin, M. Cardona, A. Trokiner, and V. I. Ozhogin, 2003, "Isotopic disorder in Ge single crystals probed with ^{73}Ge NMR," Phys. Rev. B **68**, 104201.

Ves, S., I. Loa, K. Syassen, F. Widulle, and M. Cardona, 2001, "Raman lineshapes of GaP under pressure," Phys. Status Solidi B **223**, 241–245.

Villani, S., 1976, *Isotope Separation* (American Nuclear Society, Hinsdale, IL).

Vogelgesang, R., A. D. Alvarenga, H. Kim, A. K. Ramdas, S. Rodriguez, M. Grimsditch, and T. R. Anthony, 1998, "Multiphonon Raman and infrared spectra of isotopically controlled diamond," Phys. Rev. B **58**, 5408–5416.

Vogelgesang, R., A. K. Ramdas, S. Rodriguez, M. Grimsditch, and T. R. Anthony, 1996, "Brillouin and Raman scattering in natural and isotopically controlled diamond," Phys. Rev. B **54**, 3989–3999.

Wang, C.-Z., R. Yu, and H. Krakauer, 1994, "First-principles linear response calculations of lattice dynamics for CuCl," Phys. Rev. Lett. **72**, 368–371.

Wang, D. T., A. Göbel, J. Zegenhagen, and M. Cardona, 1997, "Raman scattering on α-Sn: Dependence on isotopic composition," Phys. Rev. B **56**, 13167–13171.

Waugh, J. L. T., and G. Dolling, 1963, "Crystal dynamics of GaAs," Phys. Rev. **132**, 2410–2412.

Weber, W., 1977, "Adiabatic bond charge model for the phonons in diamond, Si, Ge, and α-Sn," Phys. Rev. B **15**, 4789–4803.

Wei, L., P. K. Kuo, R. L. Thomas, T. R. Anthony, and W. F. Banholzer, 1993, "Thermal conductivity of isotopically modified single crystal diamond," Phys. Rev. Lett. **70**, 3764–3767.

Weinstein, B. A., 1976, "Pressure-dependent optical phonon anharmonicity in GaP," Solid State Commun. **20**, 999–1003.

Widulle, F., T. Ruf, O. Buresch, A. Debernardi, and M. Cardona, 1999, "Raman study of isotope effects and phonon eigenvectors in SiC," Phys. Rev. Lett. **82**, 3089–3092.

Widulle, F., T. Ruf, A. Göbel, E. Schönherr, and M. Cardona, 1999, "Raman study of the anomalous TO phonon structure in GaP with controlled isotopic composition," Phys. Rev. Lett. **82**, 5281–5284.

Widulle, F., T. Ruf, M. Konuma, I. Silier, W. Kriegseis, M.

Cardona, and V. I. Ozhogin, 2001, "Isotopic effects in elemental semiconductors: A Raman study of Si," Solid State Commun. **118**, 1–22.

Widulle, F., J. Serrano, and M. Cardona, 2002, "Disorder-induced phonon self-energy of semiconductors with binary isotopic composition," Phys. Rev. B **65**, 075206.

Yin, T. M., and M. L. Cohen, 1982, "Theory of lattice-dynamical properties of solids," Phys. Rev. B **26**, 3259–3272.

Yu, P. Y., and M. Cardona, 1970, "Temperature coefficient of the refractive index of diamond- and zinc-blende-type semiconductors," Phys. Rev. B **2**, 3193–3197.

Yu, P. Y., and M. Cardona, 2005, *Fundamentals of Semiconductors* (Springer, Heidelberg), reprinted 3rd edition.

Zhang, J. M., M. Giehler, A. Göbel, T. Ruf, M. Cardona, E. E. Haller, and K. Itoh, 1998, "Optical phonons in isotopic Ge studied by Raman scattering," Phys. Rev. B **57**, 1348–1351.

Zhang, J. M., T. Ruf, M. Cardona, O. Ambacher, M. Stutzmann, J.-M. Wagner, and F. Bechstedt, 1997, "Raman spectra of isotopic GaN," Phys. Rev. B **56**, 14399–14406.

Zhang, J. M., T. Ruf, A. Göbel, A. Debernardi, R. Lauck, and M. Cardona, 1996, in *Proceeding of the 23rd International Conference on Physics of Semiconductors*, edited by M. Scheffler and R. Zimmermann (World Scientific, Singapore), Vol. 23, pp. 201–204.

Zhang, J. M., T. Ruf, R. Lauck, and M. Cardona, 1998, "Isotope effects on exciton energies in CdS," Phys. Rev. B **57**, 9716–9722.

Zollner, S., M. Cardona, and S. Gopalan, 1992, "Isotope and temperature shifts of direct and indirect band gaps in diamond-type semiconductors," Phys. Rev. B **45**, 3376–3385.